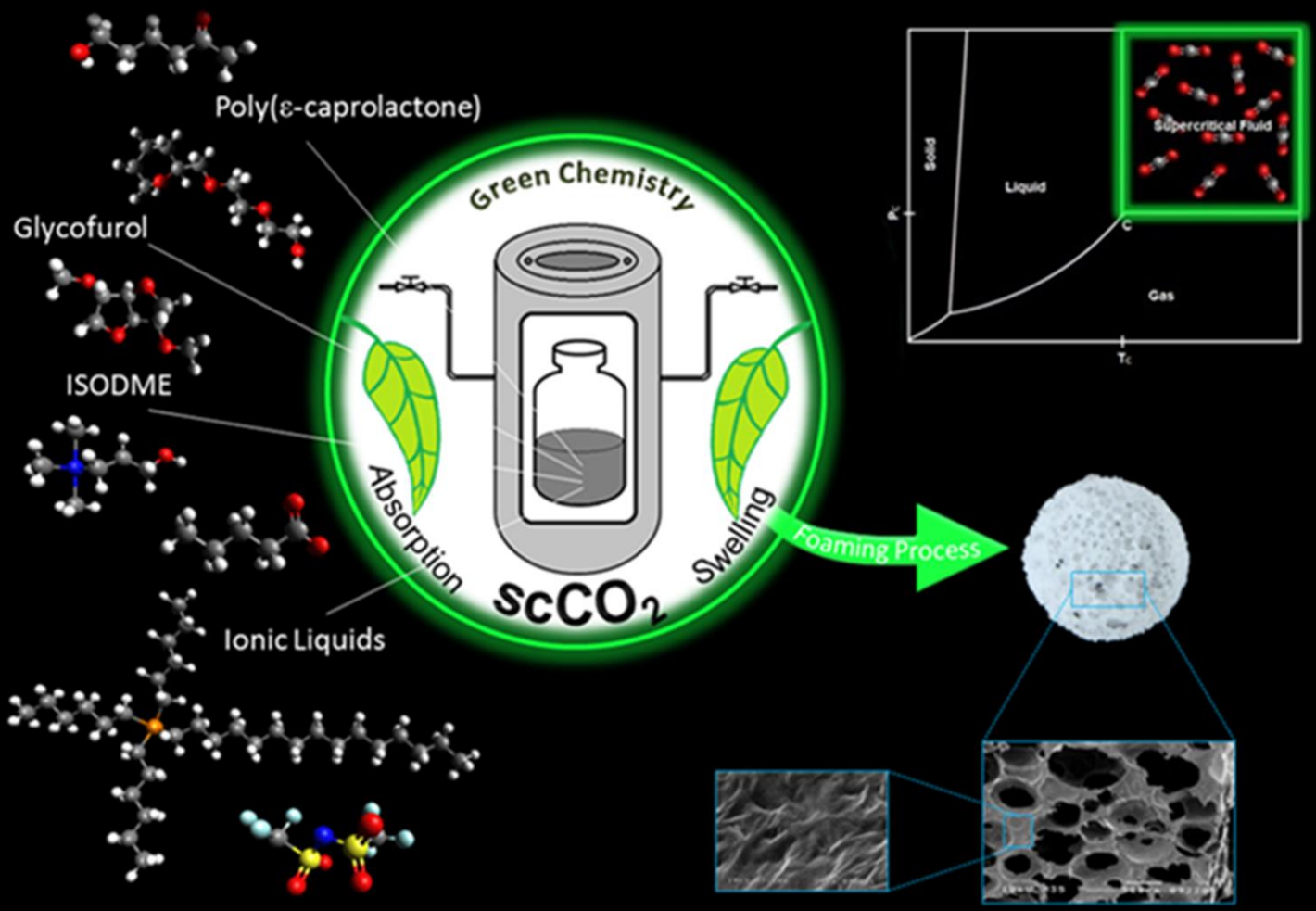

António Barbosa Soares Rosa

Poly (ε-caprolactone)/SBA-15 composite biomaterials plasticized with greener additives

September 2013

· U C ·

Universidade de Coimbra

António Barbosa Soares Rosa

Poly (ε-caprolactone)/SBA-15 composite biomaterials plasticized with greener additives

Thesis Project in the scientific area of Chemical Engineering submitted to the Faculty of Science and Technology of University of Coimbra for the degree of Master in Chemical Engineering

Supervisors:
Prof. Dr. Hermínio José Cipriano de Sousa
Prof. Dr. Mara Elga Medeiros Braga

Coimbra
2013

UNIVERSIDADE DE COIMBRA

This page was intentionally left in blank

Acknowledgements

Someone has said before that it is good to have an end to journey toward; but it is the journey that matters, in the end. So, in the same way of thinking, I would take this opportunity to thank all those that I have met throughout this journey. This work could not been possible without the help and collaboration of many people to whom I have had the good fortune to meet over these years during my university career and to whom I am sincerely grateful.

First of all, I would like to express my deepest gratitude to my advisers Professor Hermínio de Sousa and Dr. Mara Braga for the excellent guidance, interest demonstrated in this work, expert advices. It was a honor to have you two as my supervisors.

I am very grateful to Maria de Matos for all the support and help from the beginning to end of this work, my special thanks.

I would like to thank all my research group members for their help, namely, Sofia Marceneiro, Luísa Filipe, Rita Chim, Ana Cortez, Dr. Ana Dias and Luís Gomes for all the help, assistance, and availability when I needed and for the sympathy demonstrated over these months.

My special thanks to all my friends and colleagues that I had the fortune to make in this city for the friendship, help and the big memories.

To Cátia Costa and Maria João from CIEPQPF research Centre (DEQ-FCTUC) for their help in the DMA and thermal analyses, respectively.

To Pedro Prazeres from Paralab for his helpful contribution in the morphological analysis.

To José Viegas from the Escola Superior Agrária de Coimbra (ESAC) for his help in the compression tests and to everyone involved for the accomplishment of this work.

Last, but not least, words cannot express my sincere gratefulness to all my family members, especially to my mother for the constant support, caring and love and I therefore dedicate this work to her.

Abstract

There are several methods for producing foamed materials. These techniques use environmentally hazardous compounds, which contribute to the air pollution, and lead to undesirable residues in the final polymeric foam. Furthermore, purification and drying steps are often required which can degrade thermosensitive components such as drugs, proteins or other bioactive substances.

The main goal of this work was the development, processing and characterization of porous PCL/SBA–15 composite biomaterials by combining greener additives such as ionic liquids, glycofurol and isosorbide dimethyl ether with supercritical fluid process, a clean and environmentally friendly technology.

Polymeric foams of pure PCL and nanocomposite biomaterials were prepared via supercritical fluid foaming process by pressure quench method using $scCO_2$ as foaming agent, at constant operating conditions, namely pressure (20 MPa), temperature (40 °C) and soaking time (2 hours). The depressurization rate was 0.37 $L_{CO2} \cdot min^{-1}$. This technique presented several advantages over the conventional techniques. There is no need the use of organic solvents, which can be harmful to the seeding cells, human and the environment. There is also no need additional step such as drying or other methods to remove the residual solvents that can degrade the thermolabile components.

The effect of the various additives on the morphology, thermal and in the mechanical properties of the produced porous materials was assessed by Fourier Transform Infrared (FTIR), Differential Scanning Calorimetry (DSC), Thermogravimetric Analysis (TGA), Dynamical Mechanical Analysis (DMA) and compression testing. Furthermore, cytotoxicity tests were performed using LDH assay using redox reactions in SAOS–2 human osteogenic sarcoma cells to assess the biocompatibility of the foams.

The results from the cytotoxicity demonstrated that the produced foams present high biocompatibility to the cells.

The results from the FTIR and SEM–EDS have confirmed the presence of the two ILs and silica nanoparticles within the polymeric matrix which revealed to be well dispersed.

The melting temperature slightly decreased with the addition of the additives. This effect was more substantial for PG and PI composite, which decreased from 61.73 ± 0.35 °C to 55.37 ± 1.37 °C and 57.20 ± 0.69 °C, respectively.

The pore volume increased from $0.65 \pm 0.09 \times 10^{-3}$ to $0.87 \pm 0.24 \times 10^{-3}$ $cm^3 \cdot g^{-1}$ with the incorporation of small amount of SBA–15 (10 wt. %) and to $4.87 \pm 0.31 \times 10^{-3}$ with the addition of 30 wt. % of SBA–15.

The obtained results from the different techniques have demonstrated that the various additives significantly affected the morphology, the thermal and mechanical properties of the foams which confirmed their strong plasticization effect, especially Glycofurol and Isosorbide dimethyl ether.

The $scCO_2$ foaming process revealed to be a feasible technique to produce 3D porous composite accurately with real density ranging from 0.99 to 1.24 $g \cdot cm^{-3}$ by combining PCL with SBA–15 and four greener additives and supercritical carbon dioxide technology which present very interesting properties with potential applications in pharmaceutical and biomedical field.

Resumo

Existem muitos métodos para a produção de materiais porosos. Todos esses métodos usam compostos orgânicos voláteis ambientalmente perigosos, que contribuem para poluição atmosférica, e contribuem para a contaminação da estrutura final. Muitas vezes, passos adicionais são necessários como a purificação e secagem, o que contribui para um consumo elevado de energia e possível degradação de substâncias bioactivas como fármacos, proteínas ou outros compostos bioactivos.

Este trabalho teve como objectivo principal o desenvolvimento, processamento e caracterização de biomateriais compósitos porosos de poli (ε–caprolactona) (PCL) / SBA–15 combinando aditivos considerados verdes tais como líquidos iónicos, glicofurol e isossorbida éter dimetil (dois solventes usados na indústria farmacêutica) com o processo de fluido supercrítico, uma tecnologia limpa e amiga do ambiente.

As estruturas porosas da PCL pura e dos biocompósitos foram processadas via processo de *foaming* de fluido supercrítico pelo método de *pressure quench* usando o dióxido de carbono como agente de porogénico em condições de operação constante, nomeadamente pressão (20 MPa), temperatura (40 °C), tempo de saturação (2 horas) e taxa de despressurização (0.37 $L_{CO2} \cdot min^{-1}$)

Este método apresenta muitas vantagens relativamente aos métodos convencionais uma vez que não é necessário o uso de solventes orgânicos voláteis. Também não é necessário nenhum passo adicional como por exemplo a secagem ou outras técnicas para a remoção de solventes residuais, que consome enormes quantidades de energia e pode degradar os compostos bioactivos sensíveis a temperatura.

Os efeitos dos vários aditivos e das nanopartículas na morfologia, nas propriedades térmicas e mecânicas da amostra final foram analisados por diferentes técnicas com Espectroscopia de Infravermelho (FTIR), Calorimetria Diferencial de Varrimento (DSC), Análise Termogravimétrica (TGA), Microscopia Electrónica de Varrimento (SEM), Análise Dinâmica e Mecânica (DMA) e análise de compressão mecânica. Testes de citotoxicidade também foram realizados utilizando ensaio de LDH em células sarcoma osteogénicos SAOS–2 de modo a avaliar a viabilidade das células.

Os resultados de citotoxicidade demonstraram que os *foams* são citocompatíveis.

Os resultados obtidos a partir do FTIR e SEM–EDS confirmaram a presença dos dois líquidos iónicos e das nanopartículas de sílica que revelaram estar homogeneamente dispersas na matriz polimérica.

A temperatura de fusão diminui com a adição dos solventes. Este efeito foi mais significativo para o caso de PG e PI, onde decresceu de 61.73 ± 0.35 °C para 55.37 ± 1.37 °C e para 57.20 ± 0.69 °C, respectivamente.

O volume de poros aumentou de 0.65 ± 0.09 × 10^{-3} para 0.87 ± 0.24 × 10^{-3} $cm^3 \cdot g^{-1}$ com a incorporação de menor quantidade de SBA-15 (10 %) e para 4.87 ± 0.31 × 10^{-3} $cm^3 \cdot g^{-1}$ com a adição de 30 % de SBA-15.

Os resultados obtidos pelas diferentes técnicas demonstraram que as nanopartículas de sílica e os vários aditivos afectaram significativamente a morfologia, as propriedades térmicas e mecânicas. Ficou demonstrado, de uma forma clara, o grande poder plastificante dos vários aditivos utilizados, especialmente do glicofurol e isossorbida dimetil éter.

O método proposto revelou ser um método eficaz no fabrico de estruturas porosas com valores de massa específica real compreendidos entre 0.99 e 1.24 $g \cdot cm^{-3}$ usando apenas aditivos verdes e tecnologia supercrítica (CO_2) com propriedades muito interessantes com potenciais aplicações na área farmacêutica e biomédica.

Table of Contents

List of figures

List of equations

List of abbreviations and Nomenclature

Symbols

~ – approximately

$\%wt_{SBA-15}$ – Weight percentage of the silica nanoparticles

°C – Degree Celsius

3D – Three dimensional

Δh – Total deformation of the sample

ΔG_{het} – Gibbs free energy for heterogeneous nucleation

ΔG_{homo} – Gibbs free energy for homogeneous nucleation

ΔH_f – Enthalpy of fusion

ΔH_f^0 – Enthalpy of fusion of 100% crystalline polymer

µm – micrometer (s)

Å – Angstrom (s)

A – Cross section area, m^2

C_0 – Concentration of gas molecules in solution for homogeneous nucleation

C_1 – Concentration of the heterogeneous nucleation sites

CO_2 – Carbon Dioxide

cm – centimeter (s)

E – Young's Modulus (Linear elastic modulus), MPa

E' – Storage Modulus, MPa

E'' – Loss Modulus, MPa

F – Force, N

f_0 – Frequency factor for homogeneous nucleation

f_1 – Frequency factor for heterogeneous nucleation

g – Gram (s)

h – Hour (s); final height of the material

h_0 – Initial height of the material

J – Joule (s)

kg – Kilogram (s)

L – Liter (s)

L_{CO2} – Liters of carbon dioxide

LD_{50} – A dose lethal to 50% of the specified animals or microorganisms

min – Minutes

mL – milliliter (s)

M_n – number average molecular weight, $g \cdot mol^{-1}$

N – Nucleation rate of mixed nucleation

N_{het} – Heterogeneous nucleation rate

N_{homo} – Homogeneous nucleation rate

nm – Nanometer (s)

N'_{homo} – Homogeneous nucleation rate in the presence of heterogeneous nucleation

P_c – Critical Pressure, MPa

Si – Silicon

T – Absolute temperature, K

tan δ – damping parameter

T_c – Critical Temperature, °C

T_g – Glass transition temperature, °C

T_m – Melting temperature, °C

v/v – Volume in volume

Abbreviations/Acronyms

ATR – Attenuated Total Reflectance

BET – Brunauer, Emmet and Teller

BJH – Barret, Joyner and Halenda

CBA – Chemical Blowing Agent

CFC's – Chlorofluorocarbons

DMEM – Dulbecco's Modified Eagles's Medium

DSC – Differential Scanning Calorimetry

et al. – *et alii*, "and others"

FBS – Fetal Bovine Serum

FDA – Food and Drug Administration

FTIR – Fourier Transform Infrared

GF – Glycofurol

GPa – Giga Pascal

GRAS – Generally Recognize as Safe

HCFC's – Hydrochlorofluorocarbons

i.e. – *id est*, "that is"

IL, ILs – Ionic Liquid, Ionic Liquids

ISO – International Organization for Standardization

ISODME – Isosorbide Dimethyl Ether

KCl – Potassium Chloride

LDH – Lactate dehydrogenase

MPa – Mega Pascal

NaCl – Sodium Chloride

PB – Tridecyl(tetrahexyl)phosphonium bistriflamide

PBA – Physical Blowing Agent

PCL – Poly (ε–caprolactone)

PG – Poly (ε–caprolactone)/Glycofurol

PI – Poly (ε–caprolactone)/Isorsorbide dimethyl ether

PIPB – Poly (ε–caprolactone)/Isorsorbide dimethyl ether/Tridecyl(tetrahexyl)phosphonium bistriflamide

PGPB – Poly (ε–caprolactone)/Glycofurol/Tridecyl(tetrahexyl)phosphonium bistriflamide

PP – Poly (ε–caprolactone)/N,N,N-Trimethyelethanolammonium pentanoate

PS10 – Poly (ε–caprolactone)/SBA-15 10 wt. %

PS10G – Poly (ε–caprolactone)/Glycofurol/SBA-15 10 wt. %

PS10GPB – Poly (ε–caprolactone)/Glycofurol/ Tridecyl(tetrahexyl)phosphonium bistriflamide/SBA-15 10 wt. %

PS10I – Poly (ε–caprolactone)/ Isorsorbide dimethyl ether /SBA-15 10 wt. %

PS10IPB – Poly (ε–caprolactone)/ Isorsorbide dimethyl ether / Tridecyl(tetrahexyl)phosphonium bistriflamide/SBA-15 10 wt. %

PS10P – Poly (ε–caprolactone)/ N,N,N-Trimethyelethanolammonium pentanoate/SBA-15 10 wt. %

PS10PB – Poly (ε–caprolactone)/ Tridecyl(tetrahexyl)phosphonium bistriflamide/SBA-15 10 wt. %

PS30 – Poly (ε–caprolactone)/SBA-15 30 wt. %

PS30G – Poly (ε–caprolactone)/Glycofurol/SBA-15 30 wt. %

PS30I – Poly (ε–caprolactone)/ Isorsorbide dimethyl ether /SBA-15 30 wt. %

PS30P – Poly (ε–caprolactone)/ N,N,N-Trimethyelethanolammonium pentanoate/SBA-15 30 wt. %

PS30PB – Poly (ε–caprolactone)/ Tridecyl(tetrahexyl)phosphonium bistriflamide/SBA-15 30 wt. %

PPB – Poly (ε–caprolactone)/Tridecyl(tetrahexyl)phosphonium bistriflamide

SBA-15 – Santa Barbara Amorphous type 15

SCF – Supercritical Fluid

$scCO_2$ – Supercritical Carbon Dioxide

SEM – Scanning Electron Microscopy

KCl – Potassium Chloride

TGA – Thermogravimetric Analysis

TIPS – Thermally Induced Phase Separation

TMEAP – N, N, N-Trimethyelethanolammonium pentanoate

VOC – Volatile Organic Compound

Geek letters

ε – Compressive strain

κ – Boltzmann's constant

σ – Compressive stress

χ_c – Degree of crystallinity

Subscripts

1 – Bottom part of the sample

This page was intentionally left in blank

1. Introduction

1.1. Polymeric foams

Polymeric foams or cellular polymers generally consist at least in two phases, a solid–polymer matrix and gaseous voids derived from a blowing agent. Other solid phase may be present into the polymeric matrix, which may be inorganic, ceramic or metal, generating a hybrid/composite material (Landrock, 1995; Lee *et al.*, 2005; Brun *et al.*, 2011). Naturally occurring foams have been known for very long time, such as sponges and corks. The development and production of the polymeric foams started in the first half of the 20th century, and its chronology is presented in Figure 1 (Lee *et al*., 2007; Lee and Scholz, 2009).

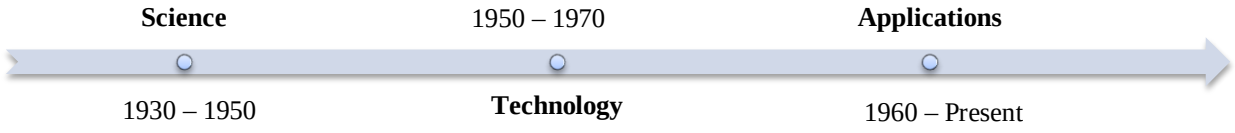

Figure 1 – Foam development timeline.

Foams can be classified using numerous criteria. They can be rigid or flexible, depending upon their glass transition temperatures are below or above the room temperature. According to the size of the foam cells, foams can be categorized by diameter of the voids as macrocellular (>100 µm), microcellular (1–100 µm), ultramicrocellular (0.1–1 µm) and nanocellular (0.1–100 µm). They can also be divided into either closed or open cell foams. In closed cell foams, the voids are not interconnected and the cavities are surrounded by complete cell wall while in open cell foams the cell walls are broken and the voids are interconnected (Lee *et al.*, 2005; Brun *et al.*, 2011; Landrock *et al.*, 1995). The applications of polymeric foams are widespread because of their high strength–to–weight ratio, excellent thermal and sound insulations properties, high energy/mass absorption, materials savings, flexibility of generating desired morphologies to meet specific applications, etc. (Zeng *et al.*, 2003; Zhai *et al.*, 2006). Polymeric foams with larger closed pore can be used in packaging, cushioning, and construction of low housing. Foams with cell size less than 10 µm are used in aerospace and automotive industries. Polymers with open cells are widely used in membranes separations, acoustic insulation, battery separations and biomedical fields such as controlled release systems and scaffolding (Bao *et al*., 2011).

Cellular polymers are usually prepared by chemical or physical foaming process, depending upon the nature of the gas formation which can be classified as physical blowing agent (PBA) and chemical blowing agent (CBA). Chemical blowing agents are compounds that produce gases due to chemical reactions and/or via thermally induced decomposition in the foaming process while physical blowing agents are non–reactive (inert) substances that gasify under foaming conditions. Typically CBA include water, azodicarbonamide, sodium bicarbonate, citric acid derivatives, etc. (Eaves, 2004; Ashida, 2007; Landrock, 1995). The PBA are usually liquids with low boiling points, such as hydrofluorocarbons, chlorofluorocarbons, hydrochlorofluorocarbons, hydrofluorocarbons, liquid carbon dioxide, C_5–hydrocarbons (Lee *et al.*, 2005; Ashida, 2007; Lee *et al*. 2007). Numerous methods have been utilized for the production of polymeric foams. The most commonly used production methods are thermally induced phase separation (TIPS), extrusion using chemical blowing agent (CBA), and casting and leaching. In the TIPS process, the foaming agent, usually a low boiling organic liquid such as pentane and hydrochlorofluorocarbons, is dissolved in the polymer which, by temperature quench, induces the phase separation and formation of porous structure. In the extrusion process, a CBA is added to the polymer and upon heating the CBA decomposes into gaseous components, resulting in the desired porous matrix. In the casting and leaching method, the polymer is dissolved in a high volatile solvent and casting the solution into a mold containing a solid porogen (usually a water soluble salts such as NaCl or KCl), which is leached out, leaving a highly porous polymeric structure (Jacobs *et al.* 2008; Jacobs *et al*., 2004; Duarte *et al.*, 2012).

All these methods, above mentioned, use environmentally hazardous compounds such as chlorofluorocarbons (CFC's), hydrochlorofluorocarbons (HCFC's), which contribute to the air pollution and generation of aqueous waste streams by the emission of harmful substances. These solvents also lead to unwanted contamination in the final polymeric foam. Furthermore, purification and drying steps are often required which can degrade thermosensitive components such as drugs, proteins and/or growth factor, thus, contributing to higher consumption of energy (Nalawade *et al*., 2006; Jacobs *et al*., 2008). Due to all these problems concerning the environment, there is a clear need to consider either solvent–free processes or alternative solvents. Recently, a number of research groups have proposed new and cleaner/greener methods to replace the conventional organic solvents. These methods include supercritical fluids (Cooper *et al.*; 2003, Duarte *et al.*, 2012; Jacobs *et al.*, 2008; Nalawade *et al.*, 2006), ionic liquids (Cooper *et al.*, 2003; Duarte *et al.*, 2012; Silv*a et al.*, 2012) and fluorous solvents *(*Cooper *et al*., 2003).

Polymeric foams reveal low mechanical strength, poor surface quality, and low thermal and dimensional stability. According to Chen *et al*., there are two approaches to solve this issue without compromising the lightweight of the polymer, (1) decrease the average cell size without decreasing the foam density or (2)use nanofillers to reinforce the polymer matrix (Chen *et al.*, 2012).

A polymer nanocomposite can be defined as a material having particles (or fillers) dispersed into a polymeric matrix, where at least one of the constituent phases has one dimension in the nanometer scale, less than 100 nm (Ajayan *et al*., 2003; Liao *et al*., 2012). The incorporation of nanoparticles in the polymeric matrix provides significant improvement in a wide variety of properties including thermal stability (Liao *et al.*, 2012; Lee *et al.*, 2005), mechanical properties (compressive strength, stiffness), fire retardance (Liao *et al.*, 2012; Jacobs *et al*., 2008; Lee *et al.*, 2005), biocompatibility and biodegradation rate (Liao *et al.*, 2012). The presence of nanoparticles acts as heterogeneous nucleation sites. The extremely fine dimensions and large surface area of nanoparticles provide a much more intimate contact between the particles, polymer matrix and gas (Zeng *et al.*, 2003). They lower the energy barrier for cell nucleation, increase the cell nucleation rate which results in high cell density with a reduced cell size (Zhai *et al.*, 2006; Jacobs *et al.*, 2008). As more bubbles start to nucleate concurrently, there is a less amount of gas available for bubble growth, leading to a reduction of cell size (Lee *et al.*, 2005).

Numerous methods have been reported for the production of nanocomposite foams including in-situ polymerization (Nalawade *et al.*, 2006), melt intercalation, solution intercalation and supercritical carbon dioxide technology (Shieh *et al.*, 2009; Liao *et al.*, 2012; Tsimpliaraki *et al.*, 2011; Salerno *et al*., 2012). The commonly used nanoparticles are clay, mostly montmorillonite (Shieh *et al.*, 2009; Zeng *et al.*, 2003), carbon nanofibers, spherical nanosilica (Zhai *et al*., 2006), nanocrystals, gold nanoparticles (Jacobs *et al*., 2008), calcium hydroxyapatite (Salerno *et al*., 2011; Mou *et al.*, 2011; Delabarde *et al.*, 2012), tricalcium phosphate (Xue *et al.*, 2009), calcium carbonate (Jiao *et al.*, 2006). Silicon–based materials have been used in numerous industries, which include electronic, building and construction (for production of glass, concrete, etc.), food industry (as preservative and thinning agents), and biomedical applications/medicine. In the past few decades, Si–based materials, especially mesoporous silicas, have been studied as carriers for drug and bioactive substances delivery systems because their extraordinary physicochemical properties, such as stable mesoporous structures, adjustable pore sizes with narrow distributions, large surface areas, large pore volumes, high biocompatibility. Their structures can be easily manipulated depending upon

the desired properties as a drug carrier. SBA–15 (Santa Barbara Amorphous type 15) is one of the most Si–based material studied in this field and it is characterized by hexagonal packed one–dimensional nanochannels (Xu *et al*., 2012; Jaganathan and Godin, 2012; Gargiulo *et al*., 2012).

Much of the research for fabrication of porous scaffolds for tissue engineering focus on poly (α–hydroxy acids), such as poly (lactic acid), poly (ε–caprolactone), poly(glycolic acid), and its copolymer poly (lactic–glycolic acid) (Liao *et al.*, 2012). Other polymers have been reported in the literature for the fabrication of porous nanocomposites including polystyrene, poly (methylmethacrylate) (Zeng *et al*., 2003) and polycarbonate (Zhai *et al.*, 2006). High porosity, proper pore size, appropriate degradation rate, biodegradability and biocompatibility are important characteristics required for this type of applications, which will be a temporary support for cell seeding and growth (Tsivintzelis *et al.,* 2007). For cell delivery and tissue ingrowth are needed scaffolds with porosity superior to 90 % and for implantation into orthopedic defects porosity less than 80 % are recommended. Pore sizes and pore interconnections greater than 200 μm are proposed for vascularization (White *et al.*, 2012).

1.2. Biodegradable polymers

The interest in biodegradable polymers is increasing over the year as well as their applications in pharmaceutical (drug, peptides and proteins delivery), medical (wound dressings, orthopedic fixation devices such as pins, rods and screws) and tissue engineering fields (scaffolds) (Takahashi *et al.*, 2012, Mishra *et al.*, 2008). Biodegradable polymers can be classified as natural or synthetic. Natural polymers include proteins (collagen, soy, fibrin, gelatin, etc.) and polysaccharides (alginate, chitosan, starch, dextran, hyaluronic acid) and derivatives. Despite their great capacity to mimic the naturally environment of certain tissues, these classes of materials have poor mechanical properties and great limitation in processability of porous structure, due to their high melting point, in the fabrication of scaffolds (Duarte *et al.*, 2012). These problems can be overcome with the employment of biodegradable synthetic polymers, which is less expensive and better processable and present the advantages of being tailored in mechanical properties and degradation kinetics depending of the nature of applications (Mishra *et al.*, 2008; Gunatillake and Adhikari, 2003). There are numerous families in these classes of polymers including polyesters, polyorthoesters, polyanhydrides, polyphosphazenes, polyamides, etc. (Liu *et al.*, 2007, Mishra *et al.*, 2008). Poly (α–hydroxy acids) are the major classes of synthetic biodegradable polymers that had

been studied by the scientific community. Polyesters such as poly (glycolic acid), poly (ε–caprolactone), poly (lactic acid), and poly (β–hydroxybutyrate valerate) have been successfully used in biomedical research and applications for their properties, structure and biological compatibility (Liu *et al.*, 2007; Gunatillake and Adhikari, 2003). Among this class of polymer, poly (ε–caprolactone) is one of the most studied.

Poly (ε–caprolactone) (PCL) is semicrystalline, hydrophobic and Food and Drug Administration (FDA) approved biodegradable aliphatic polyester for in specific applications such as drug delivery systems (Rai *et al.*, 2005; Wiria *et al.*, 2007; Woodruff and Hutmacher, 2010; Sant *et al.*, 2011). It has a glass transition temperature (T_g) of –60 °C and melting point ranging between 59–64 °C, depending upon its crystalline nature (Karimi *et al.*, 2012, Sinha *et al.*, 2004, Woodruff and Hutmacher, 2010). PCL is synthesized by the ring–opening polymerization of the cyclic monomer ε–caprolactone (Gunatillake and Adhikari, 2003, Takahashi *et al.*, 2012). PCL has flexible mechanical properties, the elastic modulus is about 0.3 GPa and it can be stretched to a strain about 0.3 (~ 30 % elongation) at a yielding stress about 11 MPa. Its physical, chemical and mechanical properties can be modified efficiently by co–polymerization or blending with other materials such as lactides, glycolides, calcium hydroxyapatite and silica that are suitable for biomedical applications (scaffolds and soft/hard tissues repairing) (Dash and Konkimalla, 2012; Liu, 2007) and drug delivery (Kelly *et al.*, 2013). PCL can be degraded by hydrolysis to produce 6–hydroxycaproic acid which is metabolized via citric acid cycle (Mishra *et al.*, 2008; Liu, 2007; Gunatillake and Adhikari, 2003). PCL degrades at much slower rates than polyglycolide, poly (D, L–lactide) and its copolymers and tests *in vivo* have shown that its takes 2–4 years to degrade completely, which makes this class of polymers suitable for long term applications. Previous studies have shown that PCL reveals low toxicity and do not significantly influence the function of host cells and tissues (Woodruff and Hutmacher, 2010; Liu, 2007). The chemical structure of PCL is shown in Figure 2.

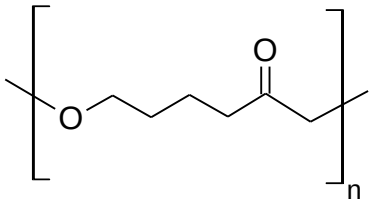

Figure 2 – Chemical structure of poly (ε-caprolactone).

1.3. Green solvents

Supercritical fluid is an environmental friendly and versatile alternative technique to conventional manufacturing/processing methods of polymer foaming (Nalawade *et al.*, 2006; Jenkins *et al.*, 2006; Tsimpliaraki *et al.*, 2011) and is currently being used as "green" solvent for a range of polymer applications, including polymer synthesis, powder coating, dyeing, impregnation, purification, extraction, preparation of drug delivery systems, composites formation and used as blowing agent to produce porous polymeric materials (Quirk *et al.*, 2004; Nalawade *et al.*, 2006; Liao *et al.*, 2012; Davies *et al.*, 2008). A supercritical fluid (SCF) can be defined as a substance which its critical temperature (T_c) and critical pressure (P_c) are exceeded (Liao *et al.*, 2012; Nalawade *et al.*, 2006; Anastas, 2010). The pressure–temperature phase diagram for a pure fluid it is well–known and it can be found in the literature (Gopalan *et al.*, 2003; York *et al.*, 2004; Anastas, 2010).

Carbon dioxide (CO_2) is by far the most commonly used SCF due to its unique properties. It is nontoxic, nonflammable, noncorrosive, relatively inexpensive, once it is generated in large quantities as a by–product in numerous chemical and biochemical industries such as ammonia, hydrogen and ethanol also in electrical power plants in fossil fuels burning. It is also readily available in high purity and it is "generally recognized as safe" (GRAS) solvent. Compared with others substances, its supercritical conditions are easily achieved (T_c = 31.1 °C and P_c = 7.38 MPa). Supercritical carbon dioxide ($scCO_2$) exhibits intermediate properties of both gaseous and liquid states. The special combination of liquid–like density which provides high solvent power with gas–like viscosity which provides high diffusion rates makes it an excellent solvent for various applications, including polymer synthesis and processing (Kazarian, 2000; Xu *et al.*, 2004; Nalawade *et al.*, 2006; Quirk *et al.*, 2006; Anastas, 2010, Yañes *et al.*, 2011; White *et al.*, 2012). The solvent properties (diffusivity, viscosity, solvent strength and polarity) of CO_2 can be easily adjusted over a wide range by varying the pressure and/or temperature. The presence of $scCO_2$ can swell and plasticize many polymers (amorphous and semi–crystalline), lowering their glass transition temperature (T_g), viscosity, interfacial tension and increasing the chain flexibility consequence of an increasing in the free volume fraction (White *et al.*, 2012; Jenkins *et al.*, 2006; Nalawade *et al.*, 2006; Anastas, 2010). $scCO_2$ can also lower the melting temperature of semi–crystalline polymers (Kiran, 2009; York *et al.*, 2004). $scCO_2$ penetrates more easily and deeper into polymers compared with liquid solvents (Goodship and Ogur, 2004; Yañes *et al.*, 2011). Furthermore, its low critical temperature makes it very attractive for processing

thermosensitive compounds, such as pharmaceutical drugs and other bioactive compounds (Liao *et al.*, 2012). It can be removed from polymeric matrix just by a simple depressurization, as being a gas under ambient conditions, and it can be recovered and reused, therefore, does not contribute to the greenhouse effect (Nalawade *et al.*, 2006; Liao *et al.*, 2012). scCO_2 is good solvent for most non–polar (and some polar) low molecular substances, and it is poor solvent for most high molecular weight polymers, except amorphous fluoropolymers and silicones (Davies *et al.*, 2008). Amorphous polymers behave differently to semi–crystalline materials. The CO_2 is absorbed only into amorphous regions and not in crystalline one. For this reason greater amount of plasticization is found to occur (Goodship and Ogur, 2004).

The interest in a novel class of material, which goes by the name of ionic liquids, has increased exponentially in the recent years in both academic and industrial field mainly due to their exceptional properties, such as non–flammability, high thermal and chemical stability, negligible vapor pressure, high ionic conductivity, ease recovery, and high solvating capacity for both polar and nonpolar compounds (Zhao, 2006; Ueki and Watanabe, 2008; Chen *et al.*, 2013). Ionic liquids (ILs) can be defined as organic salts that are liquids at low temperature (usually < 100 °C) and it is constituted by a combination between an anion and a cation. ILs are considered to be green alternative for the replacement of volatile organic compounds (VOC's) in a wide variety of chemical and biochemical process (Mohammad and Inamuddin, 2012; Chen *et al.*, 2013). They have been successful implemented as solvents in bioprocessing (separation and purification processes), chemical synthesis, organic catalysis, polymerization, electrochemistry, extraction processes, nanotechnology and gas separations. ILs have also shown many other innovative applications, including heat transfer fluids, lubricants, azeotrope–breaking liquids, stationary phases for chromatography, matrices for mass spectrometry, supports for immobilization of enzymes, plasticizers, and so on (Zhao *et al.*, 2006; Tomé *et al.*, 2011; Chen *et al.*, 2013).

ILs have been designated as "designer solvents", their physical–chemical properties, such as viscosity, density, hydrophilicity, polarity, acid–basic character can be tailored for a range of applications by varying the structures of cations or anions or their combinations (Zhao *et al.*, 2006; Ueki *et al.*, 2008; Mohammad and Inamuddin, 2012). The chemical structures of the two ILs used in this work are presented in Figure 3

.

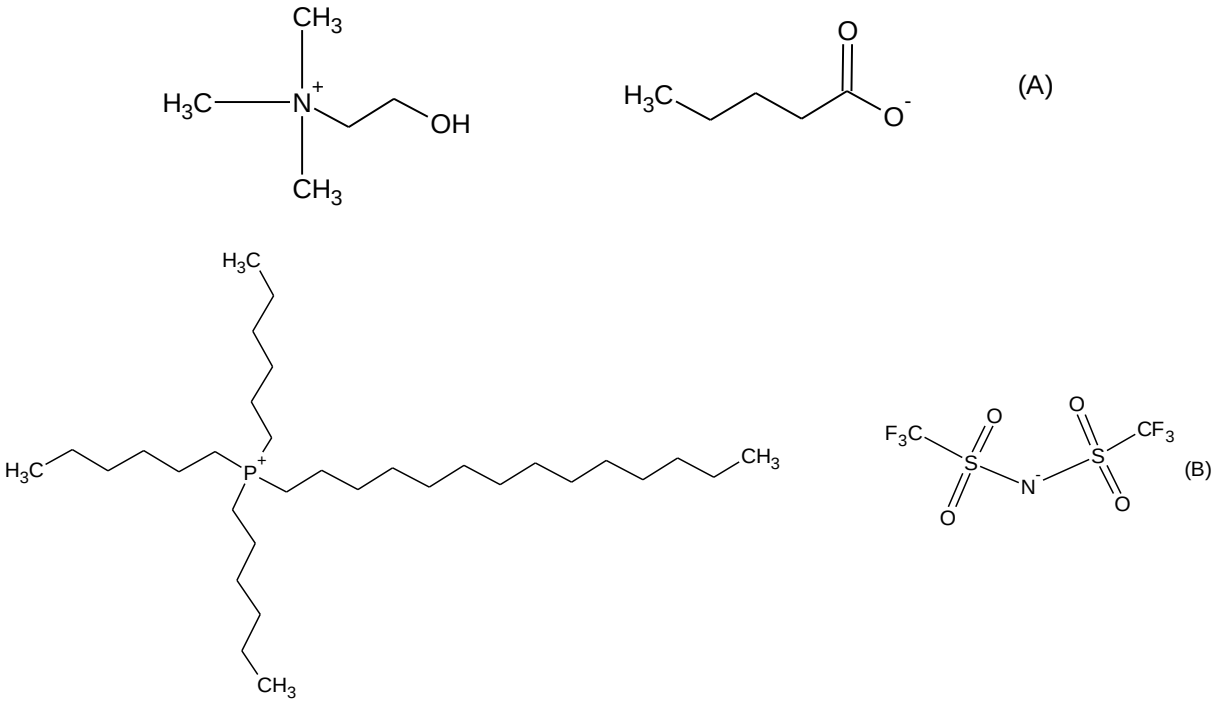

Figure 3 – Chemical structure of (A) N, N, N – trimethylethanolammonium pentanoate and (B) tetradecyl(trihexyl) phosphonium bistriflamide.

Other types of solvents commonly used due to their favorable properties include glycofurol (GF) and isosorbide dimethyl ether (ISODME). GF and ISODME are water–miscible, non–volatile and non–toxic solvents used in parenteral pharmaceutical formulations (intravenous or intramuscular injectable) and in others therapeutic applications such as skin depigmentation, creams and ointments and intranasal doses of benzodiazepine (Boongird *et al.*, 2011; Tran *et al.*, 2012). Glycofurol has high biocompatibility (Boongird *et al.*, 2011) and an LD_{50} in mouse IV of 3.5 $mL \cdot kg^{-1}$ body weight (Row*e et al.*, 2009) and it have been used as a polymer solvent for the preparation of microspheres (Allhenn and Lamprecht, 2011). Their chemical structures are shown in Figure 4.

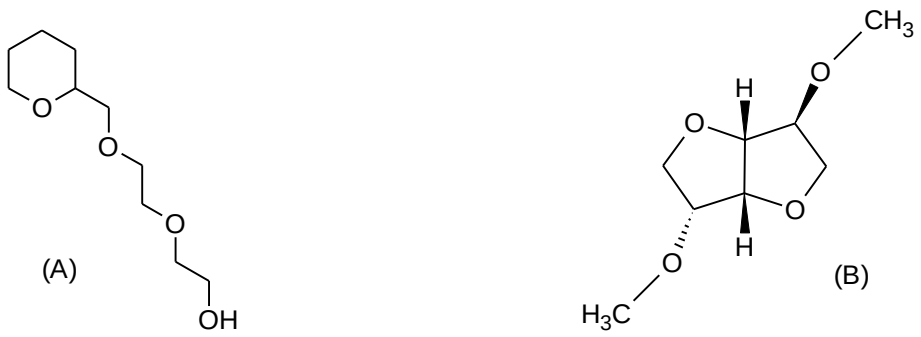

Figure 4 – Chemical structure of (A) glycofurol and (B) ISODME**.**

1.4. Supercritical carbon dioxide foaming process

Supercritical CO_2 foaming process is an established and well documented method and it can be divided into three steps. In the first step, the polymer is saturated with $scCO_2$ at constant pressure and temperature leading to a formation of a homogenous solution composed by CO_2 and polymer. Secondly, once the system reaches the equilibrium, the phase separation can be induced by a thermodynamic instability which is usually a temperature increase (temperature soak method) or a pressure decrease (pressure quench method) resulting in cell nucleation. Finally, growth of these cells, coalescence and expansion, to form the polymeric foam (Karimi *et al.*, 2012; White *et al.*, 2012; Liao *et al*., 2012). All these steps are schematically represented in Figure 5.

During the saturation step, the glass transition and melting temperatures of polymer are lowered due to the interactions between polymer segments and the gas molecules (Gualandi *et al.*, 2010; Karimi *et al.*, 2012). As a result, the density and the viscosity of the polymer is reduced and the mobility of polymer chains is increased (Liao *et al*., 2012). With the pressure reduction, the concentration of the CO_2 also decreases leading to an increasing in T_g of polymer and vitrification occurs with the porous structured fixed in the glassy state (Jacobs *et al.*, 2008; White *et al.*, 2012; Liao *et al*., 2012).

The final polymeric foam morphology and structure depends mainly in the foaming conditions, such as, pressure, temperature, saturation time and depressurization rate (Tsimpliaraki *et al.*, 2011; Chen *et al.*, 2012; Liao *et al.*, 2012).

Nucleation and growth of the foam cells

The study of cell nucleation and growth is crucial to understand the mechanism dominating cellular foaming as well the effect of the processing parameters on the final cell structures of the foam (Sun *et al*., 2004). As mentioned above, the nucleation of bubbles/cells can be either homogeneous, heterogeneous or the combination of these two mechanisms (Colton and Suh, 1987; Lee and Scholz, 2009). Homogeneous nucleation occurs when cells form in a single phase system while heterogeneous nucleation, where are at least two phases due to the presence of fine particles/fillers, the cells will nucleate at the interface between these two phases (Colton, 1987).

Numerous methods have been developed to describe the nucleation and growth of cells in the foaming process. More detailed information can be found in the literature (Colton and Suh, 1987). Colton developed a method based in classical nucleation theory, and according to this author, the rate of homogeneous nucleation N_{homo} is given by the equation (1) (Colton and Suh, 1987)

$$N_{homo} = C_0 f_0 exp\left(\frac{-\Delta G_{homo}}{\kappa T}\right) \quad (1)$$

Where C_0 is the concentration of gas molecules, f_0 is the frequency factor of the gas molecules joining the nucleus, κ is the Boltzmann's constant and T is the absolute temperature. The term ΔG_{homo} is the Gibbs free energy (activation energy barrier) for homogeneous nucleation.

In heterogeneous nucleation, there is a slightly change in the classical equation and the rate of heterogeneous nucleation is given by the equation (2).

$$N_{het} = C_1 f_1 exp\left(\frac{-\Delta G_{het}}{\kappa T}\right) \quad (2)$$

Where C_1 is the concentration of the heterogeneous nucleation sites, f_1 is the frequency factor of the gas molecules for heterogeneous nucleation joining the nucleus. The term ΔG_{het} is the Gibbs free energy (activation energy barrier) for heterogeneous nucleation.

The presence of heterogeneous nucleation sites does not exclude the homogeneous nucleation. Homogeneous nucleation can still occur in regions of material that heterogeneous sites do not exist and if the activation energy barrier can be overcome. In this instance, heterogeneous nucleation will be favored over the homogeneous due to its lower energy barrier and consequently heterogeneous bubbles will nucleate before the homogeneous ones (Colton and Suh, 1987). The nucleation rate of the mixed nucleation can be obtained by combining the, where N'_{homo} is the homogeneous nucleation rate in the presence of heterogeneous nucleation.

$$N = N'_{homo} + N_{het} \quad (3)$$

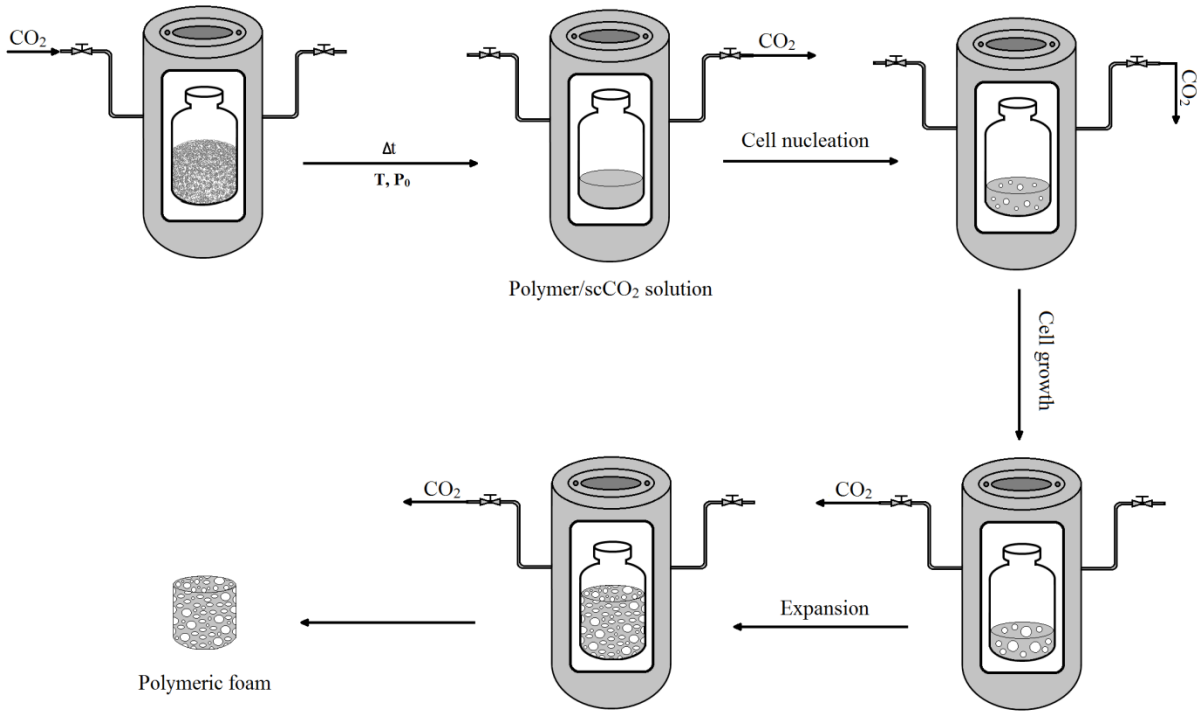

Figure 5 – Schematic representation of $scCO_2$ foaming process.

1.5 Applications in (bio) medical and pharmaceutical fields

Porous biodegradable polymers matrices are widely used in various areas including in pharmaceutical applications (drug delivery devices) (Takahashi *et al.*, 2012), biomedical applications (tissue engineering scaffolds and implants for organ replacement) (Léonard *et al.*, 2008; Takahashi *et al.*, 2012; Salerno *et al.*, 2012) and regenerative medicine (Polini *et al.*, 2011; Takahashi *et al.*, 2012).

The use of scaffold biomaterial is one of the most promising approaches in tissue engineering area. The major goal of tissue engineering is to repair or regenerate an injured or lost tissue (Rinki *et al.*, 2009; Reverchon and Cardea, 2012). The scaffolds serve as temporary artificial matrix for cells to attach, migrate, proliferate and differentiate and also used to delivery growth factors or other bioactive species to the growing cells (Singh *et al.*, 2004; Liao *et al.*, 2012).

In biomedical applications, the porous structures matrices are very important because they act as a size selective membrane permitting just the nutrients and wastes to permeate avoiding the migration of unwanted cells or tissues to the healing site (Singh *et al.*, 2004).

An ideal scaffold for tissue engineering and guided tissue regeneration must meet some fundamentals requirements including highly regular and three dimensional (3D) reproducible structure, high porosity, suitable pore size which depends on the specific tissue to be replaced, good biocompatibility, nontoxicity, biodegradability, tuned degradation rate, adequate mechanical properties capable to maintain the predesign structure and support the specific loading applied to the original tissue. The pore interconnectivity and the permeability of the scaffolds play an important role, influencing the diffusion of nutrients, removal of metabolic wastes, i.e., preventing the migration of undesirable cells and tissues to the healing site allowing only the nutrients and waste to permeate, and the promotion of blood vessel and bone tissue ingrowth (Rinki *et al*., 2009; Reverchon and Cardea, 2012).

Previous studies reveal that the success of regeneration of certain cells can be influenced by specific geometric parameters (Jenkins *et al*., 2006). According to the values reported in the literature, the optimal pore size value for construct vascularization is approximately 5 µm and the ones to allow cell and tissue ingrowth are from 200 to 400 µm (Salerno *et al.*, 2012). For cell delivery and tissue ingrowth are needed scaffolds with porosity superior to 90 % and for implantation into orthopedic defects porosity less than 80 % are recommended (White *et al.*, 2012). Although, others authors reported that pore size ranging from 100 to 500 µm are required to allow vascularization and tissue ingrowth (Fanovich *et al*., 2013). Micropores and mesopores are also required for fast degradability and efficient loading, transport and release of bioactive compounds (de Matos *et al*., 2013). Material surface roughness is another important factor because they can enhance cell adhesion and growth (Reverchon *et al*., 2008)

Objectives

This work focused in the processing, characterization of PCL/SBA–15 composite biomaterials with greener solvents such as ionic liquids, glycofurol or isosorbide dimethyl ether using supercritical carbon dioxide foaming process, a clean and environmentally friendly technology, and the study of the effects of these additives on the morphology, thermal and mechanical properties of the final foams. The ionic liquids used was N, N, N–trimethylethanolammonium pentanoate and tetradecyl(trihexyl) phosphonium bistriflamide ($[P_{6,6,6,14}][NTf_2]$). In this work the desired temperature and pressure were 40 °C and 20 MPa, respectively. The soaking time was 2 hours and the depressurization rate was 0.37 $L_{CO2}\cdot min^{-1}$.

2. Materials and Methods

2.1. Materials/Chemicals

PCL (CAS [24980–41–4]), in pellet form, with a number average molecular weight (M_n) of 45000 $g \cdot mol^{-1}$, glycofurol (tetraglycol CAS [31692–85–0]), isosorbide dimethyl ether (CAS [5306–85–4]), methanol G.C. (CAS [67–56–1], purity >= 99.8 %) were obtained from Sigma–Aldrich. Acetone (CAS [67–64–1], purity min 99.5 %) was acquired from ACS Basic Scarlau, Spain. N, N, N–Trimethylethanolammonium pentanoate (purity > 95 %) was provided by Iolitec. Silica mesoporous SBA–15 type (average BJH framework pore diameter 8.5 nm, total pore volume 0.93 $cm^3 \cdot g^{-1}$, surface area 718 $m^2 \cdot g^{-1}$) were supplied by Claytec (USA). Tetradecyl(trihexyl) phosphonium bistriflamide (purity > 98 %) was obtained from Cytec Industries (France). Carbon dioxide was purchased from Praxair (Spain) with a stated purity of 99.998 %, v/v. All reagents were used as received, except PCL. PCL was powderized in order to increase the superficial area and facilitate the physical mixture and the interaction with $scCO_2$.

2.2. Methods

2.2.1. Preparation of PCL in the powder form

Approximately 12 g of PCL was dissolved in ~200 mL of acetone at room temperature under stirring. After complete solubilization, the solution PCL–acetone was precipitated by adding slowly, drop by drop, ~20 mL of methanol and later 20 mL of water. Then the suspension was left for sedimentation/decantation. Later the phase separation, the supernatant was removed and the precipitated poured in petri dishes at room temperature to dry and remove the solvent. PCL powder was sieved using a test sieve (width 0.500 mm, Retsch 5657 Haan w., Germany) to homogenize the particle size distribution, and then stored in proper flasks.

2.2.2. Foam production using Supercritical Carbon Dioxide Technology

Prior to the foaming process, 1.2 g of PCL and SBA–15 (10 wt. % or 30 wt. %) were manually mixed inside a glass flask until complete homogenization and then the proper additive (98 %, molar) was added.

Porous structures samples of pure and nanocomposite PCL were prepared with the batch foaming technique using supercritical carbon dioxide as foaming agent. The experimental apparatus, presented in Figure 6, consists in a high–pressure liquid pump, high pressure vessel (23 cm^3), temperature–controlled water bath (Thermoscientific, Haake AC 150), a manometer (Lab DMM, REP transducer), a mass flow meter (series GFM, Dwyer), a magnetic stirrer plate to homogenize the high pressure mixture, high pressure valves and fittings used to connect the system (High Pressure Equipment Company, Erie, USA).

Firstly, the intended materials, previously prepared, were placed inside the sealed high pressure cell which was immersed into the thermostatic water bath at the desired temperature (heated by a controller) and then filled with CO_2 until the operational pressure was attained. The system was maintained at constant temperature and pressure over a given period of time (soak time), which is a period of time that was assumed to be sufficient for the saturation of the nanocomposite polymeric matrix, according to the preliminary and previously studies that were made (de Matos *et al.*, 2013). After this stage, the high pressure cell was depressurized to ambient pressure at constant depressurization flow rate. During this stage the temperature was kept constant. In this work the desired temperature and pressure were 40 °C and 20 MPa, respectively. The soaking time was 2 hours and the depressurization rate was 0.37 $L_{CO2}{\cdot}min^{-1}$. All the assays were performed in duplicate.

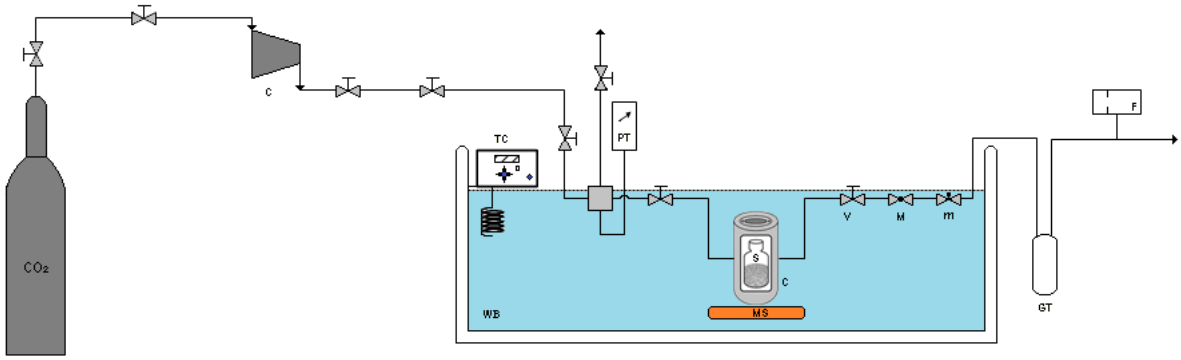

Figure 6 – Schematic diagram of the experimental apparatus. CO_2 Cylinder; V – valve; C – compressor; TC – temperature controller; WB – water bath; PT – pressure transducer; C – high pressure cell; S – sample; M – macrometric valve; m – micrometric valve; GT – glass trap; F – mass flow meter.

2.3. Characterization methods

2.3.1. Physical characterization

The infrared spectra of the pure and composite material were obtained using a Fourier Transform Infrared (FTIR) spectrometer (Jasco FT/IR–4200, Japan) using the attenuated total reflectance (ATR) system with a resolution of 4 cm^{-1} at 256 scans, in the spectral region from 4000 to 500 cm^{-1} in order to identify the functional groups of the various substance used.

The mean pore diameter, pore volume and surface area were determined by nitrogen adsorption using a ASAP 2000 Micromeritics equipment (model 20Q–34001–01). Surface area and mean pore diameter were calculated by the Brunauer, Emmet and Teller (BET) method and the pore volume by the Barret, Joyner and Halenda (BJH) method.

Helium picnometry (Quanta–Chrome, MPY–2) was the technique used to determine the real density of the foams. The results presented are the average and standard deviation of three samples.

2.3.2. Morphological analysis

The morphologies of the foamed samples were characterized by scanning electron microscopy (SEM) using a scanning microscope (Jeol JSM–5310, Japan) with an operating voltage of 10 kilovolts. The mean pore size of the samples was evaluated from the SEM images using Gwyddion software version 2.31. Samples were cryofractured on liquid nitrogen. This decision was made based on the fact that when a fracture meets a void or a cell, it will propagate along its weakest axis and therefore, it provide a maximum projected surface area of the cells (Gosselin and Rodrigue, 2005). Then the samples were sputter–coated with gold for 25 seconds (~150 nm of film thickness) before being observed by the microscope.

A scanning microscope (Phenton world, Pro X) equipped with EDS was also used.

2.3.3. Thermal analysis

Thermogravimetric analyses were carried out using a TGA analyzer (TA Instruments, model Q500). Analyses were performed on samples weighing 7–8 mg from 25 to 600 °C at a heating rate of 10 °C·min^{-1}, under nitrogen flow atmosphere. The degradation temperature (T_d) and mass loss of the used materials was determined using TA instruments universal software.

The melting temperatures, glass transition temperatures, enthalpies of fusion and crystallinity of the foamed samples were measured using DSC calorimeter (TA Instruments, model Q100).

Differential scanning calorimetry measurements were performed using DSC calorimeter (TA Instruments, model Q100). Samples weighing 7–8 mg were sealed in aluminum pans and heated at a constant rate of 10 °C·min^{-1} over a temperature range from –80 to 300 °C.

The degree of crystallinity of the polymer and nanocomposites is defined as the following equation (Kong and Hay, 2002; Fukushima *et al*., 2009; Delabarde *et al*., 2012):

$$\chi_c(\%) = \frac{\Delta H_f(T_m)}{\Delta H_f^0(T_m^0) \times \left(1 - \frac{\%wt_{SBA-15}}{100}\right)} \times 100 \quad (4)$$

Where $\Delta H_f(T_m)$ is the experimental enthalpy of fusion obtained from the DSC scan measured at the melting point, T_m and ΔH_f^0 (T_m^0) is the enthalpy of fusion of 100 % crystalline polymer measured at the equilibrium point, T_m^0 and $\%wt_{SBA-15}$ is the weight percentage of the silica nanoparticles. The value of the ΔH_f^0 of 100 % crystalline PCL is reported in the literature to be 139.5 J·g^{-1}(Chasin and Langer, 1990; Jenkins *et al.*, 2006). The analyses were performed in duplicate.

2.3.4. Dynamical Mechanical Analysis

Dynamical mechanical analysis is an important versatile technique widely used to determine the storage modulus, E', the loss moduli, E'' and the damping parameters, tan δ, by the application of an oscillating force to a sample. The damping parameter is defined as the ratio between loss and storage modulus (Menard, 2008).

$$tan\,\delta = \frac{E''}{E'} \quad (5)$$

This technique can be used to determine more accurately the glass transition temperature (T_g) compared with the DSC technique due to its high sensitiveness (Menard, 2008).

The T_g, according to the literature, it can be obtained by the maximum value of E'' or by the tan δ peak, depending upon the authors (Martínez–Hernández *et al.*, 2007). In this work, the T_g of the samples were obtained by the maximum value of E''.

The glass transition temperature was measured using a dynamical mechanical analyzer (Netzsch, model 242) operating in the compression mode. Samples were cut in cylindrical shape with a diameter varying from 12–16 mm and thickness from 2–5 mm. The test was

performed from –150 to 20 °C at a heating rate of 10 °C·min^{-1}, and three different frequencies were used (1, 5 and 10 Hz). The results presented are the average and standard deviation of two samples.

The compressive properties of the foam were examined using a TA.TX Express Enhanced texture analyzer (Stable Micro Systems Company) equipped with 5 kg of load cell capacity. Samples in circular shapes with a diameter ranging from 16–18 mm and thickness from 9–10 mm were compressed to a total of 25 % using a compression rate of 1 mm·s^{-1}. The compression tests were performed at room temperature and the force was applied vertically down, in the direction of foaming, how is presented in the Figure 7. This analyses were performed in duplicate.

The Young's Modulus (linear elastic modulus, E) was obtained from linear regression on the elastic region of the strain–stress curve. The compressive strength was the stress produced at 25 % strain (ultimate stress) (Salerno *et al*., 2010; White *et al*., 2012). The compressive stress, σ, was calculated by the equation (6).

$$\sigma = \frac{F}{A} \tag{6}$$

Where F is the applied force (N) on the sample and A the initial cross section area (m^2). The compressive strain, ε, can be defined as the ratio of total deformation (Δh) to the initial height of the material (h_0).

$$\varepsilon = 1 - \frac{h_0 - h}{h_0} = 1 - \frac{\Delta h}{h_0} \tag{7}$$

(A)

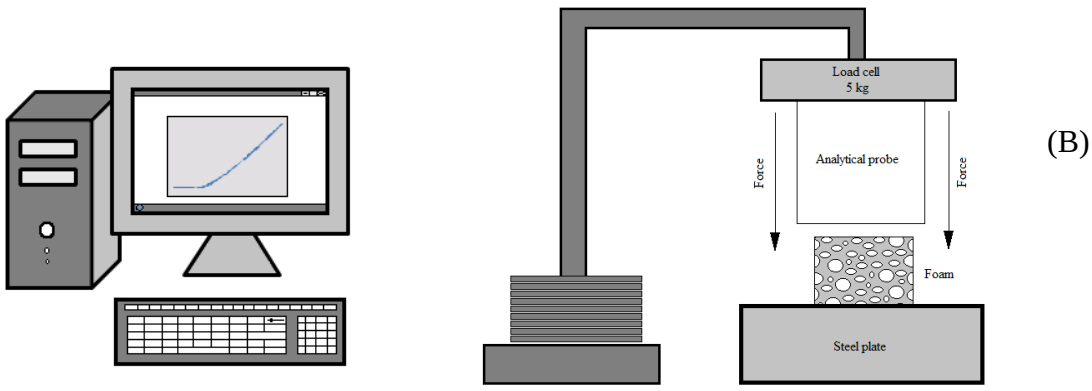

(B)

Figure 7 – Experimental apparatus for compression test; (A) computer and (B) texture analyzer equipment.

2.3.6. Cytotoxicity studies

Cell viability were assessed by Lactate dehydrogenase (LDH) assay using redox reactions in SAOS-2 human osteogenic sarcoma cells (HTB–85, LGD Standards, ATCC, Manassas, VA) according to the direct contact test ISO 10993–5:1999 standard (Puga *et al.*, 2012).

The cells were cultured in Dulbecco's Modified Eagles's Medium (DMEM, Sigma-Aldrich) F12-HAM with phenol red supplemented with 10 % Fetal Bovine Serum (FBS) and 1 % penicillin/streptomycin. After reaching the confluence, cells were placed in 24–well culture plates (2×10^5 cells per well) and allowed to adhere overnight. Then, 0.5 mL of the supernatant of each well was removed and the materials were introduced to the wells, all foamed samples (~50 mg) and liquids materials (1 and 5 %, v/v) were sterilized with ultraviolet light for 30 minutes and the plates were incubated at 37 °C, 5 % CO_2 and 90 % of relative humidity.

After 24 and 72 hours of incubation, aliquots were transferred into 96 well plates, and further analysis of the absorbance at 490 nm in an ELISA microplate reader (BioRad, Model 680) was preformed according to the manufacturer instructions. Culture medium, cells in culture medium and cells in culture medium with lysis factor were used as blank, negative control and positive control, respectively, in each plate. The viability (%) was estimated by the equation (8).

$$Viability\ (\%) = 100 - \left[\frac{\left(Abs_{sample} - Abs_{C^-}\right)}{\left(Abs_{C^+} - Abs_{C^-}\right)} \times 100\right] \quad (8)$$

Where Abs_{sample} is the absorbance of the sample, Abs_{C}^{-} is the absorbance of the negative control and Abs_{C}^{+} is the absorbance of the positive control.

The cytotoxicity and the adsorption tests were performed by Maria de Matos under supervision of Dr. Carmen Alvarez–Lonrenzo, Department of Pharmacy and Pharmaceutical Technology of University of Santiago de Compostela.

3. Results and discussion

3.1. Morphological characterization

3.1. 1. Macroscopic analysis

The effects of the various additives and silica nanoparticles on the final morphologies and in the mechanical properties of the processed foams were investigated.

Macroscopic visualization of all the processed samples is illustrated in Figure 8. From these images, it is evident that the morphology of the foams obtained for the pure processed PCL and its composites was clearly different.

Adding the solvents to the polymeric matrix, the pores diameter appeared to decrease for all samples except for PG composite which appeared to have larger pores diameter, as shown in the Figure 8. This difference may be due to solubility of $scCO_2$ in the solution (polymer–additive). According to Karimi and coworkers, smaller pore size and higher cell density are obtained when more gas is dissolved into a polymer (Karimi *et al.*, 2012).

The incorporation of SBA–15 10 wt. % into the matrix slightly increased the height of the samples (for the same mass of polymer), probably due to higher porosity of the produced samples. Opposite results were found when SBA–15 30 wt. % was added, which the height decreased.

For the PCL/SBA–15 30 wt. %/additives composites, the foams were not very consistent (slightly brittle) mainly in the external part, probably due to high amount of silica nanoparticles.

Comparing PS30 composite with the ones which had the additives, it was clear the change in their morphologies. Adding the additives the pore size of the voids increased. It noticeable, as can be observed in Figure 8, that the pore size distribution was irregular.

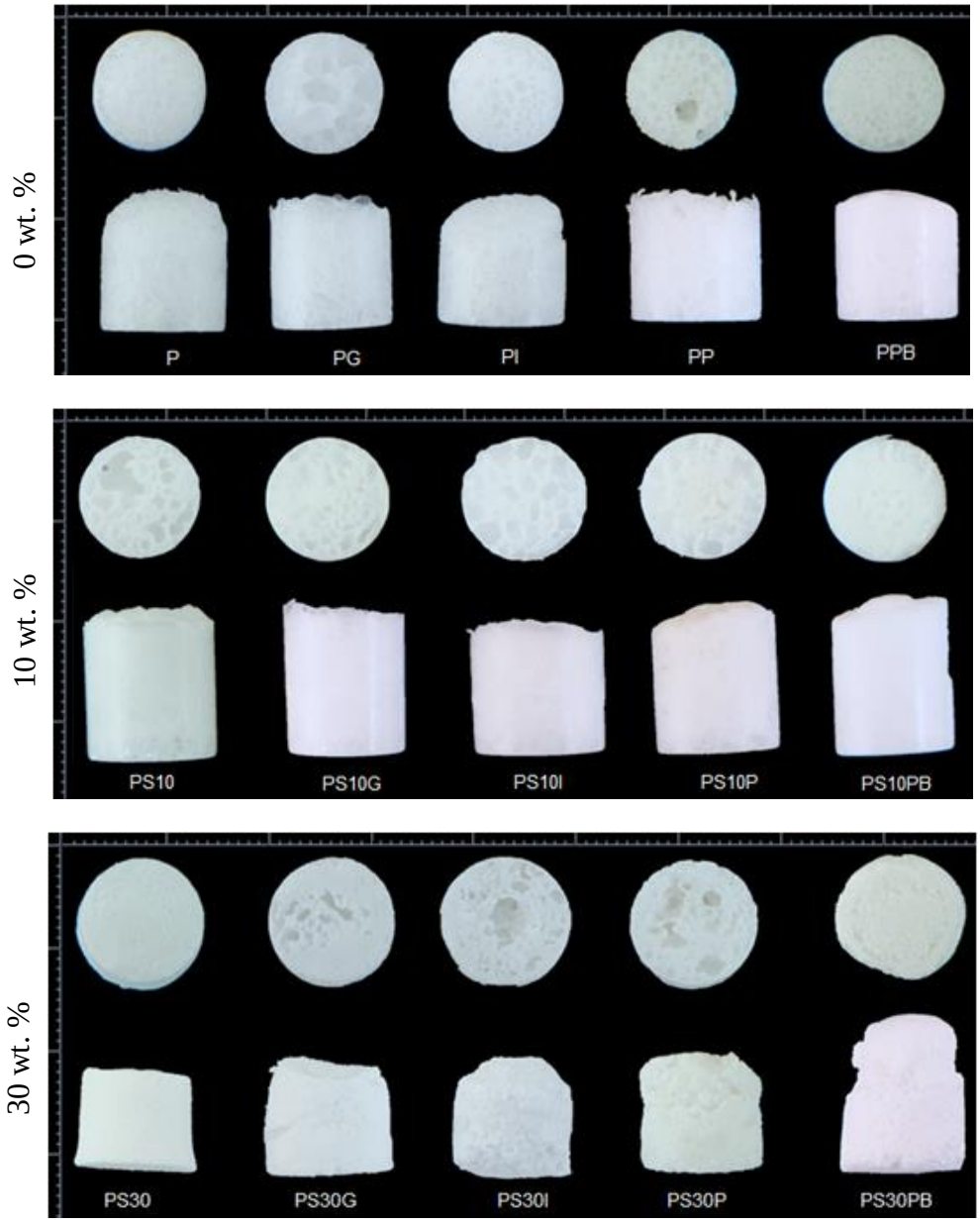

Figure 8 – Digital images (cross section (top) and side view (bottom)) of pure and composite samples obtained from the $scCO_2$ foaming process after 2 h, 20 MPa, 40 °C and 0.37 $L_{CO2} \cdot min^{-1}$.

It was also made a formulation combining PCL/Glycofurol/Phosphonium bistriflamide, PCL/Isosorbide dimethyl ether/Phosphonium bistriflamide, respectively, and the same formulation comprising SBA–15 10 wt. %. Figure 9 shows the digital images of the foams obtained by $scCO_2$ foaming process.

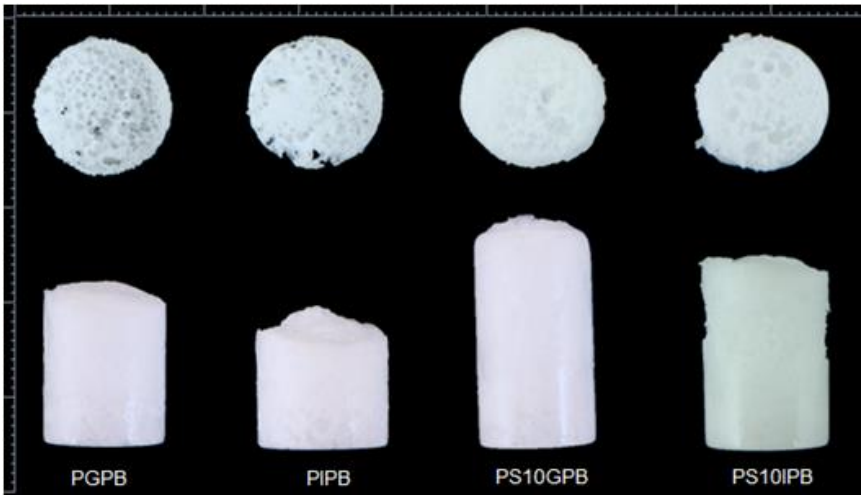

Figure 9 – Optical images (cross section (top) and side view (bottom)) of the mixture of two additives prepared by $scCO_2$ foaming process for 2 h, 20 MPa, 40 °C and 0.37 $L_{CO2} \cdot min^{-1}$.

PGPB and PIPB exhibited lower pore size and more regular pore size distribution compared with the ones with just a single additive probably due to their high $scCO_2$ solubility.

The incorporation of the silica nanoparticles (SBA–15) in the polymeric matrix induced an increase on the height of the samples, possibly due to an increase in the porosity of the samples. Between all processed samples, PS10GPB composite was the one which presented higher sample volume/height.

In all formulations, except those incorporating 30 wt. % of Si NPs, there was a formation of a thin skin around the surface of the porous composites. This effect has been described in the literature as very common in the $scCO_2$ foaming process and was attributed to the rapid diffusion of the dissolved fluid from the samples borders (Jacobs *et al*., 2008; Tsimpliaraki *et al*., 2011).

These results revealed that the influence of the additives and the nanoparticles on the morphology of the final porous structures was very significant.

A more detailed study of the final morphology of the produced foams was evaluated using a scanning electron microscope.

3.1.2. Scanning Electron Microscopy (SEM)

The morphological study of the processed samples was examined by SEM. The influence of the CO_2, additives and SBA–15 nanoparticles on the final structure of processed PCL is illustrated in Figure 10.

As can be observed in the Figure 10, the porous character samples were evident for almost all processed samples. It is clear that large pores diameter and heterogeneous pore size

distributions were obtained for almost all cases. In some cases, particularly for the composites comprising 30 wt. % of nanoparticles, smaller pores were obtained and extended all over the foam structure.

As it can be observed in Figure 10, the morphology of the processed samples was strongly dependent upon the additive and the amount of Si NPs used. Different foams morphologies were obtained by varying the additives and the Si NPs.

From the SEM images analysis, which results are listed in Table 1, it was observed that the processed PCL exhibited extremely large mean pore diameter 1606 µm.

The addition of the additives to the polymeric matrix resulted in a decrease in the pores diameter for all processed samples except for PG composite which increased to 1792 µm. This result is the same found in the macroscopic analysis.

Generally, the mean pore diameter decreased with the increase of the amount of Si NPs. In the samples containing small amount of Si NPs (10 wt. %) the mean pore diameter ranged from 194 to 1341 µm. The composite materials incorporating 30 wt. % of Si NPs showed mean pore diameter ranging from 117 to 1515 µm. The effect of the nanoparticles on the morphology of the foams has been discussed by several authors. Similar results were reported by Tsimpliaraki *et al*. in the foaming of PDLLA with clay via $scCO_2$ process (Tsimpliaraki *et al*., 2011). The same effect was observed by Zhai *et al*. who foamed polycarbonate/nanosilica using $scCO_2$ as foaming agent (Zhai *et al*., 2006).

As mentioned above (in the introduction section), the presence of inorganic particles within the polymeric matrix affect the foaming process, favoring heterogeneous nucleation. The nanoparticles act as nucleating sites, providing more intimate contact between particles, polymer and gas lowering the energy barrier for cell nucleation, thus increasing the nucleation rate and resulting in pores with smaller diameter (Zhai *et al.*, 2006; Jacobs *et al.*, 2008).

It is very clear that the addition of the different additives to the polymeric matrix had significant impact in the final structure of the samples, as it can be observed in Figure 10 and Figure 11, respectively.

PS10GPB and PS10IPB composites (samples incorporating Si NPs 10 wt. % and the mixture of two additives) showed more regular pore size distribution with mean pore diameter varying between 347 and 794 µm and also the pores seemed to be interconnected, however none appropriate technique was used in this work to confirm this finding.

Table 1 – Results of morphological analysis of SEM images obtained $scCO_2$ foaming process for 2 h, 20 MPa, 40 °C and 0.37 $L_{CO2} \cdot min^{-1}$.

Sample	Mean Pore diameter, µm
PCL	1606
PG	1792
PI	640–1137
PP	1671
PPB	805
PS10	194–567
PS10G	723–1194
PS10I	1341
PS10P	491–848
PS10PB	779–1080
PS30	117–224
PS30G	223–816
PS30I	224–505
PS30P	816–1515
PS30PB	294–429
PGPB	669–1212
PIPB	1624
PS10GPB	794
PS10IPB	347–553

Pore size is one of the key factor they applications in the tissue engineering area. For this technique, it was demonstrated that mesopores and macropores can be simultaneously obtained. These values are in the same range of those normally required for certain types of biomedical applications such as in hard tissue engineering. Macrospores (200–900 µm and 1.2–2.0 mm) for allowing the cell diffusion and vascularization and mesopores (2–50 nm) for fast degradability, efficient loading, transport and release of bioactive compounds (Salgado *et al*., 2004; de Matos *et al*., 2013).

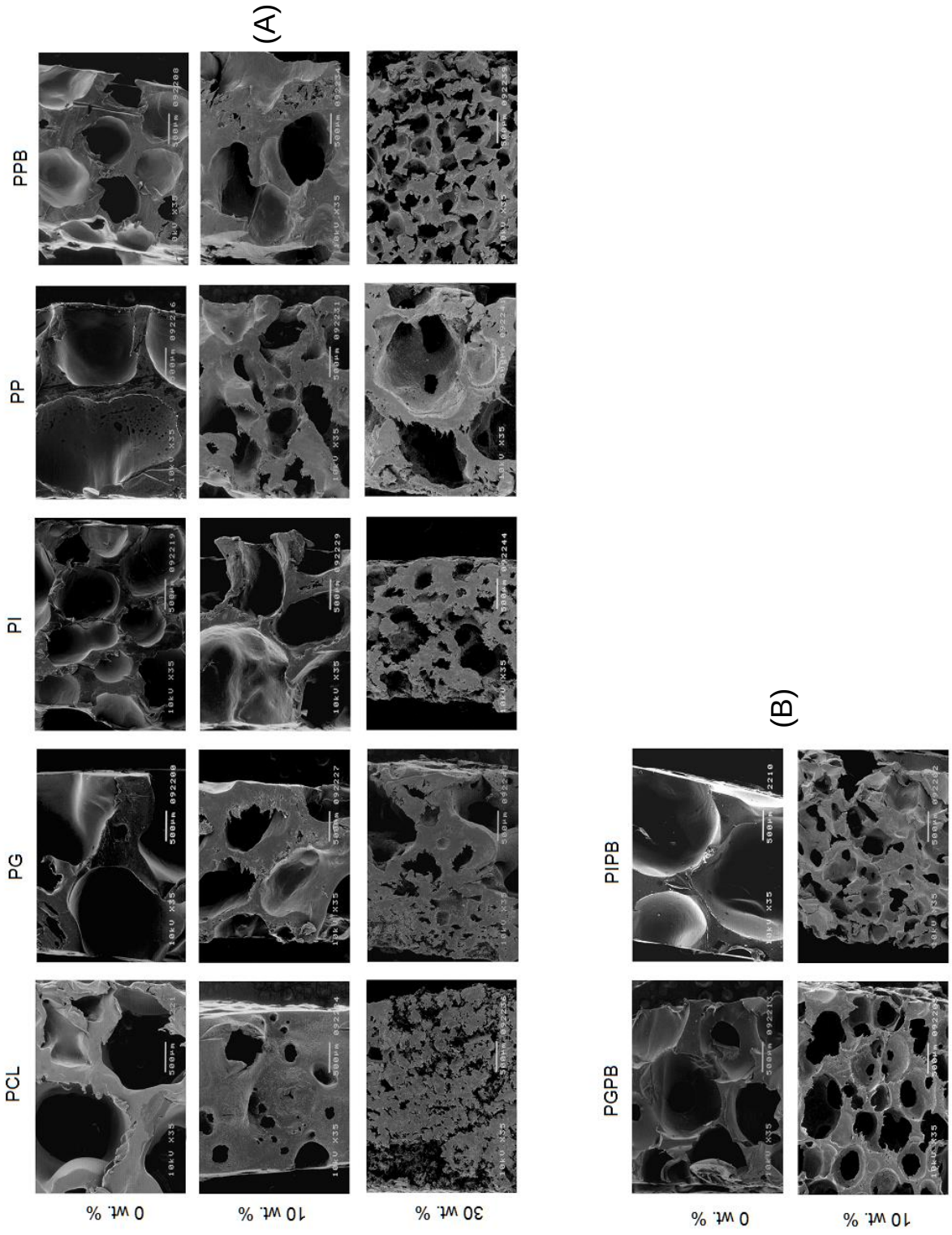

Figure 10 – SEM cross section micrographs of samples prepared by $scCO_2$ foaming process for 2 h, 20 MPa, 40 °C and 0.37 $L_{CO2} \cdot min^{-1}$ of (A) single additive and (B) mixture of two additives.

Figure 11 shows the SEM micrographs at higher magnification which can allow an analysis more detailed of the surface of the foams. It can be seen clearly the differences in the inner surface of the cells. Microfibrous internal structure (for the samples comprising 0 and 10 wt. % of SBA–5) and roughly surface (for all incorporating 30 wt. % of SBA–15) were obtained. It was also observed that the inner surface of some pores were porous, particularly in the formulation with 30 wt. % of SBA–15 and some samples comprising 10 wt. % of Si NPs (PS10 and PS10P). These effects could be very important and interesting for cell adhesion and growth (Reverchon *et al*., 2008). From these results it was very clear that the incorporation of Si NPs into the polymeric matrix enhanced the roughness of the foams surface. Similar results were described by Salerno and colleagues (Salerno *et al*., 2010).

From the SEM micrographs shown in Figure 11, it can be observe clearly the presence of the Si NPs, for both amount (10 and 30 wt. %), within the polymeric matrix of the composite foams. The presence in the composite comprising 30 wt. % was more visible. Nevertheless, the presence of these NPs was confirmed by EDS (Figure 12).

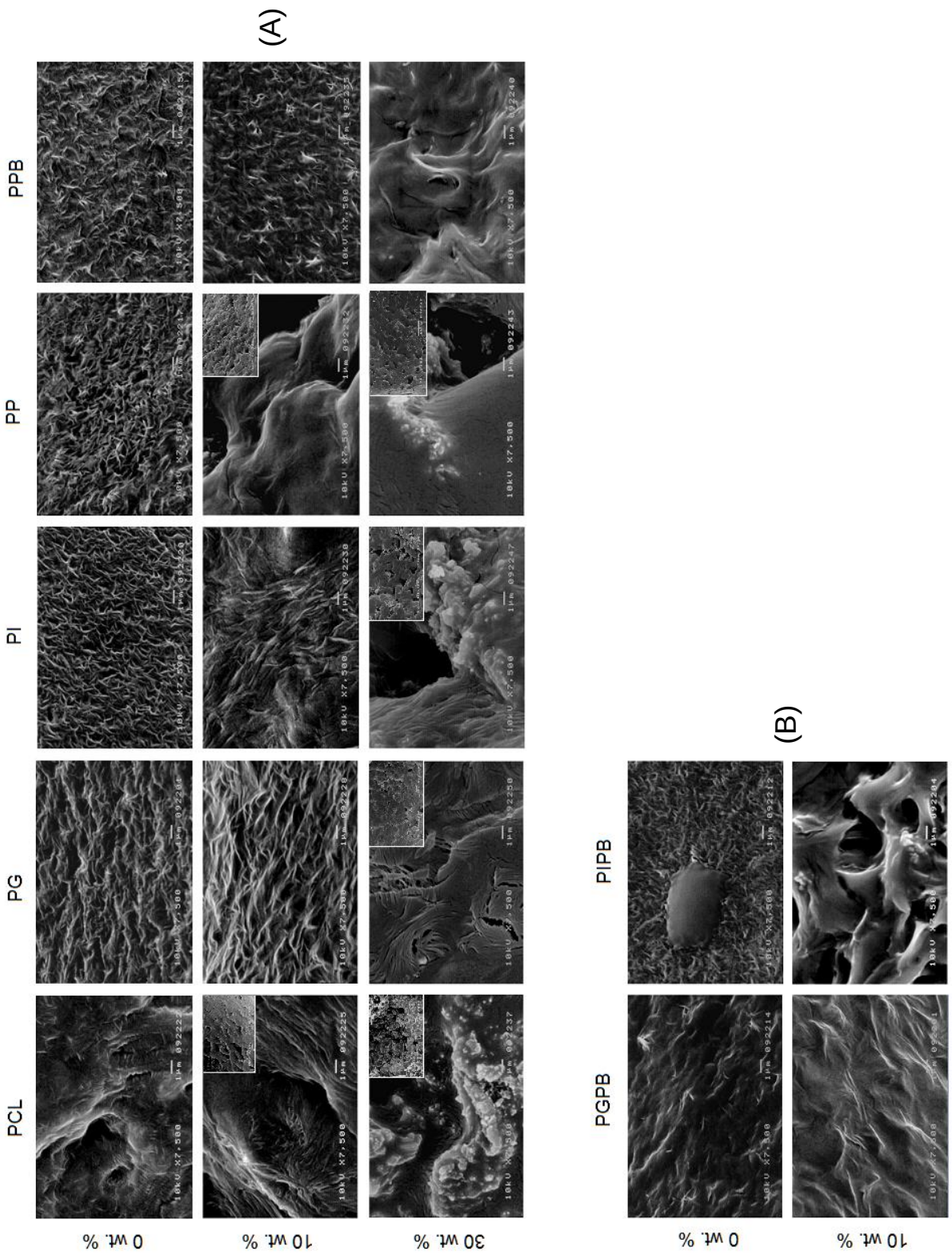

Figure 11 – SEM surface micrographs of processed samples by $scCO_2$ foaming process for 2 h, 20 MPa, 40 °C and 0.37 $L_{CO2} \cdot min^{-1}$ (A) single additive and (B) mixture of two additives.

Energy–Dispersive X–ray Spectroscopy (EDS) was used to identify and quantify the several chemical elements in order to confirm the existence of the Si NPs and ILs in the polymeric matrix.

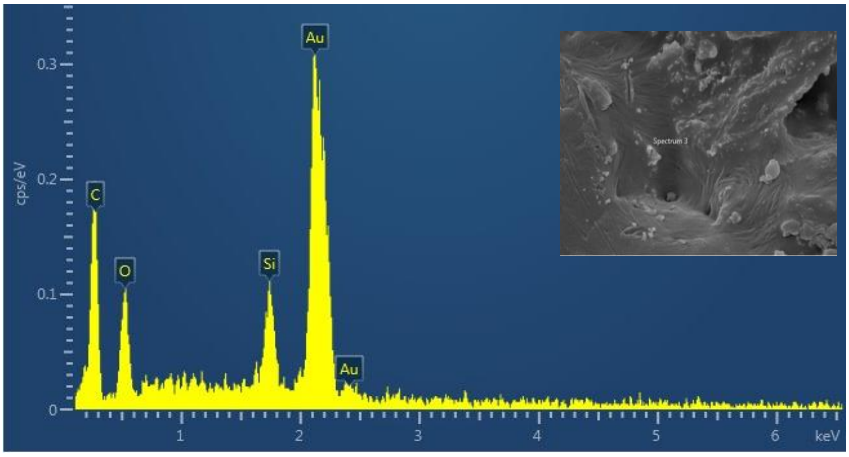

Figure 12 – EDS spectrum of PS10 composite biomaterial.

The results from EDS confirmed the presence of Si element and the other elements from the two IL used (N, F, P and S). All these evidences demonstrated the inclusion of the Si and the ILs into the polymeric foam.

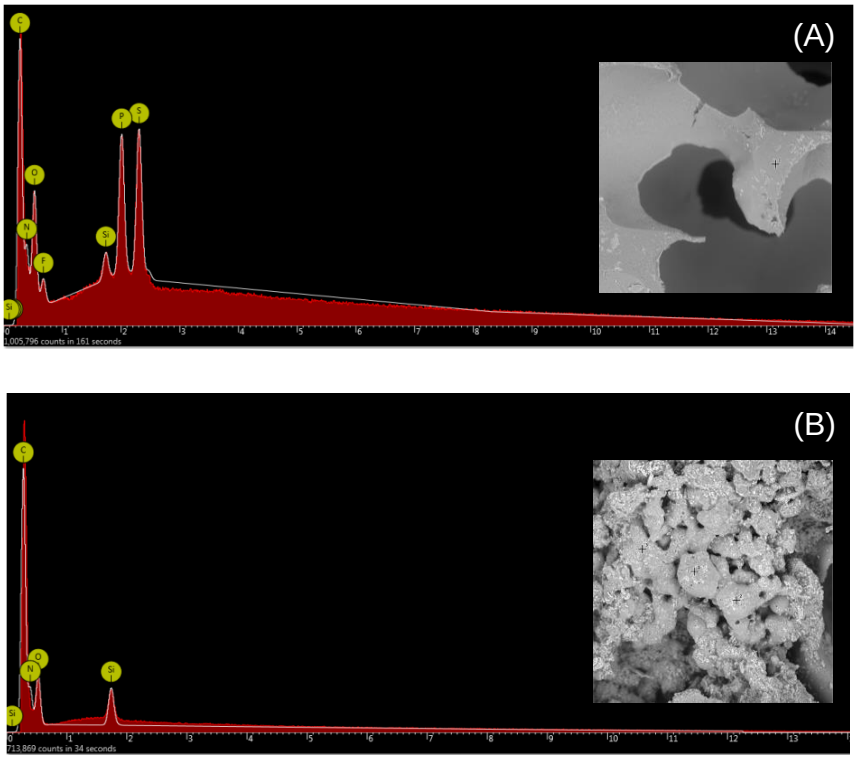

Figure 13 – EDS spectrum of (A) PS10GPB and (B) PS10P composite biomaterial.

EDS elemental mapping were also performed. The results, shown in Figure 14, revealed that all the elements, N, F, Si, S and P (proportionally to the corresponding color intensity) were homogeneously dispersed into the polymeric matrix.

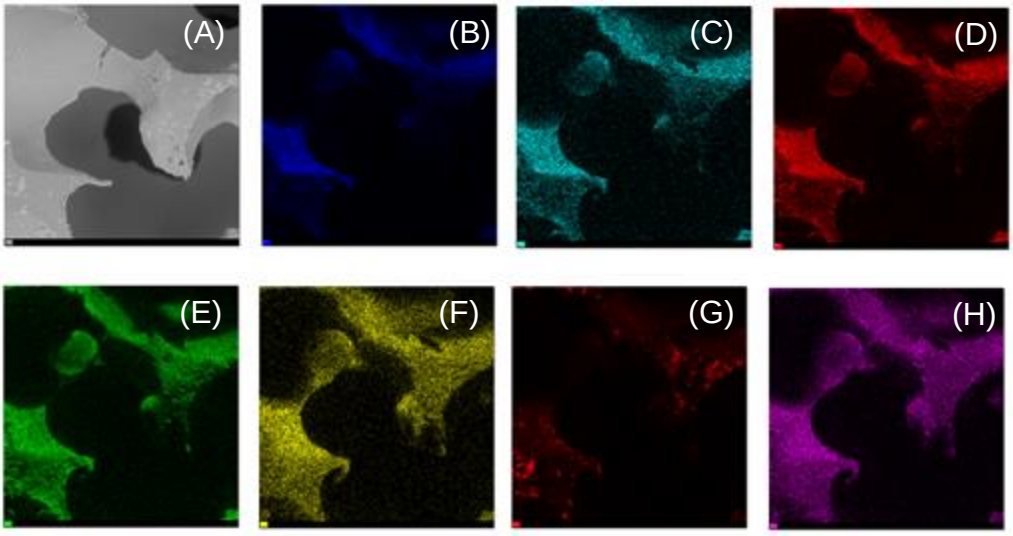

Figure 14 – EDS element mapping image of PS10GPB composite biomaterial (A) SEM image (B) Fluorine (C) Nitrogen (D) Oxygen (E) Carbon (F) Phosphorous (G) Silicon (H) Sulfur.

These macroscopic results will be investigated using more accurate and quantitative methods such as nitrogen adsorption and helium picnometry.

3.2. Physical characterization

3.2.1. Fourier Transform Infrared–Attenuated Total Reflectance (FTIR–ATR)

FTIR analysis was performed to identify any changes in the chemical structure that could have occurred during the foaming process and to confirm the presence of other component or interactions with other phase. The FTIR spectra of the pure substances, processed PCL and composites are illustrated in Figure 15.

Figure 15A shows the spectra of PCL in the form of pellet, powder and PCL processed via supercritical CO_2 technology. Comparing the FTIR spectra of the pure PCL (in the pellet and powder form) with the processed PCL, the spectra are the same, which reveals that there were no changes in the chemical structure of PCL after the foaming process. The characteristic absorption band at 2800–3000 cm^{-1} is attributed to CH_2 stretching (Pankajakshan *et al.*, 2008; Ghasemi–Mobarakeh *et al.*, 2008; Salerno *et al.*, 2012). The peak observed at 1720 cm^{-1} is

assigned to the C=O (carbonyl group) stretching (Pankajakshan *et al*., 2008; Ghasemi–Mobarakeh *et al*., 2008; Salerno *et al*., 2012) and C–O and C–C stretching in the range of 1290 to 1300 cm^{-1} (Pankajakshan *et al*., 2008; Ghasemi–Mobarakeh *et al*., 2008; Salerno *et al*., 2012).

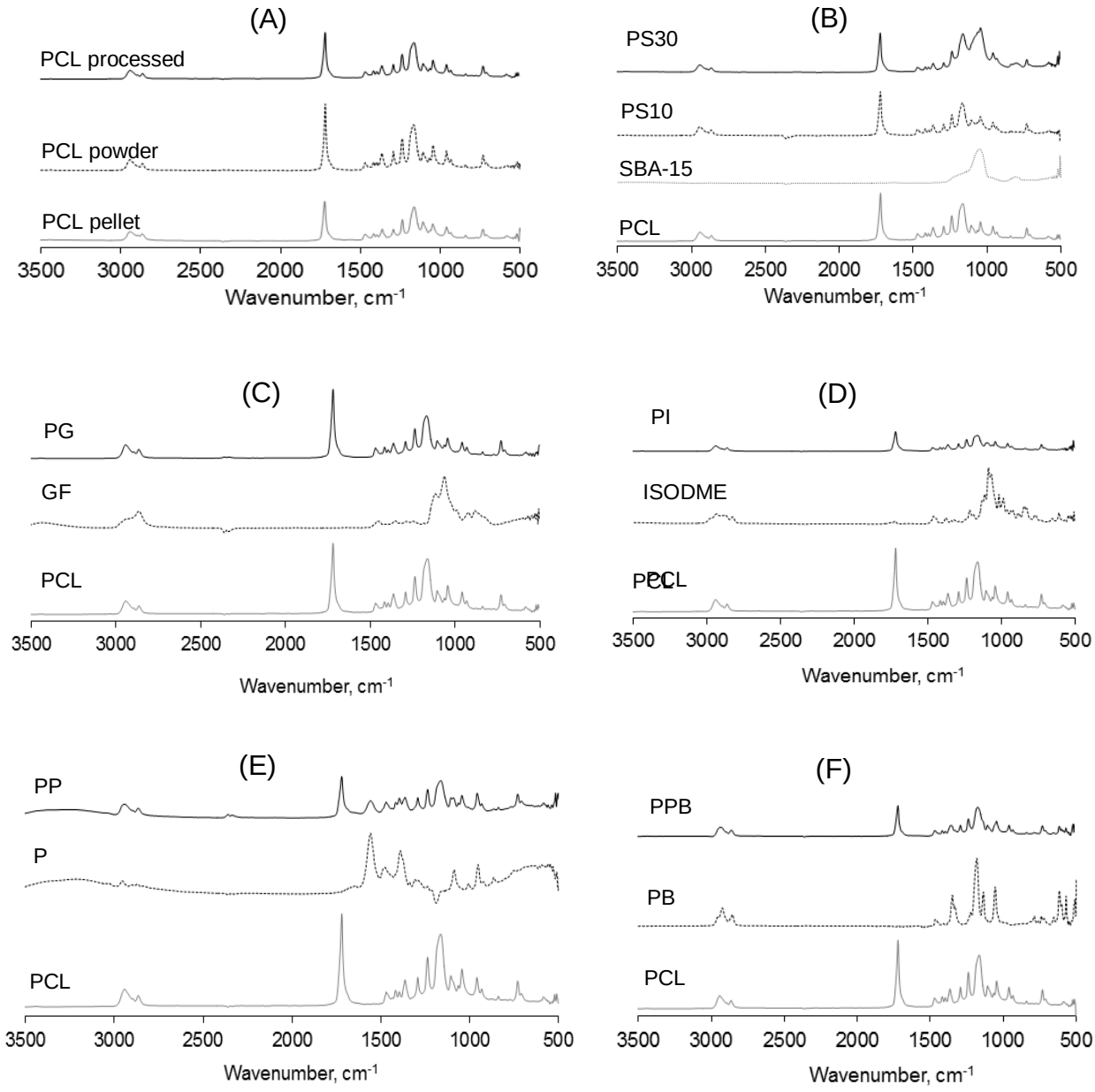

Figure 15 – FTIR-ATR spectra of various processed foams via $scCO_2$ foaming process for 2 h, 20 MPa, 40 °C and 0.37 $L_{CO2} \cdot min^{-1}$.

For pure SBA–15 shown in Figure 15B, the absorption peak (very intense) at 1051 cm^{-1} is attributed to Si–O–Si asymmetric stretching vibrations and the symmetric stretching vibrations of Si–O–Si appear at 808 cm^{-1} (Al–Oweini and El–Rassy, 2009, Yan and Li, 2010). For PCL/SBA–15 30 wt. % composite foam, the characteristic bands of silica were present,

which confirmed the existence of the Si NPs in the final polymeric foam. However, for the composite comprising 10 wt. % of SBA–15 these bands were inexistent, probably due to small amount and well dispersed Si NPs into the polymeric matrix. These trends were verified for all composites containing SBA–15 10 wt. %.

The spectra of PCL/additives are shown in the Figure 15C–F. For pure $[P_{6,6,6,14}][Tf_2N]$, the spectrum is characterized by CF_3 stretching vibration at 1181 cm^{-1}, C–S stretching vibration at 1349 cm^{-1} and $–SO_2–N–$ stretching vibration at 1055 cm^{-1} (Dias *et al*., 2012). Comparing pure PCL with their composite biomaterial, slight deviations were observed in the spectrum, which may indicate possible interactions between the PCL and the additive.

For pure N, N, N–Trimethylethanolammonium pentanoate, the absorption bands observed in the region of 3600–2400 is assigned to O–H stretching and the peak found at 1560 cm^{-1} is attributed to C–N stretching.

As can be seen in the Figure 15E, these characteristics absorption peak of IL can be identified in the PCL/PP composite spectrum, which indicates there were clearly interactions between the PCL and the IL.

The pure ISODME presented three main peaks, as shown in Figure 15D, in the range 3000–2800 cm^{-1} which correspond to CH_2, at 1092 cm^{-1} attributed to C–O stretching and lastly at 846 cm^{-1} which is the characteristic of C–H (from the ring) stretching absorption band. Differences were found in the PI composite spectrum when compared with the pure spectrum, indicating that there was interaction between PCL and ISODME.

For pure GF spectrum, the absorption bands observed in the region of 3600–3183 and 3000–2800 cm^{-1} are assigned to O–H and CH_2 stretching, respectively. The peak found at 1070 belongs to C–O stretching. Compared with the PG composite spectrum, a slightly modification could be seen in the region of 3600–3183 cm^{-1} and the absorption peak at 1170 cm^{-1} shifted to 1163 cm^{-1}, indicating that there may be chemical interaction between PCL and GF.

The FTIR spectra of all processed samples are presented in Figure A1 in Appendix A.

3.2.2. Density and porosimetry

Helium picnometry

Figure 16 shows the real density of the processed samples. The density of the pure processed PCL was about 1.11 ± 0.002 $g \cdot cm^{-3}$.

By the incorporation of the additives, the density of the composite biomaterials suffered a little change. The density of PG composite slightly increased to 1.13 ± 0.000 g·cm^{-3}. By the contrary, the density PI, PP and PPB decreased. For the composite including the mixture of two additives (PGPB and PIPB), the density lowered to 0.98 ± 0.004 and 0.99 ± 0.001 g·cm^{-3}, respectively. This result may be attributed to the lower density of the various additives used (ρ_{GF} = 1.09 g·cm^{-3}, ρ_{TMEAP} = 0.94 g·cm^{-3}, ρ_{PB} = 1.07 g·cm^{-3}, ρ_{ISODME} = 1.15 g·cm^{-3}).

The incorporation of Si NPs into the polymeric matrix resulted in an increase of the density of the foams, because the density of the NPs is greater (1.82 g·cm^{-3}) than the density of the PCL. The true density of the processed foams increased with the increasing of Si NPs. Similar results were found by Tsimpliaraki and coworkers using clay nanoparticles (Tsimpliaraki *et al.*, 2011).

It was not possible to realize the porosity, pore size distribution and pore volume studies of the produced foams by mercury intrusion within the stipulated time. However, this technique will be performed in the future for the scientific paper.

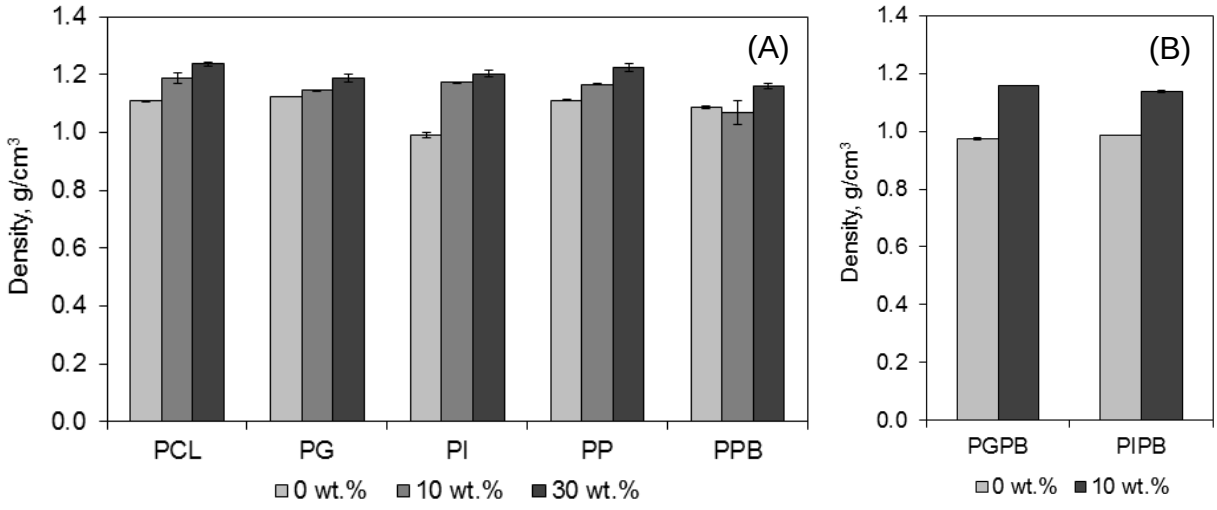

Figure 16 – Density of processed samples prepared by $scCO_2$ foaming process for 2 h, 20 MPa, 40 °C and 0.37 L_{CO2}·min^{-1} (A) single additive and (B) mixture of two additives.

3.2.3. Nitrogen adsorption

The nitrogen adsorption results are listed in Table in Appendix A. According with the IUPAC classification the different adsorption–desorption isotherms were of type II and IV, respectively indicating essentially mesoporous (pore sizes between 20 and 500 Å) and macropores (pore sizes > 500 Å) nature of the materials (Webb and Orr, 1997).

Surface area

The surface area of all processed foams is reported in Figure 17. The foamed PCL demonstrated a BET surface area of 0.86 ± 0.23 $m^2 \cdot g^{-1}$. This value is slightly higher than the value previously reported in the literature (0.78 ± 0.08 $m^2 \cdot g^{-1}$) (de Matos *et al*., 2013).

The influence of the various additives on the surface area was investigated. Adding the additives to the polymeric matrix the surface area decreased for all foamed samples except for PPB composite. This result may be explained by an increase of the pores diameter and decrease of cell density of the produced samples. PG composite showed the lower value, 0.70 ± 0.19 $m^2 \cdot g^{-1}$. The same effect was verified for the samples with the mixture of two additives, which decreased down to 0.67 ± 0.08 $m^2 \cdot g^{-1}$ for PGPB and 0.81 ± 0.25 $m^2 \cdot g^{-1}$ for PIPB, respectively.

The incorporation of the NPs into the polymeric matrix had a significant impact on the surface area of the foams mainly in the composite with higher amount of SBA–15 (30 wt. %), as it can be seen in Figure 17. The same effect was described in the literature (de *Matos et al.*, 2013).

For the composites comprising 10 wt. % of SBA–15 the surface area decreased except for PG and PGPB. PS30 composite showed the higher value of surface area (2.786 $m^2 \cdot g^{-1}$) due to the high surface area of the Si NPs. This difference can be explained by the results obtained from SEM images of the foams where for the composites incorporating higher amount of Si NPs (30 wt. %) was evident the existence of extremely small pore diameter extended all over the surface and for the composites with 10 wt. % was not verified.

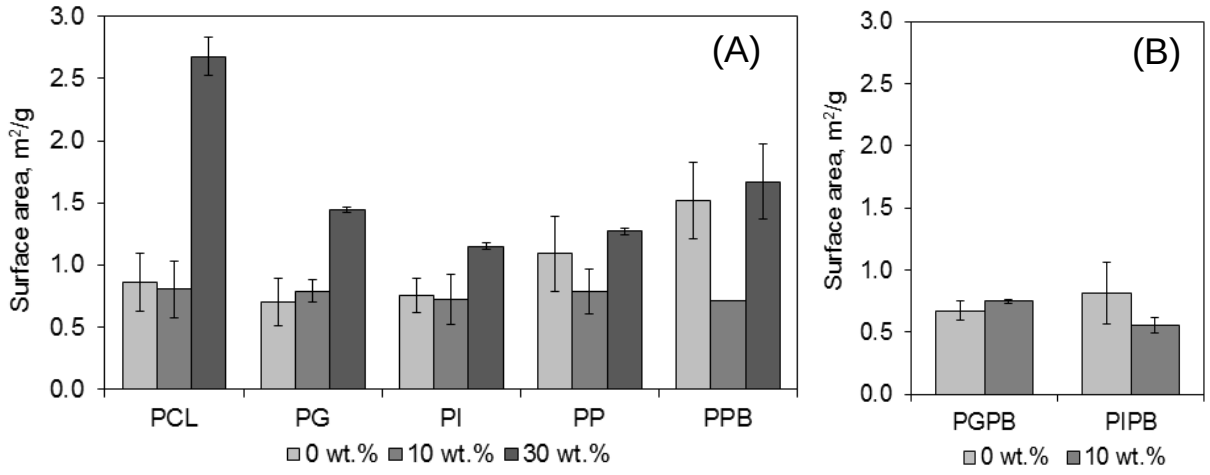

Figure 17 – Surface area of produced samples obtained by $scCO_2$ foaming process after 2 h, 20 MPa, 40 °C and 0.37 $L_{CO2} \cdot min^{-1}$ (A) single additive and (B) mixture of two additives.

Pore volume

Figure 18 displays the results of pore volume of prepared foams. The foamed PCL revealed a total pore volume of $0.65 \pm 0.09 \times 10^{-3}$ $cm^3 \cdot g^{-1}$. This value is much lower than that reported in the literature ($1.56 \pm 0.01 \times 10^{-3}$ $cm^3 \cdot g^{-1}$) (de Matos et al., 2013). This discrepancy may be due to the different silica type and processing parameters used in the fabrication of the foams.

The addition of the various additives to the polymeric matrix resulted in slightly decrease of the pores volume for all fabricated foams (single and mixture of two additives), excluding the PPB composite. PG composite exhibited the lower value of pore volume ($0.45 \pm 0.06 \times 10^{-3}$ $cm^3 \cdot g^{-1}$).

The integration of the Si NPs into the polymeric matrix led to an increase of pore volume. This effect was observed for all the composite biomaterials and for both Si NPs content 10 wt. % and 30 wt. %, respectively. Increasing the content of Si NPs from 10 to 30 wt. %, it was verified a considerable increase in the value of pore volume, as expected. The Si NPs contain pores with small diameter and high pore volume, and its incorporation at a high amount will consequently increase the pore volume. The composite which presented higher value of pore volume was PS30 ($4.87 \pm 0.31 \times 10^{-3}$ $cm^3 \cdot g^{-1}$). These results are in agreement with those found in the literature (de Matos et al., 2013).

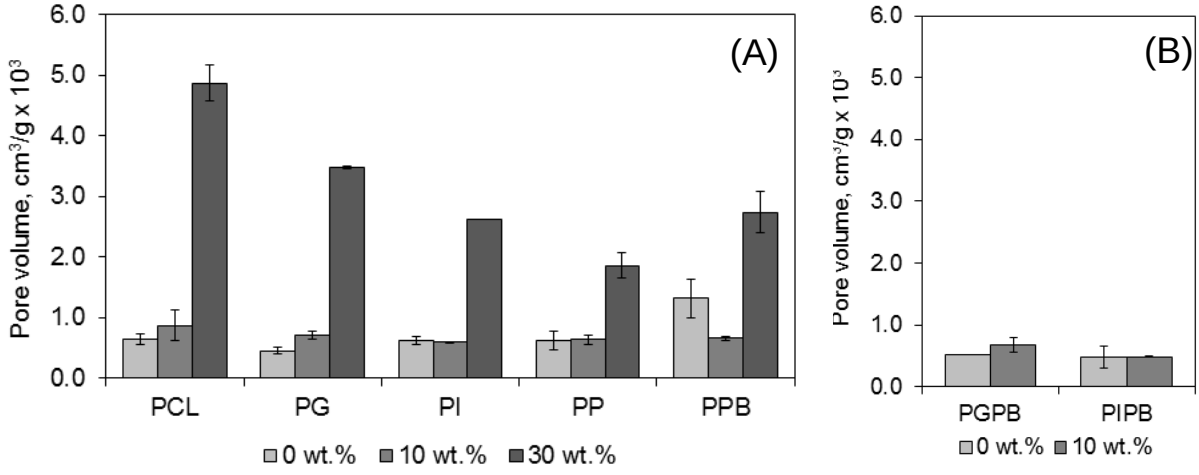

Figure 18 – Pore volume of samples obtained by $scCO_2$ foaming process after 2 h, 20 MPa, 40 °C and 0.37 $L_{CO2} \cdot min^{-1}$ (A) single additive and (B) mixture of two additives.

Pore diameter

The pore diameter of the produced foams was investigated and the results are illustrated in Figure 19. The mean pore diameter of porous PCL was determined to be 30.86 ± 4.20 Å. This value is also much lower than that reported in the literature (80.32 ± 5.69×10^{-3} $cm^3 \cdot g^{-1}$) (de Matos et al., 2013).

The pore diameter remained approximately constant after the addition of the additives to the polymeric matrix. For the composite combining the mixture of two additives (PIPB) the pore diameter decreased to 23.06 ± 1.53 Å.

The addition of the SBA-15 NPs into the polymeric matrix had a substantial effect on the pore diameter, which was found to increase with the increasing of the amount of SBA–15, as can be seen in Figure 19. This increment may be attributed to the larger number of pores presented in the polymeric matrix that were measure by this technique. The largest pore diameter was observed for PS30G composite 96.07 ± 1.05 Å.

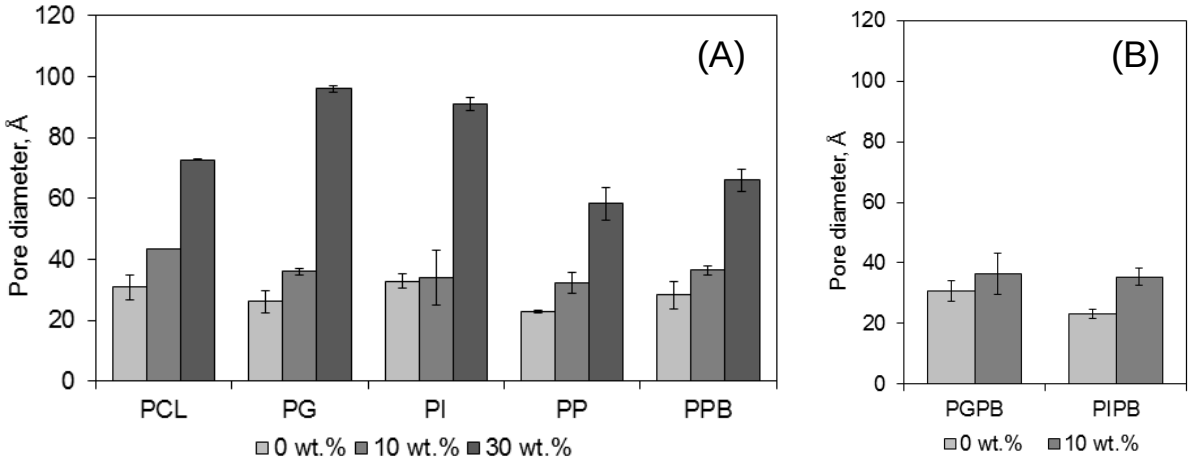

Figure 19 – Pore diameter of samples obtained by $scCO_2$ foaming process after 2 h, 20 MPa, 40 °C and 0.37 $L_{CO2} \cdot min^{-1}$ (A) single additive and (B) mixture of two additives.

3.3. Thermal and mechanical characterization

The thermal properties of material depend upon their chemical structures and the thermal stability of the composites materials depends on the interaction between polymers chains and the inorganic network and the resulting uniform distribution of the inorganic nanoparticles on the polymeric matrix (Chen *et al.*, 2012).

3.3.1. Thermogravimetric Analysis

The results of degradation temperature of the composite biomaterials are presented in Figure 20. The thermal degradation temperature of PCL remained almost the same after the $scCO_2$ foaming process. Similar results were found and reported in the literature (de Matos *et al.*, 2013).

The effect of the various additives on the thermal properties of foams was evaluated. By the addition of Glycofurol and ISODME into the polymeric matrix, the degradation temperature slightly increased which indicate an increase in the thermal stability of the produced foams. For the composites with the ILs, the degradation temperature remained approximately constant.

It was possible to verified a little increase in thermal degradation temperature with the addition of SBA–15 30 wt. %. In the contrary, the degradation temperature of the composites containing SBA–15 10 wt. % remained almost the same and decreasing in some case (PS10PB decreased down to 391.16 ± 6.65 °C). In general, the incorporation of SBA–15 (30 wt. %) into the polymeric matrix resulted in an increase in the temperature of degradation of all prepared samples which probably may be due to the formation of more stronger structures between the Si NPs, polymer and the additives.

In the formulations combining PCL with two additives, the thermal degradation temperature increased from 405.91 ± 2.83 to 410.56 ± 0.23 °C. Adding silica nanoparticles (SBA–15 10 wt. %), the degradation temperature remained nearly constant.

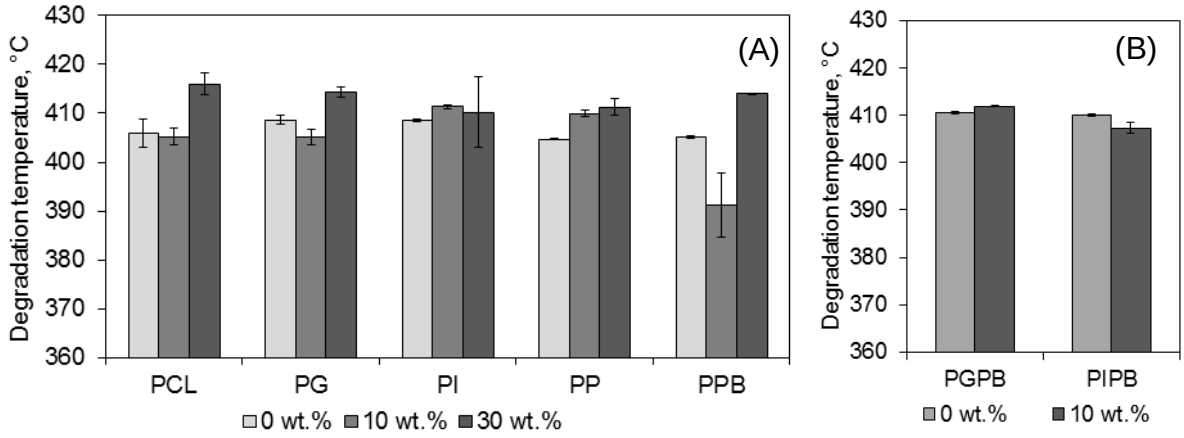

Figure 20 – Degradation temperature of processed samples obtained by $scCO_2$ foaming process for 2 h, 20 MPa, 40 °C and 0.37 $L_{CO2} \cdot min^{-1}$ of (A) single additive and (B) mixture of two additives.

TGA was used to determine the amount of NPs present in final polymeric matrix. TGA give us information about the mass loss of a sample and provides excellent quantitative compositional information. Figure 21 shows the mass loss results obtained of all processed samples by $scCO_2$ foaming technology. The percentages of mass loss of all pure compounds were around 99 % (and above), which means that, at the end of the test, almost all the materials had been completely degraded. For all the composites comprising 10 wt. % of Si NPs the total mass loss was in the range of approximately 89 to 94 % which means that the NPs were dispersed homogeneously within the polymeric matrix. For the composite with 30 wt. % content of SBA-15, the residual mass that remained in the polymeric matrix was about 77–88 %. By considering the sample formulation, it can be seen that the amount of nanoparticles present in the final polymeric did not correspond to the initial amount of SBA-15 which means heterogeneity of the produced foams. This result was expected because the mixture PCL/SBA-15/additives was not stirred and the Si NPs tend to deposit due do its superior density (1.82 $g \cdot cm^{-3}$). In all experiments only the $scCO_2$ was stirred. It was decided not to use the magnetic stirrer inside the vial glass, in direct contact with the polymer melt, because after the foaming process a big hole (corresponding to the volume of the magnetic stirred) was left in the final polymeric foam was undesirable because later characterization test.

The use of magnetic stirrer inside the vial glass would minimize the problem of heterogeneity of the fabricated foams. However, it is relevant to mention that it is very complicated to stirrer the polymer melt using a magnetic stirrer due its high viscosity.

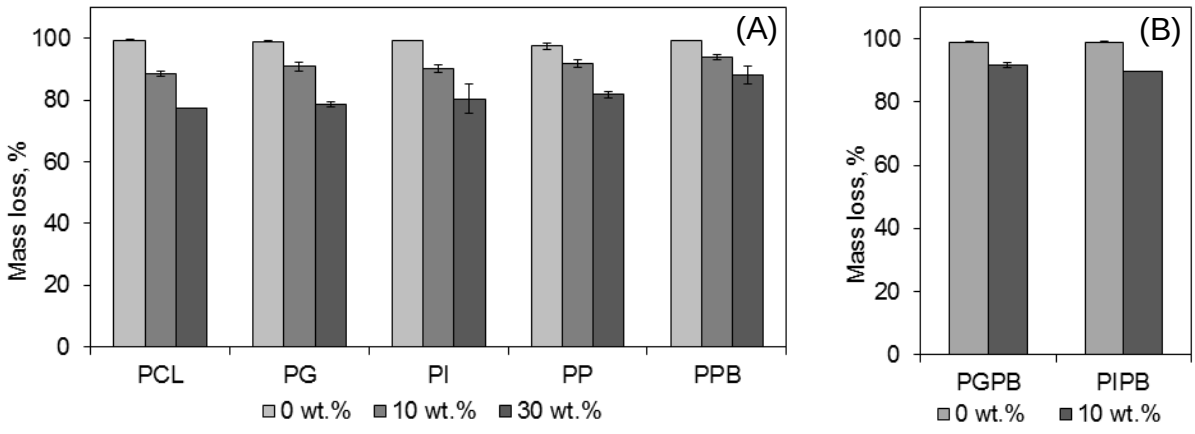

Figure 21 – Mass loss of processed samples by $scCO_2$ foaming process for 2 h, 20 MPa, 40 °C and 0.37 $L_{CO2} \cdot min^{-1}$ (A) single additive and (B) mixture of two additives.

3.3.2. Differential Scanning Calorimetry (DSC)

Differential scanning calorimetry has been a very important technique to study the thermal properties such as melting temperature and crystallinity of polymers. All results of the thermal properties of the polymeric foams are listed in Table B2 in Appendix B.

The melting temperature of pure PCL was calculated to be 62.31 ± 0.49 °C. This value is in agreement with the ones found in the literature (Lebourg *et al.*, 2008, Salerno *et al.*, 2010, Fanovich *et al.*, 2013) and reported by the supplier for this molecular weight, 56–64 °C.

Marginally change was observed in the thermal properties of the prepared foams after the $scCO_2$ foaming process. The melting temperature of pure processed PCL decreased to 61.73 ± 0.75 °C. Similar effect was verified and reported in the literature (de Matos *et al.*, 2013).

The effect of the various additives in the melting temperature of the polymeric foams is presented in Figure 22. As it can be seen, the addition of the additives to the polymeric matrix had huge impact in the thermal properties of the foams. The melting temperature of all produced foams decreased. This tendency was verified for the samples integrating the mixture of two additives (PGPB and PIPB). The temperature reduction was more significant in the case of glycofurol (which decreased 11 %) and isosorbide dimethyl ether (decreased ~8 %). These results showed that the PCL was clearly modified with the ionic liquids and with the others two solvents which confirm the plasticization effect of these materials.

The T_m of the processed foams increased with the incorporation of SBA–15 10 wt. % into the polymeric matrix for all samples. Mixed results were obtained for the higher amount of Si NPs (30 wt. %). The melting temperature decreased for PS30, PPB and PP composites while increased for PG and PI composites, respectively. For the composites comprising two additives, the addition of the Si NPs to the polymeric matrix the T_m decreased. This reduction was more pronounced in the PS10PG composite, from 59.52 ± 0.32 to 56.26 ± 0.02 °C.

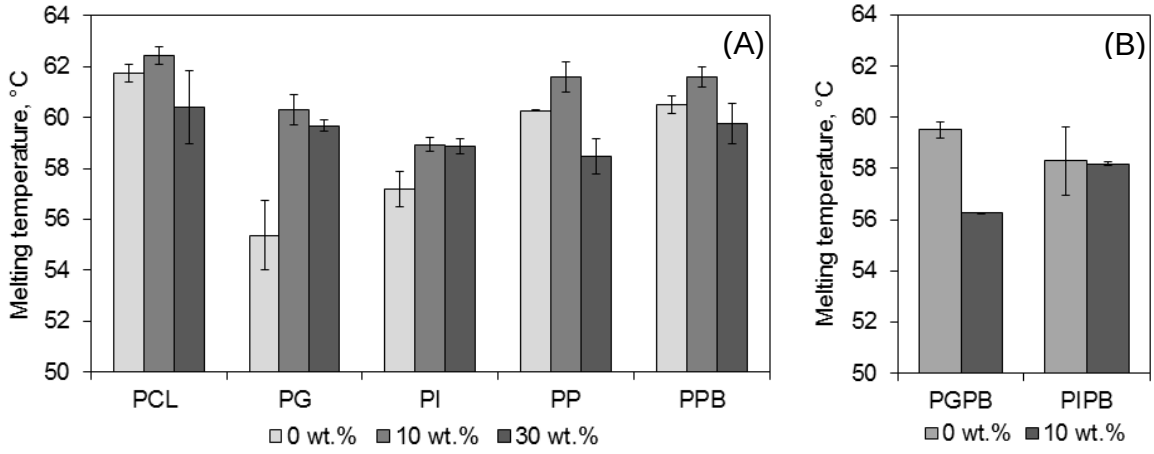

Figure 22 – Melting temperature of processed samples by $scCO_2$ foaming process for 2 h, 20 MPa, 40 °C and 0.37 L_{CO2}·min^{-1} (A) single additive and (B) mixture of two additives.

The effect of the different additives and silica nanoparticles on the crystallinity of the obtained foams was evaluated. The degree of crystallinity of pure unprocessed PCL was determined to be 75.56 ± 0.71 %. The percentage of crystallinity of PCL reported in the literature range from 60 to 70 %, slightly lower than the value obtained in this work.

As shown in the Figure 23, it is clear the change in the crystallinity of the prepared polymeric foams after the $scCO_2$ process, decreasing from 75.56 ± 0.71 to 63.73 ± 4.99 %.

The degree of crystallinity of the foams slightly decreased with the addition of the various additives. This effect was more substantial for the PG (56.88 %) and PI composite (56.43 %), respectively.

The incorporation of SBA-15 into the polymeric matrix resulted in a reduction of the degree of crystallinity of the foams. Opposite results were reported in the literature, where the incorporation of nanoparticles leads to an increment in the percentage of crystallinity of the samples (Shieh *et al.*, 2009).

Combining PCL with the two additives, the degree of crystallinity of the samples decreased when compared with pure processed PCL and with the same formulation combining only one additive. The addition of small amount of SBA–15 (10 wt. %) to the polymeric matrix led to a reduction of the degree of crystallinity for PS10GPB and an increment for the PS10IPB composite.

This effect may be attributed to the increased difficulty in arranging the polymer chain due to the nanoparticles prohibiting movement of the polymer segments.

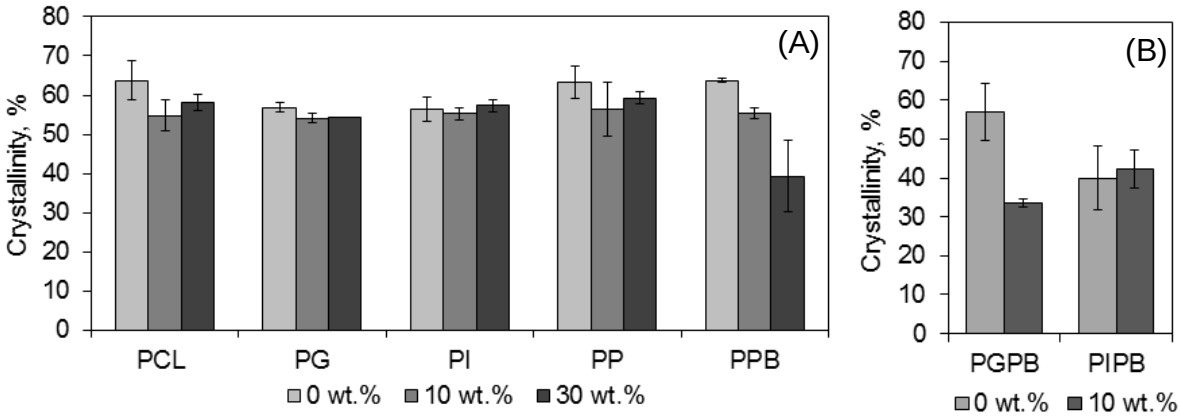

Figure 23 – Degree of crystallization of processed samples by $scCO_2$ foaming process for 2 h, 20 MPa, 40 °C and 0.37 $L_{CO2}{\cdot}min^{-1}$ (A) single additive and (B) mixture of two additives.

3.3.3. Dynamical and mechanical analysis

Figure 24 shows the effect of the different additives on the T_g of the final foamed samples. Foamed PCL showed a glass transition temperature, T_g, at –19.98 °C. This value is different with the one reported in the literature –60 °C.

The influence of the additives on the glass transition temperature was evaluated. As it can be observed in the Figure 24, the T_g of the composite materials decreased with the addition of the additives. The minimum value of T_g was observed for PG composite.

It was clear that the incorporation of Si NPs into the polymeric matrix affect the T_g of the produced foams. For the composites comprising 10 wt. % of Si NPs mixed results were found. The T_g increased for PS10 and PS10PB composites and decreased for PS10G, PS10I and PS10P, respectively. The same trend was verified for the amount of 30 wt. %, the T_g increased for PS30, PS30I and PS10PB. For PS30G and PS30P the T_g of the samples decreased. Generally, the T_g increased with the increase of the amount of SBA–15.

This finding suggests that the additives make the samples to become more elastic, which is in agreement with previous reported studies (Duarte *et al*., 2012).

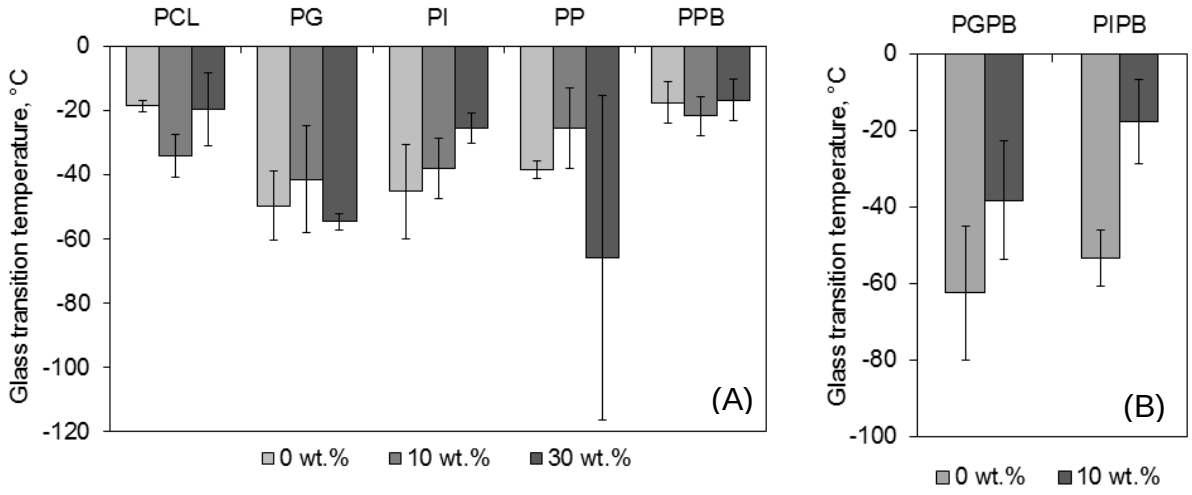

Figure 24 – Glass transition temperature of the processed foams by $scCO_2$ foaming process for 2 h, 20 MPa, 40 °C and 0.37 $L_{CO2} \cdot min^{-1}$ (A) single additive and (B) mixture of two additives.

Figure 25 presents the dynamical mechanical response of the different processed foams as a function of temperature in terms of E'. There was a substantial decrease in the storage modulus (E') for all samples foams by increasing the temperature.

By the addition of the various additives there was significant depression in the storage modulus E', which means that the samples foam became more elastic. PGPB composite presented the lowest value of E'.

These results showed that the porous structure samples were clearly modified with the addition of the additives.

Figure 25B shows the influence of the Si NPs on the value of E'. It can be seen that the value of E' decreased with the addition of 10 wt. % of SBA–15 (PS10) and increased incorporating 30 wt. % of SBA–15 (PS30) may be due to the smaller pore diameter with high cell density indicating the reinforcement of the composite materials. This result showed that PS10 composite was more elastic than pure processed and unprocessed PCL.

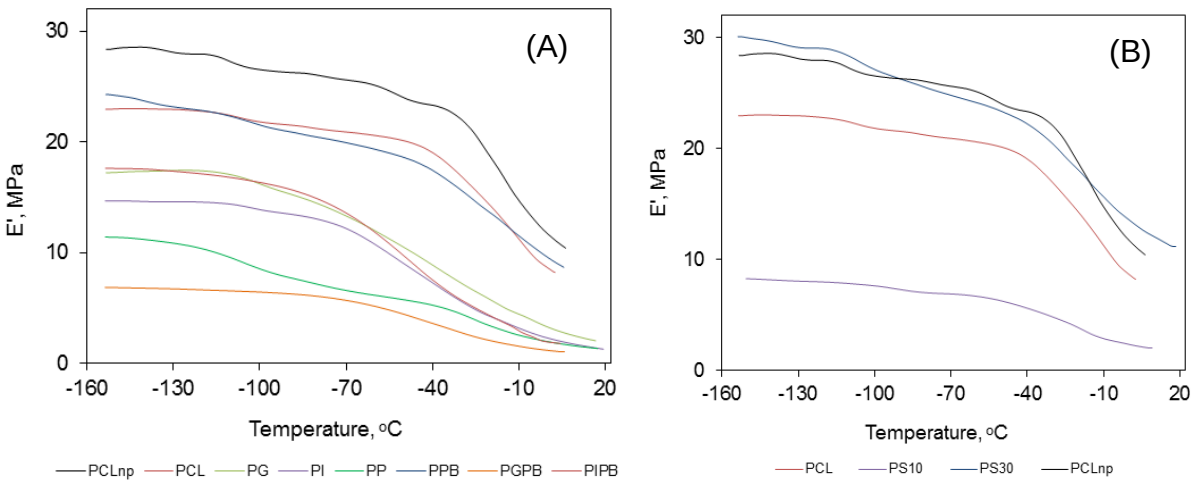

Figure 25 – Storage modulus of processed samples by $scCO_2$ foaming process for 2 h, 20 MPa, 40 °C 0.37 L_{CO2}·min^{-1}.

3.3.3. Mechanical properties

Besides the morphological features, mechanical properties of the foams are another important key factor for its applications in biomedical field/tissue engineering.

The mechanical properties of the foam were characterized by compression tests. The compression tests were carried out in order to determine the compressive strength and Young's modulus of the polymeric foams. The results of the tests are summarized in Table C1 in Appendix C.

The compressive strengths of the foamed samples were very similar for all samples. The larger value were obtained for PS30 (0.31 MPa) and PS10IPB (0.33 MPa).The sample with the smallest value of compressive strength was PS10GPB (0.11 MPa) (top part).

Figure 26 shows the effect of the various used additives in the Young's Modulus of the polymeric foam. PS10GPB showed the smallest value of the Young's Modulus (1.92 MPa), which indicated that this sample was more elastic than the others composites. PS30 has the highest value of Young's Modulus (4.32 MPa). In general, the addition of the additives to the polymeric matrix contributed to a slightly increase in the Young's Modulus of the foams.

The Young's Modulus and the compressive strength increased as the content of SBA–15 nanoparticles increases. This increment was more significant in the case of higher amount of SBA–15 (30 wt. %). Similar results were found by Yang and coworkers (Yang *et al.*, 2013) and according to these authors, this mechanical improvement could be attributed to the well developed and uniform pore size with small pore size and high pore density. They also

reported that it can be attributed to the increase of the T_g. Increasing the T_g, the mobility of chain segments is limited resulting in pore walls much stronger (Yang *et al*., 2013).

All the composite foams exhibited the typical stress–strain behavior/curves of an elastomeric material under a compression load, i.e., a linear slope curve in the initial stage, as can be seen in Figure C1 in Appendix C (Lebourg *et al*., 2008, Salerno *et al*., 2012).

The mechanical properties of all formulations were inferior to those required for applications in bone tissue engineering area. The value of compressive strength was smaller than that of trabecular bone, 7–10 MPa, and the Young's Modulus was also smaller, 0.05–0.5 GPa (Bassi *et al*., 2011). These values are also smaller than the target value for cartilage repair, 0.5–1 MPa (Annabi *et al.*, 2011).

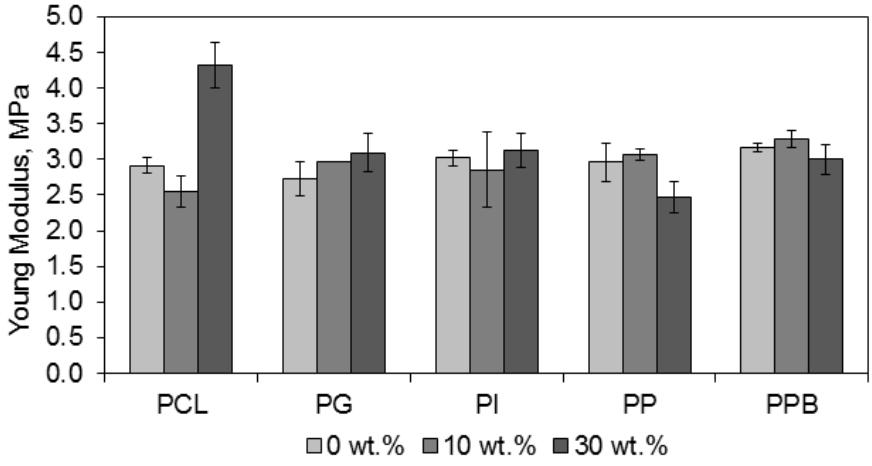

Figure 26 – Young's modulus of processed samples by $scCO_2$ foaming process for 2h, 20 MPa, 40 °C and 0.37 $L_{CO2}{\cdot}min^{-1}$.

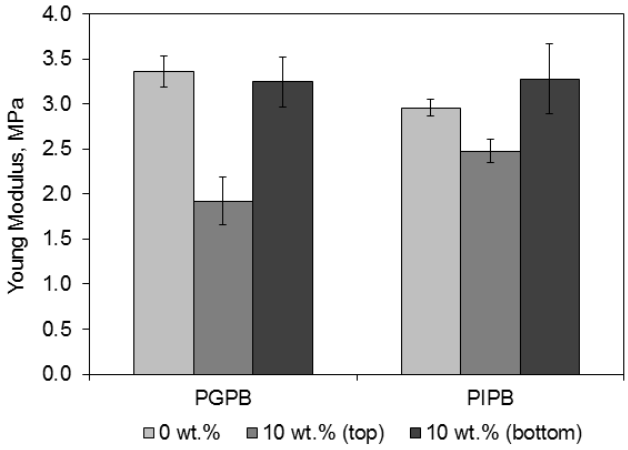

Figure 27 – Young's modulus of the mixture of two additives by $scCO_2$ foaming process for 2 h, 20 MPa, 40 °C and 0.37 $L_{CO2}{\cdot}min^{-1}$.

The effect of combining two additives on the mechanical properties of the prepared foams was studied. The Young's modulus of both PGPB and PIPB marginally increased with the addition of the two additives to the polymeric matrix.

By the addition small amount of SBA–15 (10 wt. %), it can be seen that different parts of the same samples reveal different mechanical behavior, i.e., different values of Young's Modulus and compressive strength, as shown in the Figure 27 and Figure 29, respectively. These results may indicate heterogeneity in the final foamed structure. The top part of the samples revealed lower value of Young's Modulus while the bottom part showed a higher value for both formulations, PS10GPB and PS10IPB, respectively.

Identic results were obtained for the values of compressive strength. The top part of the foam revealed lesser value of compressive strength while the bottom part exhibited high value for PS10GPB composite. For the PS10IPB composite opposite result was found, higher value of compressive strength was obtained for the top part and lower value was observed for the bottom part of the foam.

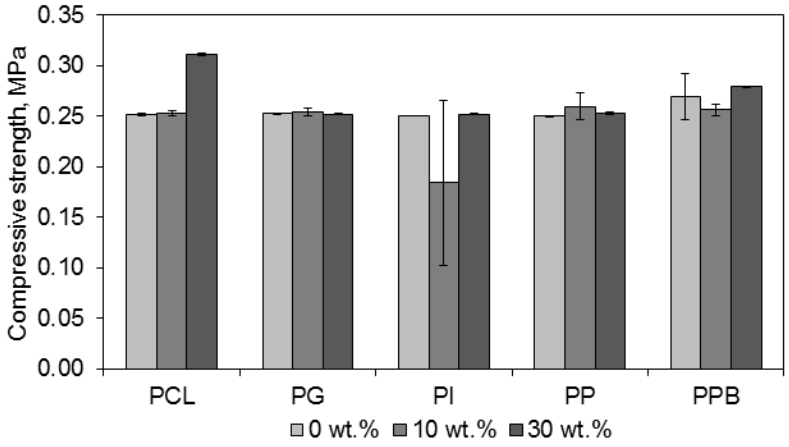

Figure 28 – Compressive strength of processed samples by $scCO_2$ foaming for 2 h, 20 MPa, 40 °C 0.37 L_{CO2}·min^{-1}.

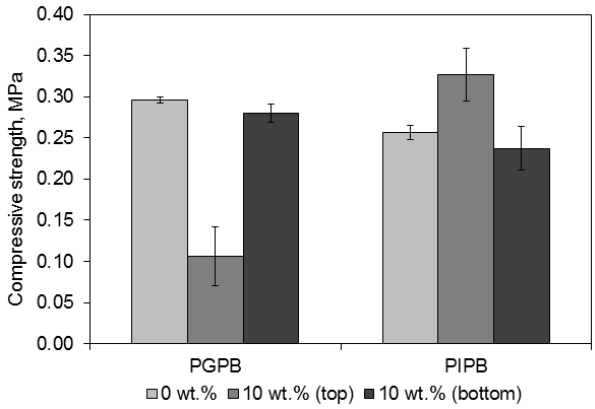

Figure 29 – Compressive strength of ternary processed samples (mixture of two additives) by $scCO_2$ foaming process for 2 h, 20 MPa, 40 °C and 0.37 L_{CO2}·min^{-1}.

Effect of porosity on mechanical properties

The mechanical behavior depends strongly on porosity and pore morphology of the samples (Lebourg *et al*., 2008). According with previous studies, increasing the porosity will decrease the compressive strength and the Young's Modulus of the foams and vice–versa (Lebourg *et al*., 2008, Yoshimura *et al*., 2012).

3.4. Cytotoxicity tests

Cell viability and proliferation on the scaffolds is one of many prerequisites for the porous structure applications in biomedical area (Oliveira *et al*., 2008). Therefore, taking this in account, it is very important to evaluate its toxicity and cell viability. Cytotoxicity tests were performed by LDH assay using SAOS–2 human osteogenic sarcoma cells. Figure 30 shows the results of cytotoxicity tests of all pure compounds.

ILs are generally classified as green solvents, but recent studies have revealed that several commonly used ILs exhibit a certain level of toxicity (Zhao *et al*., 2007). These authors have found that the cation type was the key factor influencing the toxicity of ILs while the anion type remained uncertain.

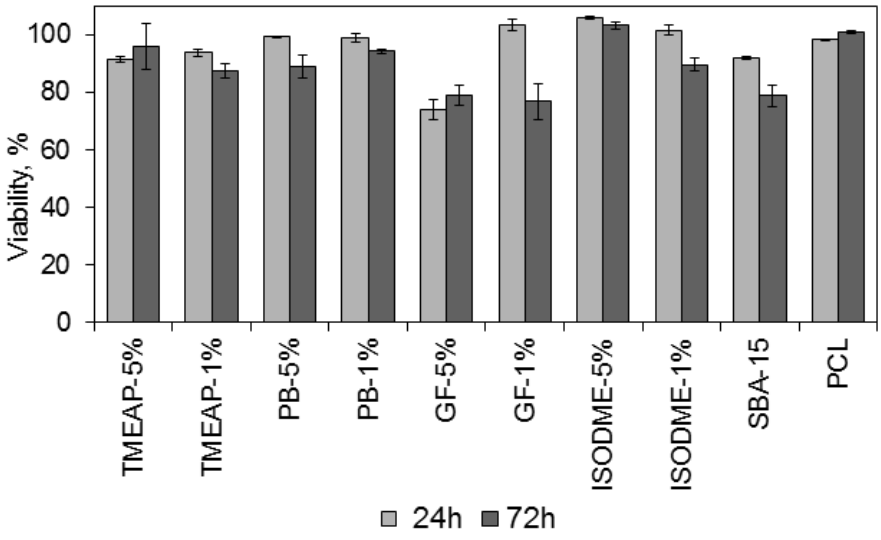

Figure 30 – Cell viability on the pure compounds after 24 and 72 hours of incubation.

Glycofurol, 5 %, exhibited the lowest cell viability percentage after 24 and 72 hours. For 1 % of concentration, for same compound, the cell viability decreased from 103.51 ± 2.03 % to

76.74 ± 6.46 %. For all the other pure compounds the cell viability percentage showed high biocompatibility, superior to 80 %. Generally, the cell viability decreased with the incubation time.

The percentage of cell viability after 24 and 72 hours of incubation are presented in Figure 31 and Figure 32, respectively. These results revealed good cell viability after 24 hours of cell seeding, around 100 %, which marginally increased for the period of 72 hours of incubation/cell seeding, which may indicated cell growth on the composites surfaces. This effect was more pronounced in the composites containing the ILs. According to the literature, the anion $[Tf_2N]^-$ decreases the cell toxicity, increasing the cell viability (Dias *et al.*, 2012).

It can be seen that the cell viability slightly decreased with the addition of 30 wt. % of SNPs for all samples compared with the others formulations, which means that for this amount of SNPs provided less viable environment for the cells. PS30P composite presented lower cell viability after 24 hours, 89.83 ± 0.68 %, which increased to 97.57 ± 1.35 %.

These results showed that all the composites porous structures materials were nontoxic to the cells. The porous structures materials revealed to be a good environment for the seeded cells (good biocompatibility to the SAOS-2 cells).

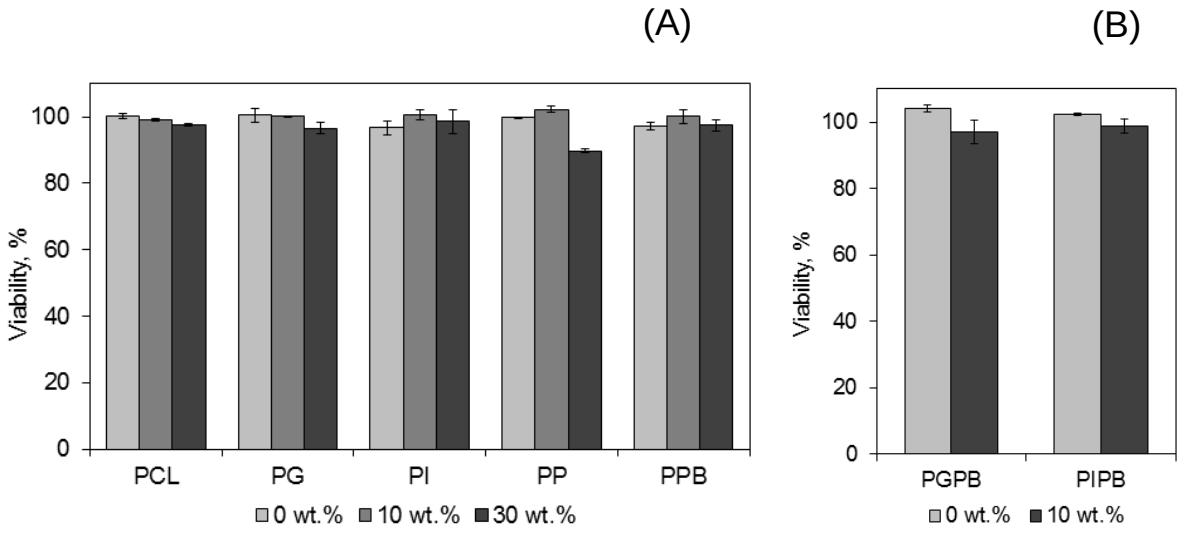

Figure 31 – Cell viability percentage on the foamed samples after 24 hours of incubation (A) single additive and (B) mixture of two additives.

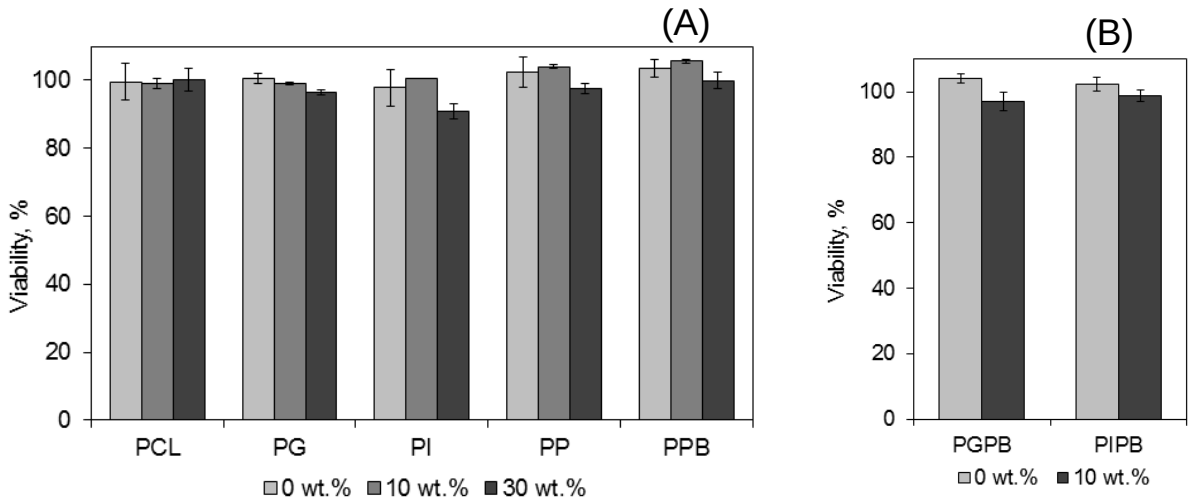

Figure 32 – Cell viability percentage on the foamed samples after 72 hours of incubation (A) single additive and (B) mixture of two additives.

4. Conclusion and future remarks

In this work, porous biodegradable composite biomaterials reinforced with SBA–15 were produced using principles of green chemistry involving the use of PCL and four different additives via supercritical fluid technology, namely supercritical carbon dioxide pressure quench method.

The supercritical foaming process, a clean and environmentally friendly technique, revealed to be a very versatile method for the fabrication of foams with very large pore diameter, in the range of 117 to 1792 μm.

Different formulations were tested at the same operating conditions and the effects of the additives on the final morphology and in the mechanical properties of the foams were evaluated.

The optical images showed that 3D porous structures could be reproduced accurately by $scCO_2$ foaming process via pressure quench method.

From the SEM analysis, it was noticeable that the structure of the prepared foams was strongly dependent on the type of additive used and the amount of nanoparticles.

The pore diameter of the prepared foams decreased with the increase of Si NPs. The composites combining two additives and SBA–15 NPs showed more regular pore size distribution with mean pore diameter varying between 347 and 794 μm and also the pores seemed to be interconnected.

The presence of the two ILs and the Si NPs within the polymeric matrix was confirmed by SEM–EDS which revealed to be homogeneously dispersed.

The thermal and mechanical results revealed the strong plasticization effect of the various additives. The different additives have been demonstrated to be a suitable porogenic agent to generate pore structure within the polymeric matrix.

TGA results showed that the Si NPs were uniform distributed within the polymeric matrix for all samples comprising 10 wt. % of SBA-15 Opposite results were found for the composite biomaterials comprising 30 wt. %, where the samples were found to be heterogeneous.

The cytotoxicity tests showed that the prepared polymeric foams were cytocompatible, i.e., nontoxic to the cells which can be potentially suitable for applications biomedical fields.

All these results revealed that $scCO_2$ foaming process is a feasible method to produce foam (3D porous structures accurately) with very interesting properties which can be applied in different fields, using only greener solvents, which do not present any risks to human and

environment and this technique is performed at low processing temperature which cannot degrade thermo labile compounds.

The interconnectivity of the pores is another important parameter to study in the future works.

It is recommended to evaluate the cell adhesion and proliferation on the produced samples.

In the mechanical characterization it is suggested to use an equipment with more load capacity in order to study the entire mechanical behavior of the foam, i.e., until the break.

It would be very interesting to study the variation of the heterogeneity along the foam.

It also would be interesting to study the influence of CO_2 in the melting and glass transition temperatures of the produced samples by comparison with other samples prepared by another method without CO_2.

5. References

Ajayan, P. M., Schadler, L. S., & Braun, P. V. (Eds.). (2003). *Nanocomposite Science and Technology*: Wiley-VCH Verlag GmbH & Co. KGaA.

Al-Oweini, R., & El-Rassy, H. (2009). Synthesis and Characterization by FTIR Spectroscopy of Silica Aerogels Prepared Using Sveral $Si(OR)_4$ and $R''Si(OR')_3$ Precursors. *Journal of Molecular Structure 919*, 140-145.

Allhenn, D., & Lamprecht, A. (2011). Microsphere Preparation Using the Untoxic Solvent Glycofurol. *Pharmaceutical Research, 28*, 563-571.

Anastas, P. T. (Ed.). (2010). *Green Solvents* (Vol. 4): Wiley-VCH Verlag GmbH.

Annabi, N., Fathi, A., Mithieux, S., Weiss, A. S., & Dehghani, F. (2011). Fabrication of Porous PCL/Elastin Composite Scaffolds for Tissue Engineering Applications. *Journal of Supercritical Fluids, 59*, 157-167.

Ashida, K. (2007). *Polyurethane and Related Foams: Chemistry and Technology*. Boca Ranton CRC Press Taylor & Francis.

Bao, J.-B., Liu, T., Zhao, L., & Hu, G.-H. (2011). A Two-Step Depressurazation Batch Process for the Formation of Bi-modal Cell Structure Polystyrene Foams Using $scCO_2$. *Journal of Supercritical Fluids, 55*, 1104-1114.

Bassi, A. K., Gough, J. E., Zakikhani, M., & Downes, S. (2011). The Chemical and Physical Properties of Poly(e-Caprolactone) Scaffolds Functionalised With Poly(Vinyl Phosphonic Acid-Co-Acrylic Acid). *Journal of Tissue Engineering* doi: 10.4061/2011/615328

Boongird, A., Nasongkla, N., Hongeng, S., Sukdawong, N., Sa-Nguanruang, W., & Larbcharoensub, N. (2011). Biocompatibility Study of Glycofurol in Rat Brains. *Experimental Biology and Medicine, 236*, 77-83.

Brun, N., Ungureanu, S., Deleuze, H., & Backov, R. (2011). Hybrid Foams, Colloids and Beyond: From Design to Applications. *Chemical Society Reviews, 40*, 771-788.

Chansin, M., & Langer, R. (Eds.). (1990). *Biodegradable Polymers as Drug Delivery Systems*: Marcel Dekker, Inc.

Chen, B.-K., Shih, C.-C., & Chen, A. F. (2012). Ductile PLA Nanocomposites With Improved Thermal Stability. *Composites: Part A, 43*, 2289-2295.

Chen, B. K., Wu, T.-Y., Chang, Y.-M., & Chen, A. F. (2013). Ductile Polylactic Acid Prepared with Ionic Liquids. *Chemical Engineering Journal, 215-216*, 886-893.

Chen, L. , Rende, D. , Schadler, L. S., & Ozisik, R. (2013). Polymer Nanocomposite Foams. *Journal of Materials Chemistry A*. doi: 10.1039/c2ta00086e

Colton, J. S., & Suh, N. P. (1987a). Nucleation of Microcellular Foam: Theory and Practice. *Polymer Engineering and Science, 27*(7), 500-503.

Colton, J. S., & Suh, N. P. (1987b). The Nucleation of Microcellular Thermoplastic Foam with Additives: Part I: Theorical Considerations. *Polymer Engineering and Science, 27*(7), 485-492.

Colton, J. S., & Suh, N. P. (1987c). The Nucleation of Microcellular Thermoplastic Foam with Additives: Part II: Experimental Results and Discussion. *Polymer Engineering and Science, 27*(7), 493-499.

Cooper, A. I. (2003). Porous Materials and Supercritical Fluids. *Advanced Materials, 15*(13), 1049-1059.

Dash, T. K., & Konkimala, V. B. (2012). Poly-e-Caprolactone Based Formulations for Drug Delivery and Tissue Engineering: A Review. *Journal of Controlled Release, 158*, 15-33.

Davies, O. R., Lewis, A. L., Whitaker, M. J., Tai, H., Shakesheff, K. M., & Howdle, S. M. (2008). Applications of Supercritical CO_2 in the Fabrication of Polymer Systems for Drug Delivery and Tissue Engineering. *Advanced Drug Delivery Reviews, 60*, 373-387.

Delabarde, C., Plummer, C. J. G., Bourban, P.-E., & Manson, J.-A. E. (2012). Biodegradable Polylactide.Hydroxyapatite Nanocomposite Foam Scaffolds for Bone Tissue Enginnering Applications. *Journal of Materials Science: Materials in Medicine 23*, 1371-1385.

de Matos, M. B. C., Piedade, A. P., Alvarez-Lorenzo, C., Braga, M. E. M., & de Sousa, H. C.. (2013). Dexamethasone-Loaded Poly(ε-Caprolactone)/Silica Nanoparticles Composites Prepared by Supercritical CO_2 foaming/mixing and Deposition. *International Journal of Pharmaceutics,* In Press.

Dias, A. M. A., Marceneiro, S., Braga, M. E. M., Coelho, J. F. J., Ferreira, A. G. M., Simões, P. N., . . . de Sousa, H. C. (2012). Phosphonium-Based Ionic Liquids as Modifiers for Biomedical Grade Poly(Vinyl Chloride). *Acta Biomaterialia, 8*, 1366-1379.

Duarte, A. R. C., Silva, S. S., Mano, J. F., & Reis, R. L. (2012). Ionic Liquids as Foaming Agents of Semi-Crystalline Natural-Based Polymers. *Green Chemistry, 14*(7), 1949-1955.

Eaves, D. (Ed.). (2004). *Handbook of Polymer Foams*. Shawbury, UK: Rapra Technology Limited.

Fanovich, M. A., Ivanovic, J., Misic, D., Alvarez, M. V., Zizovic, I., & Eggers, R. (2013). Development of Polycaprolactone Scaffold with Antibacterial Activity by an Integrated Supercritical Extraction and Impregnation Process. *Journal of Supercritical Fluids, 78*, 42-53.

Fukushima, K., Tabuani, D., & Camino, G. (2009). Nanocomposites of PLA and PCL Based on Montmorillone and Sepiolite. *Materials Science and Engineering C, 29*, 1433-1441.

Gargiulo, N., Attianese, I., Buonocore, G. G., Caputo, D., Lavorgna, M., Mensitieri, G., & Lavorgna, M. (2013). a-Tocopherol Release from Active Polymer Films Loaded with Functionalized SBA-15 Mesoporous Silica. *Microporous and Mesoporous Materials, 167*, 10-15.

Ghasemi-Mobarakeh, L., Prabhakaran, P., Morshed, M., Nasr-Esfahani, M.-H., & Ramakrishna, S. (2008). Electrospun Poly(e-Caprolactone)/Gelatin Nanofibrous Scaffolds for Nerve Tissue Engineering. *Biomaterials, 29*, 4532-4539.

Goodship, V., & Ogur, E. O. (2004). *Polymer Processing with Supercritical Fluids* (Vol. 15): Rapra Review Report.

Gopalan, A. S., Wai, C. M., & Jacobs, H. K. (Eds.). (2003). *Supercritical Carbon Dioxide: Separations and Processes*. Washington ACS Division of Industrial and Engineering Chemistry, Inc.

Gosselin, R., & Rodrigue, D. (2005). Cell Morphology Analysis of High Density Polymer Foams. *Polymer Testing, 24*, 1027-1035.

Gualandi, C., White, L. J., Chen, L., Gross, R. A., Shakesheff, K. M., Howdle, S. M., & Scandola, M. (2010). Scaffolds for Tissue Engineering Fabricated by Non-Isothermal Supercritical Carbon Dioxide Foaming of Highly Crystalline Polyester. *Acta Biomaterialia, 6*, 130-136.

Gunatillake, P. A., & Adhikari, R. (2003). Biodegradable Synthetic Polymers for Tissue Enginnering. *European Cells and Materials, 5*, 1-16.

Jacobs, L. J. M. , Kemmer, M. F., & Keurentjes, J. T. F. (2008). Sustainable Polymer Foaming Using High Pressure Carbon Dioxide: A Review on Fundamentals, Process and Applications. *Green Chemistry, 10*(7), 721-812.

Jaganathan, H., & Godin, B. (2012). Biocompatibility Assessment of Si-Based Nano and Micro-Particles. *Advanced Drug Delivery Reviews, 64*, 1800-1819.

Jenkins, M. J. , Harrison, K. L., Silva, M. M. C. G., Whitaker, M. J., Shakesheff, K. M., & Howdle, S. M. (2006). Characterization of Microcellular Foams Produced from Semi-Crystalline PCL Using Supercritical Carbon Dioxide. *European Polymer Journal, 42*, 3145-3151.

Jiao, J., Xiao, M., Shu, D., Li, L., & Meng, Y. Z. (2006). Preparation and Characterization of Biodegradable Foams from Calcium Carbonate Reinforced Poly(Propylene Carbonate) Composites. *Jounal of Applied Polymer Science, 102*, 5240-5247.

Karimi, M. , Heuchel, M., Weigel, T., Schossig, M., Hofmann, D., & Lendlein, A. (2012). Formation and Size Distribution of Pores in Poly(ε-Caprolactone) Foams Prepared by Pressure Quenching Using Supercritical CO_2. *Journal of Supercritical Fluids, 61*, 175-190.

Kazarian, S. G. (2000). Polymer Processing with Supercritical Fluids. *Polymer Science, Series C, 42*(1), 78-101.

Kelly, C. A., Murphy, S. H., Leeke, G. S., Howdle, S. M., Shakesheff, K. M., & Jenkins, M. J. (2013). Rheological Studies of Polycaprolactone in Supercritical CO_2. *European Polymer Journal, 49*, 464-470.

Kiran, E. (2009). Polymer Miscibility, Phase Separation, Morphological Modifications and Polymorphic Transformations in Dense Fluids. *Journal of Supercritical Fluids, 47*, 466-483.

Kong, Y., & Hay, J. N. (2002). The Measurement of the Crystallinity of Polymers by DSC. *Polymer, 43*, 3873-3878.

Landrock, A. H. (Ed.). (1995). *Handbook of Plastic Foams: Types, Properties, Manufacture and Applications*. New Jersey: Noyes Publications.

Lebourg, M., Antón, J. S., & Ribelles, J. L. G. (2008). Porous Membranes of PLLA-PCL Blend for Tissue Enginnering Applications. *European Polymer Journal, 44*, 2207-2218.

Lee, L. J. , Zeng, C., Cao, X., Han, X., Shen, J., & Xu, G. (2005). Polymer Nanocomposite Foams. *Composites Science and Technology*(65), 2344-2363.

Lee, S.-T. , Park, C. B., & Ramesh, N. S. (2007). *Polymeric Foams: Science and Technology* CRC Press Taylor & Francis Group.

Lee, S.-T. , & Scholz, D. (2009). *Polymeric Foams* CRC Press Taylor & Francis Group.

Léonard, A., Calberg, C., Kerckhofs, G., Wevers, M., Jérôme, R., Pirard, J.-P., . . . Blacher, S. (2008). Characterization of the Porous Structure of Biodegradable Scaffolds Obtained with Supercritical CO_2 as Foaming Agent. *Journal of Porous Materials, 15*, 397-403.

Lian, Z., Epstein, S. C., Blenk, C. W., & Shine, A. D. (2006). Carbon Dioxide-Induced Melting Point Depression of Biodegradable Semicrystalline Polymers. *Journal of Supercritical Fluids, 39*, 107-117.

Liao, X., Zhang, H., & He, Ting. (2012). Preparation of Porous Biodegradable Polymer and Its Nanocomposites by Supercritical Carbon Dioxide Foaming for Tissue Engineering. *Journal of Nanomaterials*. doi: 10.1155/2012/836394

Liu, S. Q. (2007). Bioregererative Engineering: Principle and Applicatons. New Jersey: John Wiley & Sons, Inc.

Martínez-Hernádez, A. L., Velasco-Santos, C., de-Icaza, M., & Castaño, V. M. (2007). Dynamical-Mechanical and Thermal Analysis of Polymeric Composites Reinforced With Keratin Biofibers from Chicken Feathers. *Composites Part B, 38*, 405-410.

Menard, K. P. (2008). *Dynamic Mechanical Analysis: A Practical Introduction* (2nd ed.): CRC Press Taylor & Francis Group.

Meshra, N. , Goyal, A. K., Khatri, K., Vaidya, B., Paliwal, R., Rai, S., . . . Vyas, S. P. . (2008). Biodegradable Polymer Based Particulate Carriers for the Delivery of Proteins and Peptide. *Anti-Inflammatory & Anti-Allergy in Medicinal Chemistry, 7*, 240-251.

Mohammad, A., & Inammudin (Eds.). (2012). *Green Solvents II: Properties and Applications of Ionic Liquids*: Springer.

Mou, Z.-L., Zhao, L.-J. , Zhang, Q.-A. , Zhang, J., & Zhang, Z.-Q. (2011). Preparation of Porous PLGA/HA/Collagen Scaffolds with Supercritical CO_2 and Application in Osteoblast Cell Culture. *Journal of Supercritical Fluids, 58*, 398-406.

Nalawade, S. P., Picchioni, F., & Jansen, L. P. B. M. (2006). Supercritical Carbon Dioxide as Green Solvent for Processing Polymer Melts: Processing and Applications. *Progress In Polymer Science, 31*, 19-43.

Oliveira, J. M., Silva, S. S., Malafaya, P. B, Rodrigues, M. T., Kotobuki, N., Hirose, M., . . . Reis, R. L. (2009). Macroporous Hydroxyapatite Scaffolds for Bone Tissue Engineering Applications: Physical Characterization and Assessment of Rat Bone Marrow Stromal Cell Viability. *Journal of Biomedical Materials Research Part A, 91A*, 175-186.

Pankajakshan, D., Lizymol, P. P., Palakkal, M., Krishnan, K., & Krishnan, L. K. (2008). Development of Fibrin Composite-Coated Poly(ε-Caprolactone) Scaffold for Potential Vascular Tissue Engineering Applications. *Journal of Biomedical Materials Research Part B: Applied Biomaterials, 87B*, 570-579.

Polini, A., Pisignano, D., Parodi, M., Quarto, R., & Scaglione, S. (2011). Osteoinduction of Human Mesenchymal Stem Cells bu Bioactive Composite Scaffolds without Supplemental Osteogenic Growth Factors. *Plosone, 6*(10), 1-8.

Puga, A. M., Rey-Rico, A., Magariños, B., Alvarez-Lorenzo, C., & Concheiro, A. (2012). Hot Melt Poly-e-Caprolactone/Poloxamine Implantable Matrices for Tissue Sustained Delivery of Ciprofloxacin. *Acta Biomaterialia, 8*, 1507-1518.

Quirk, R. A., France, R. M., Shakesheff, K. M., & Howdle, S. M. (2004). Supercritical Fluid Technologies and Tissue Engineering Scaffolds. *Current Opinion in Solid State and Materials Science, 8*, 313-321.

Rai, B., Teoh, S. H., Hutmacher, D. W., Cao, T., & Ho, K. H. (2005). Novel PCL-Based Honeycomb Scaffolds as Drug Delivery Systems for rhBMP-2. *Biomaterials, 26*, 3739-3748.

Reverchon, E., & Cardea, S. (2012). Supercritical Fluids in 3-D Tissue Engineering. *Journal of Supercritical Fluids, 69*, 97-107.

Reverchon, E., Cardea, S., & Rapuano, C. (2008). A New Supercritical Fluid-Based Process to Produce Scaffolds for Tissue Replacement. *Journal of Supercritical Fluids, 45*, 365-373.

Rinki, K., Dutta, P. K., Hunt, A. J., Clark, J. H., & Macquarrie. (2009). Preparation of Chitosan Based Scaffolds Using Supercritical Fluids. *Macromolecules Symposia, 277*, 36-42.

Rowe, R. C., Sheskey, P. J., & Quinn, M. E. (Eds.). (2009). *Handbook of Pharmaceutical Excipients* (6th ed.). London: Pharmaceutical Press.

Salerno, A., Di Maio, E. , Iannace, S., & Netti, P. A. . (2012). Tailoring the Pore Structure of PCL Scaffolds for Tissue Enginnering Prepared via Gas Foaming of Multi-Phase Blends. *Journal of Porous Materials, 19*, 181-188.

Salerno, A., Zeppetelli, S., Di Maio, E., Iannace, S., & Netti, P. A. (2010). Novel 3D Porous Multi-Phase Composite Scaffolds Based on PCL, Thermoplastic Zein and HA Prepared Via Supercritical CO_2 Foaming for Bone Regeneration. *Composites Science and Technology, 70*, 1838-1846.

Salgado, A. J., Coutinho, O. P., & Reis, R. L. (2004). Bone Tissue Engineering: State of Art and Future Trends. *Macromulecular Bioscience, 4*, 743-765.

Sant, S., Hwang, C. M., Lee, S.-H. , & Khademhosseini, A. (2011). Hybrid PGS-PCL Microfibrous Scaffolds with Improved Mechanical and Biological Properties. *Journal of Tissue Engineering and Regenerative Medicine 5*(4), 283-291.

Shieh, Y.-T., Lai, J.-G. , Tang, W.-L. , Yang, C.-H., & Wnag, T.-L. (2009). Supercritical CO_2 Intercalation of Polycaprolactone in Layered Silicates. *Journal of Supercritical Fluids, 49*, 385-393.

Silva, S. S. , Santos, T. C., Cerqueira, M. T., Marques, A. P., Reys, L. L., Silva, T. H., . . . Reis, R. L. (2012). The Use of Ionic Liquids in the Processsing of Chitosan/Silk Hydrogels for Biomedical Applications. *Green Chemistry, 14*, 1463-1470.

Singh, L., Kumar, V., & Ratner, B. D. (2004). Generation of Porous Microcellular 85/15 Poly(DL-Lactide-co-Glycolide) Foams for Biomedical Applications. *Biomaterials, 25*, 2611-2617.

Sinha, V. R., Bansal, K., Kaushik, R., Kumria, R., & Trehan, A. . (2004). Poly-ε-Caprolactone Microspheres and nanospheres: An Overview. *International Journal of Pharmaceuticals, 278*, 1-23.

Sun, X., Liu, H. L., Li, G., Liao, X., & He, J. (204). Investigation on the Cell Nucleation and Cell Growth in Microcellular Foaming by Means of Temperature Quenching. *Jounal of Applied Polymer Science, 93*, 163-171.

Takahashi, S., Hassler, J. C., & Kiran, E. (2012). Melting Bahavior of Biodegradable Polyesters in Carbon Dioxide at High Pressures. *Journal of Supercritical Fluids, 72*, 278-287.

Tomé, L. I. N., Ramesh, L. G., Carvalho, P. J., Pastoriza-Gallego, M. J., Pineiro, M. M., & Coutinho, J. A. P. (2011). Measurements and Correlation of High-Pressure Densities of Phosphonium Based Ionic Liquids. *Journal of Chemical Engineering Data, 56*, 2205-2217.

Tran, M.-K., Swed, A., & Boury, F. (2012). Preparation of Polymeric Particles in CO_2 Medium using Non-Toxic Solvents: Formulations and Comparisons wih Phase Separation Method. *European Journal of Pharmaceutics and Biopharmaceutics, 82*, 498-507.

Tsimpliaraki, A., Tsivintzelis, I., Zuburtikudis, S. I., & Panayiotou, C. . (2011). The Effect of Surface Chemistry and Nanoclay Loading on the Microcellular Structure of Porous Poly(D,L Lactic Acid) Nanocomposites. *Journal of Supercritical Fluids, 57*, 278-287.

Tsivintzelis, I., Angelopoulou, A. G., & Panayiotou, C. . (2007). Foaming of Polymers with Supercritical CO_2: An Experimental and Therical Study. *Polymer, 48*, 5928-5939.

Ueki, T., & Watanabe, M. (2008). Macromolecules in Ionic Liquids: Progress, Challenges, and Opportunities. *Macromolecules, 41*(11), 3739-3749.

Webb, P. A., & Orr, C. (1997). *Analytical Methods in Fine Particle Technology*. Norcross, GA: Micromeritics Instrument Corporation.

White, L. J., Hutter, V. , Tai, H., Howdle, S. M., & Shakesheff, K. M. . (2012). The Effect of Proceesing Variables on Morphological and Mechanical Properties of Supercritical CO_2 Foamed Scaffolds for Tissue Engineering *Acta Biomaterialia, 8*, 61-71.

Wiria, F. E. , Leong, K. F., Chua, C. K., & Liu, Y. . (2007). Poly-e-Caprolactone/Hydroxyapatite for Tissue Engineering Scaffolds Fabrication Via Selective Laser Sintering. *Acta Biomaterialia, 3*, 1-12.

Woodruff, M. A., & Hutmacher, D. W. (2010). The Return of a Forgotten Polymer-Polycaprolactone in the 21st Century. *Progress In Polymer Science, 35*, 1217-1256.

Xu, Q. , Ren, X., Chang, Y., Wang, J., Yu, L., & Dean, K. (2004). Generation of Microcellular Biodegradable Polycaprolactone Foams in Supercritical Carbon Dioxide. *Jounal of Applied Polymer Science, 94*, 593-597.

Xu, Y. , Wang, C., Zhou, G., Wu, Y., & Chen, J. (2012). Improving the Controlled Release of Water-Insoluble Emodin From Amino-Functionalized Mesoporous Silica. *Applied Surface Scince, 258*, 6366-6372.

Yan, B., & Li, Y. (2010). Luminescent Ternary Inorganic-Organic Mesoporous Hybrids Eu(TTASi-SBA-15)phen: Covalent Linkage in TTA Directly Functionalized SBA-15. *Dalton Transactions, 39*, 1480-1487.

Yañes, F., Martikainen, L., Braga, M. E. M., Alvarez-Lorenzo, C., Concheiro, A., Duarte, C. M. M., . . . de Sousa, H. C. (2011). Supercritical Fluid-Assisted Preparation of Imprinted Contact Lenses for Drug Delivery. *Acta Biomaterialia, 7*, 1019-1030.

Yang, G., Su, J., Gao, J., Hu, X., Geng, C., & Fu, Q. (2013). Fabrication of Well-Controlled Porous Foams of Graphene Oxide Modified Poly(Propylene-Carbonate) Using Supercritical Carbon Dioxide and Its Potential Tissue Engineering Applications. *Journal of Supercritical Fluids, 73*, 1-9.

York, P., Kompella, U. B., & Shekunov, B. Y (Eds.). (2004). *Supercritical Fluid Technology for Drug Product Development*: Marcel Dekker, Inc.

Yoshimura, K., Nakano, K., Okamoto, K., & Miyake, T. (2012). Mechanical and Electrical Properties in Porous Structure of Ketjenblack/Silicone-Rubber Composites. *Sensors and Actuators A, 180*, 55-62.

Zeng, C., Han, X., Lee, L. J., Koelling, K. W. , & Tomasko, D. L. (2003). Polymer-Clay Nanocomposite Foams Prepared Using Carbon Dioxide. *Advanced Materials, 15*(20), 1743-1747.

Zhai, W., Yu, J., Wu, L., Ma, W., & He, J. (2006). Heterogeneous Nucleation Uniformizing Cell Size Distribution in Microcellular Nanocomposites Foams. *Polymer, 47*, 7580-7589.

Zhao, D., Liao, Y., & Zhang, Z. (2007). Toxicity of Ionic Liquids. *Clean, 35*(1), 42-48.

Zhao, H. (2006). Innovative Applications of Ionic Liquids as "Green" Engeneering Liquids. *Chemical Engineering Communications, 193*, 1660-1667.

6. SUPLEMMENTARY DATA

Appendix A – Physical characterization

Morphological analysis

Fourier Transform InfraRed

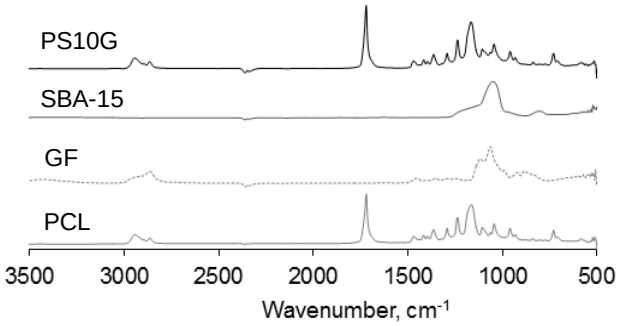

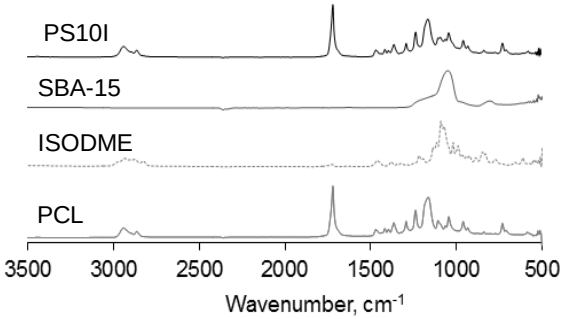

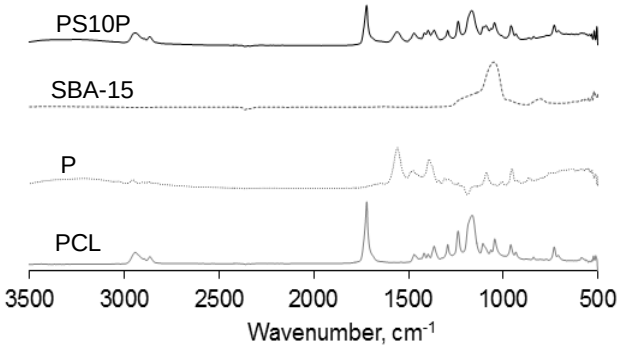

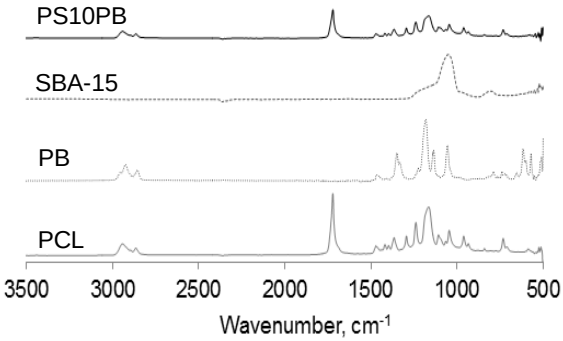

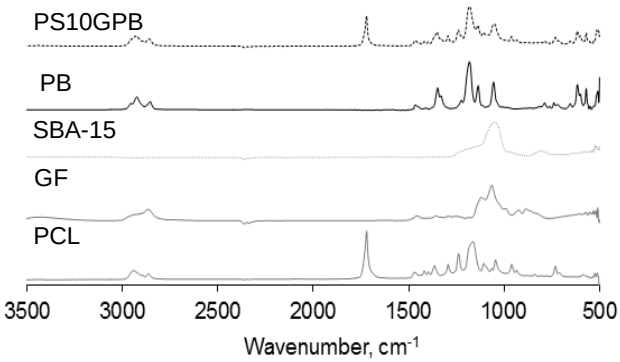

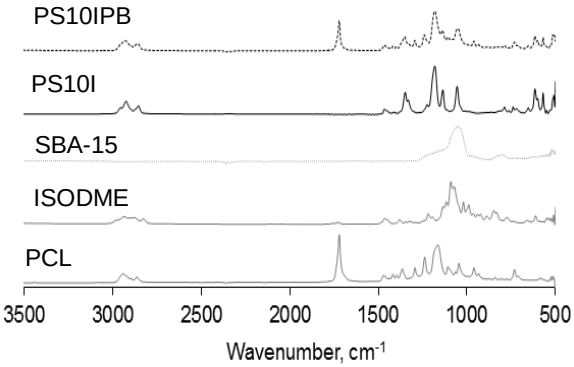

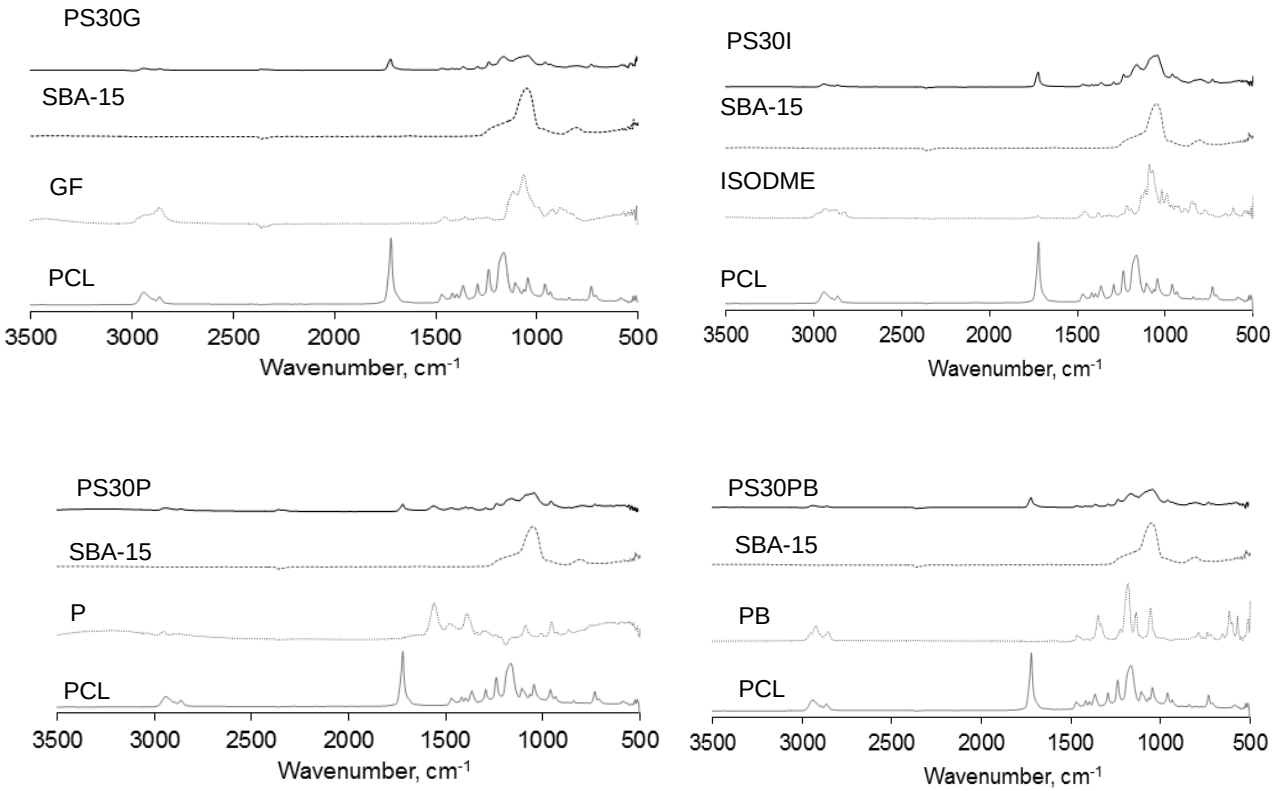

Figure A1 – FTIR spectra of the processed samples by $scCO_2$ for 2 h, 20 MPa, 40 °C and 0.37 L_{CO2}·min^{-1}.

Helium picnometry

Density

Table A1 – Density of porous materials prepared via by $scCO_2$ foaming process for 2 h, 20 MPa, 40 °C and 0.37 L_{CO2}·min^{-1}.

Sample name	Density, g·cm^{-3}
PCL	1.11 ± 0.002
PG	1.13 ± 0.000
PI	0.99 ± 0.010
PP	1.11 ± 0.001
PPB	1.09 ± 0.003
PS10	1.19 ± 0.017
PS10G	1.15 ± 0.003
PS10I	1.17 ± 0.002
PS10P	1.17 ± 0.002
PS10PB	1.07 ± 0.043
PS30	1.24 ± 0.007
PS30G	1.19 ± 0.014
PS30I	1.20 ± 0.012
PS30P	1.22 ± 0.013
PS30PB	1.13 ± 0.018

PGPB	0.98 ± 0.004
PIPB	0.99 ± 0.001
PS10GPB	1.16 ± 0.001
PS10IPB	1.14 ± 0.004

Nitrogen adsorption

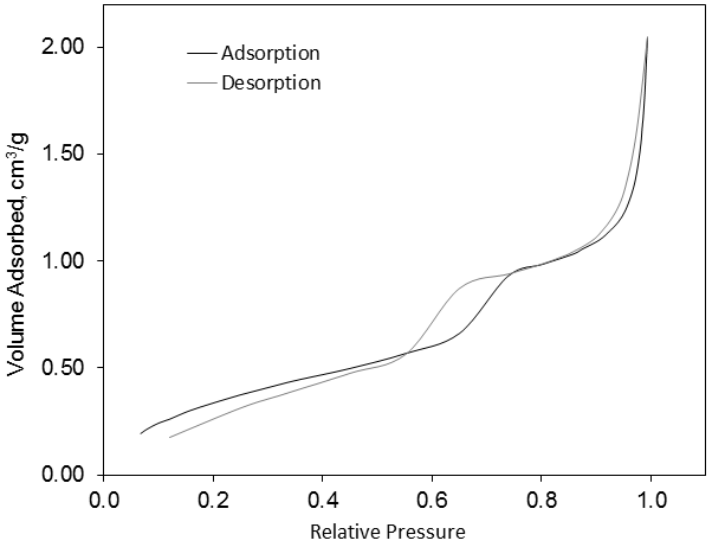

Figure A2 – Adsorption isotherm for PS30PB composite.

Table A2 – Results obtained from nitrogen adsorption for all processed samples by $scCO_2$ foaming for for 2 h, 20 MPa, 40 °C and 0.37 $L_{CO2} \cdot min^{-1}$

Sample name	Surface Area, $m^2 \cdot g^{-1}$	Pore Volume, $cm^3 \cdot g^{-1} \times 10^3$	Pore Diameter, Å
PCL	0.86 ± 0.23	0.65 ± 0.09	30.86 ± 4.20
PG	0.70 ± 0.19	0.45 ± 0.06	26.16 ± 3.61
PI	0.76 ± 0.14	0.62 ± 0.07	32.98 ± 2.31
PP	0.94 ± 0.51	0.59 ± 0.21	26.57 ± 5.43
PPB	1.39 ± 0.50	0.96 ± 0.20	28.37 ± 4.45
PS10	0.80 ± 0.23	0.87 ± 0.24	43.56 ± 0.03
PS10G	0.79 ± 0.09	0.71 ± 0.06	36.04 ± 1.18
PS10I	0.73 ± 0.20	0.59 ± 0.01	33.96 ± 9.04
PS10P	0.79 ± 0.18	0.63 ± 0.08	32.40 ± 3.44
PS10PB	0.71 ± 0.00	0.65 ± 0.03	36.50 ± 1.55
PS30	2.68 ± 0.16	4.87 ± 0.31	72. 83 ± 0.37
PS30G	1.45 ± 0.02	3.48 ± 0.01	96.07 ± 1.05
PS30I	1.15 ± 0.03	2.62 ± 0.00	91.05 ± 2.02
PS30P	1.27 ± 0.02	1.86 ± 0.21	58.45 ± 5.34
PS30PB	1.67 ± 0.30	2.74 ± 0.34	66.10 ± 3.63
PGPB	0.67 ± 0.08	0.51 ± 0.00	30.73 ± 3.50
PIPB	0.81 ± 0.25	0.47 ± 0.18	23.06 ± 1.53

PS10GPB	0.75 ± 0.02	0.68 ± 0.12	36.44 ± 6.95
PS10IPB	0.55 ± 0.06	0.49 ± 0.01	35.42 ± 2.81

Appendix B – Thermal analysis

Thermogravimetric Analysis (TGA)

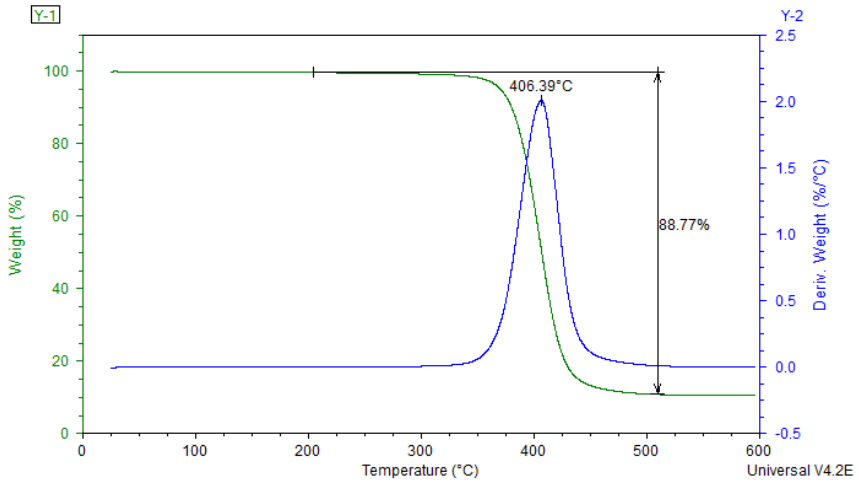

Figure B1 – TG profile for PS10 composite indicating the degradation temperature and mass loss.

Table B1 – Degradation temperature and mass loss of processed samples by $scCO_2$ foaming process for 2 h, 20 MPa, 40 °C and 0.37 L_{CO2}·min^{-1}.

Sample code	Degradation temperature, °C	Mass loss, %
GF	169.76 ± 9.66	98.45 ± 0.51
ISODME	126.22 ± 6.29	98.73 ± 0.01
TMEAP	206.91 ± 1.02	99.13± 0.12
PB	398.93 ± 5.01	99.23 ± 0.09
PCL pure	407.57 ± 0.18	99.30 ± 0.19
PCL	405.91 ± 2.83	99.44 ± 0.08
PG	408.68 ± 0.86	99.01 ± 0.11
PI	408.60 ± 0.23	99.32 ± 0.03
PP	404.66 ± 0.16	97.44 ± 1.05
PPB	405.16 ± 0.23	99.39 ± 0.01
PS10	405.23 ± 1.65	88.65 ± 0.83
PS10G	405.17 ± 1.53	90.82 ± 1.57
PS10I	411.39 ± 0.42	90.19 ± 1.32
PS10P	409.99 ± 0.57	91.80 ± 1.08
PS10PB	391.16 ± 6.65	93.89 ± 0.99

PS30	416.04 ± 2.23	77.32 ± 0.13
PS30G	414.33 ± 0.99	78.62 ± 0.86
PS30I	410.26 ± 7.29	80.42 ± 4.90
PS30P	411.25 ± 1.72	81.83 ± 1.00
PS30PB	413.99 ± 0.09	88.11 ± 3.05
PGPB	410.56 ± 0.23	99.09 ± 0.05
PIPB	410.09 ± 0.25	98.90 ± 0.18
PS10GPB	411.94 ± 0.18	91.61 ± 0.78
PS10IPB	407.34 ± 1.09	89.84 ± 0.04

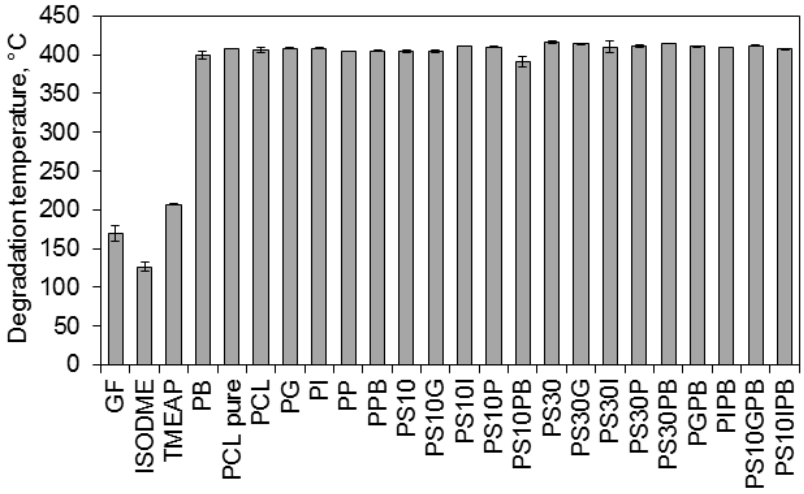

Figure B2 – Degradation temperature of pure compounds and processed samples by $scCO_2$ foaming process for 2 h, 20 MPa, 40 °C and 0.37 $L_{CO2}·min^{-1}$.

.

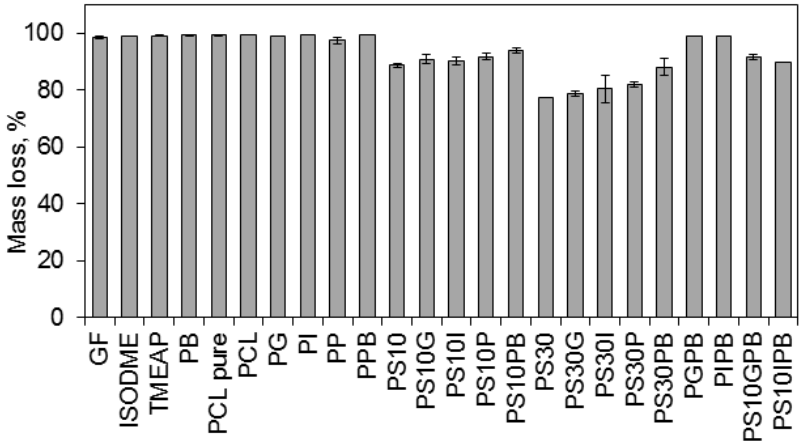

Figure B3 – Mass loss of pure compounds and processed samples by $scCO_2$ foaming process for 2 h, 20 MPa, 40 °C and 0.37 $L_{CO2}·min^{-1}$.

Differential Scanning Calorimetry (DSC)

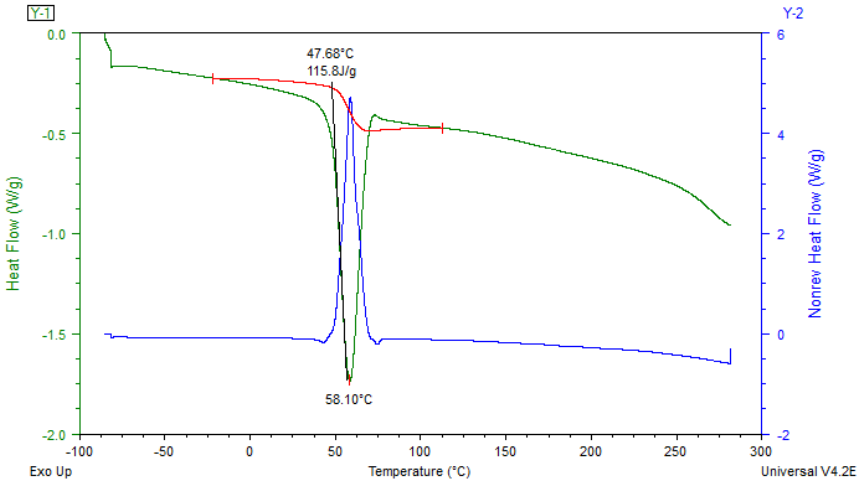

Figure B4 – DSC profile for PCL indicating the melting temperature and enthalpy.

Table B2 – Thermal properties and crystallinity of pure compounds and processed samples by $scCO_2$ foaming process for 2 h, 20 MPa, 40 °C and 0.3 $L_{CO2} \cdot min^{-1}$.

Sample code	Melting temperature, °C	Melting enthalpy, J/g	Crystallinity, %
PCL pure	62.31 ± 0.49	105.40 ± 0.99	75.56 ± 0.71
PCL	61.73 ± 0.35	88.91 ± 6.96	63.73 ± 4.99
PG	55.37 ± 1.37	79.35 ± 1.71	56.88 ± 1.23
PI	57.20 ± 0.69	78.72 ± 4.14	56.43 ± 2.97
PP	60.26 ± 0.02	88.14 ± 5.85	63.18 ± 4.19
PPB	60.50 ± 0.33	88.86 ± 0.64	63.70 ± 0.46
PS10	62.45 ± 0.36	76.28 ± 5.46	54.68 ± 3.91
PS10G	60.32 ± 0.59	75.44 ± 1.50	54.08 ± 1.07
PS10I	58.94 ± 0.27	77.06 ± 2.16	55.24 ± 1.55
PS10P	61.61 ± 0.59	78.58 ± 9.58	56.36 ± 6.57
PS10PB	61.59 ± 0.41	77.09 ± 1.87	55.26 ± 1.34
PS30	60.43 ± 1.44	80.99 ± 2.85	58.05 ± 2.04
PS30G	59.68 ± 0.23	75.40 ± 0.01	54.05 ± 0.01
PS30I	58.87 ± 0.30	79.78 ± 2.26	57.19 ± 1.62
PS30P	58.48 ± 0.70	82.56 ± 2.27	59.18 ± 1.63
PS30PB	59.76 ± 0.78	51.10 ± 12.69	37.25 ± 9.09
PGPB	59.52 ± 0.32	79.38 ± 10.12	56.90 ± 7.25
PIPB	58.31 ± 1.34	55.76 ± 11.53	39.97 ± 8.27
PS10GPB	56.26 ± 0.02	46.95 ± 1.52	33.65 ± 1.09
PS10IPB	58.19 ± 0.06	59.02 ± 6.96	42.31 ± 4.99

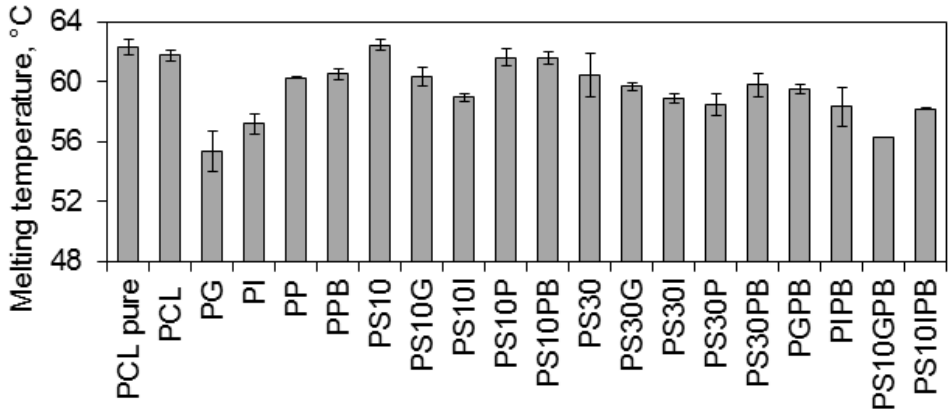

Figure B5 – Melting temperature of pure compounds and processed samples by $scCO_2$ foaming process for 2 h, 20 MPa, 40 °C and 0.37 $L_{CO2} \cdot min^{-1}$.

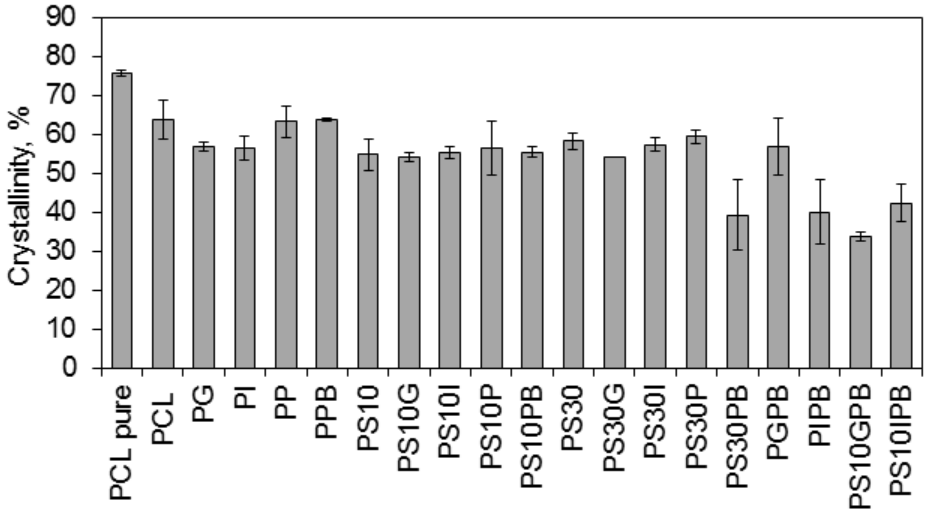

Figure B6 – Melting temperature of pure compounds and processed samples by $scCO_2$ foaming process for 2 h, 20 MPa, 40 °C and 0.37 $L_{CO2} \cdot min^{-1}$.

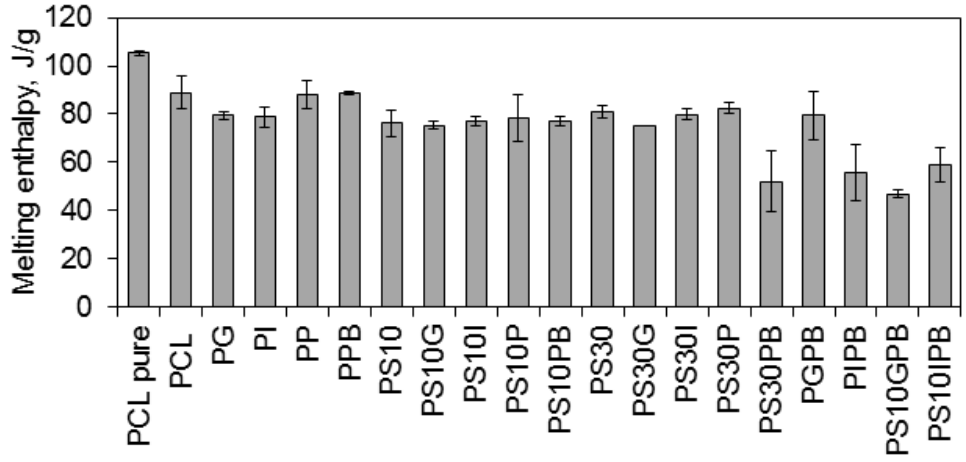

Figure B7 – Melting enthalpy of pure compounds and processed samples by $scCO_2$ foaming process for 2 h, 20 MPa, 40 °C and 0.37 $L_{CO2} \cdot min^{-1}$.

Appendix C – Mechanical analysis

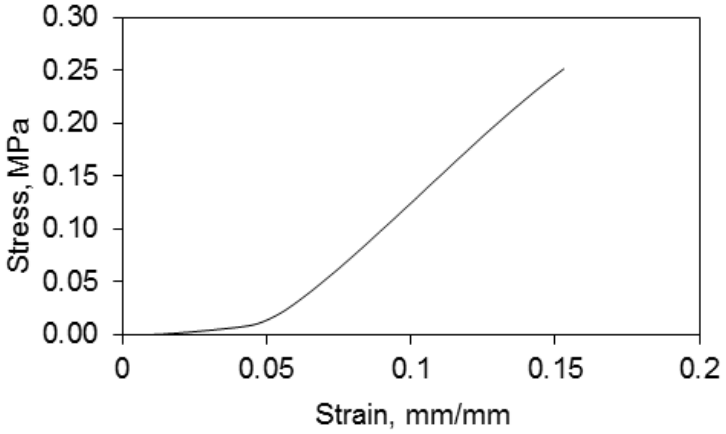

Figure C1 – Stress-strain curves of foamed samples obtained by $scCO_2$ foaming process for 2 h, 20 MPa, 40 °C and 0.37 $L_{CO2}{\cdot}min^{-1}$

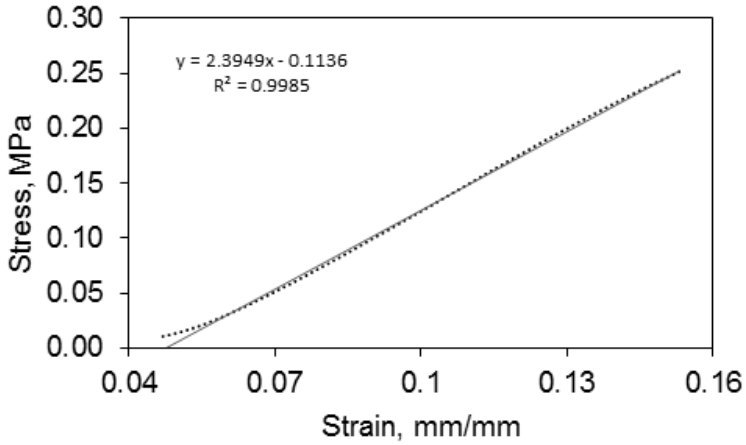

Figure C2 – Linear regression of the elastic region used to determine the Young's Modulus.

Table C1 – Mechanical properties of obtained porous structures samples obtained by $scCO_2$ foaming process for 2 h, 20 MPa, 40 °C and 0.37 $L_{CO2}{\cdot}min^{-1}$

Sample code	Young's Modulus, MPa	Compressive Strength, MPa
PCL	2.915 ± 0.10	0.252 ± 0.001
PG	2.734 ± 0.24	0.252 ± 0.001
PI	3.024 ± 0.11	0.250 ± 0.000
PP	2.958 ± 0.26	0.250 ± 0.001
PPB	3.170 ± 0.06	0.269 ± 0.023
PS10	2.547 ± 0.22	0.253 ± 0.002
PS10G	2.967 ± 0.01	0.254 ± 0.004
PS10I	2.853 ± 0.53	0.184 ± 0.081
PS10P	3.071 ± 0.08	0.259 ± 0.013

PS10PB	3.285 ± 0.12	0.256 ± 0.005
PS30	4.318 ± 0.32	0.311 ± 0.001
PS30G	3.090 ± 0.27	0.252 ± 0.001
PS30I	3.130 ± 0.24	0.252 ± 0.000
PS30P	2.476 ± 0.22	0.253 ± 0.001
PS30PB	2.998 ± 0.22	0.279 ± 0.000
PGPB	3.355 ± 0.17	0.296 ± 0.004
PIPB	2.954 ± 0.09	0.257 ± 0.008
PS10GPB	1.918 ± 0.26	0.106 ± 0.036
PS10IPB	2.418 ± 0.13	0.327 ± 0.032
PS10GPB1	3.244 ± 0.28	0.280 ± 0.011
PS10IPB1	3.278 ± 0.39	0.237 ± 0.026

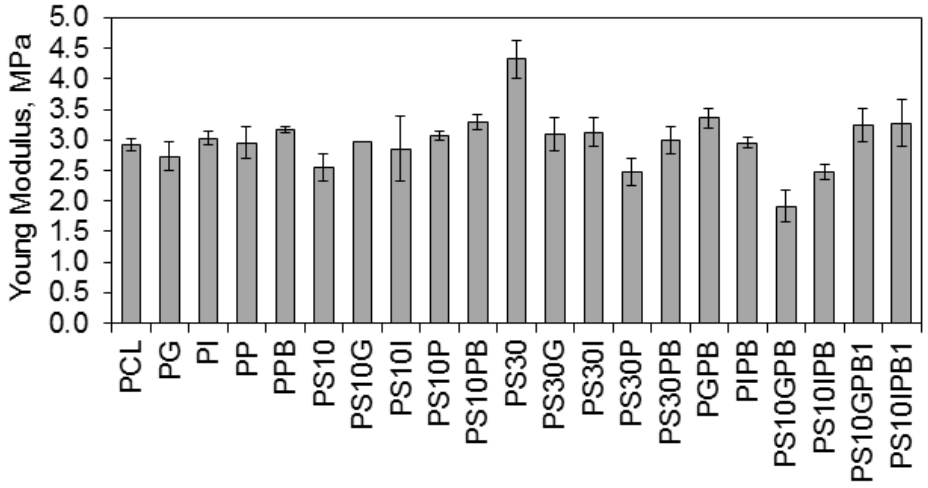

Figure C3 – Young's Modulus of prepared samples obtained by $scCO_2$ foaming process for 2 h, 20 MPa, 40 °C and 0.37 $L_{CO2} \cdot min^{-1}$.

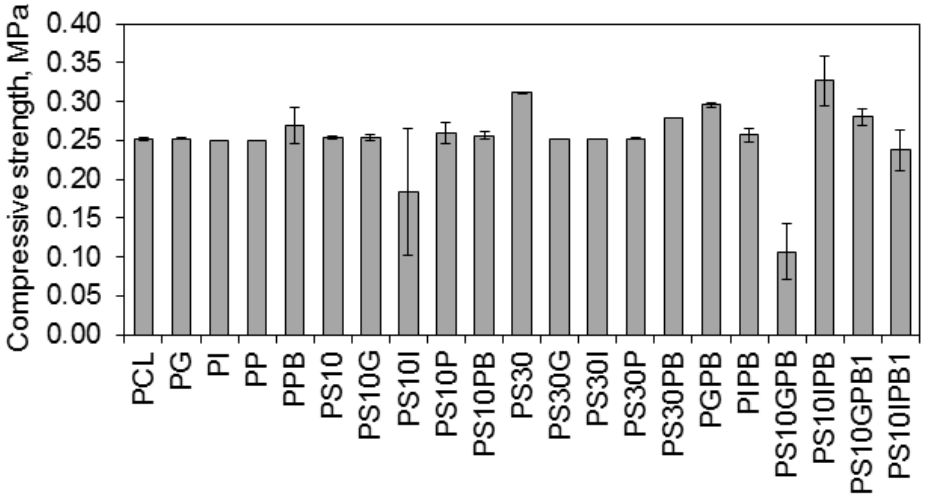

Figure C4 – Compressive strength of prepared samples obtained by $scCO_2$ foaming process for 2 h, 20 MPa, 40 °C and 0.37 $L_{CO2} \cdot min^{-1}$.

Dynamical mechanical analysis (DMA)

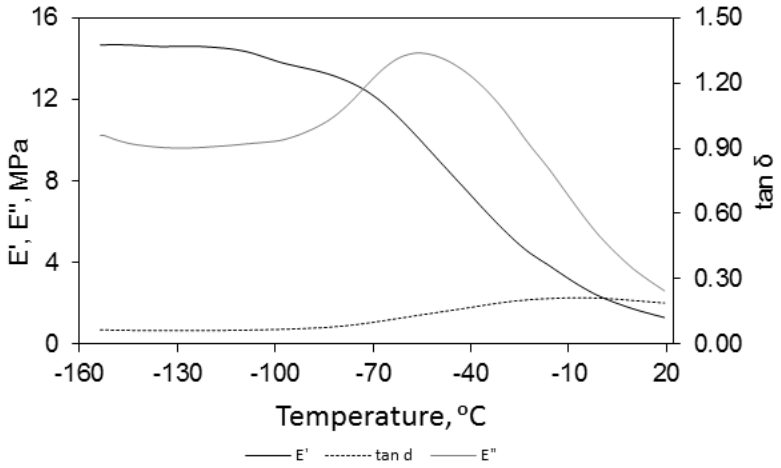

Figure C5 –Results obtained during the DMA analysis.

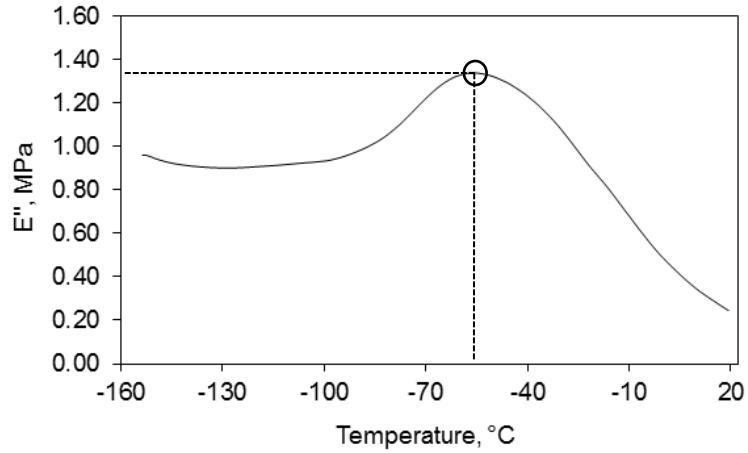

Figure C6 – Loss modulus curve obtained during the DMA analysis.

Appendix D – Pressure behavior during depressurization step

The pressure drop with time during the depressurization step at a constant flow rate was measured. As it can be seen in the Figure D1, there was a sharp drop in the first 10 minutes of depressurization which became less accentually until the end of the process. This effect may be due the rapid diffusion of CO_2 through the polymeric matrix and maybe due to the big pressure gradient between the high pressure cell and the external environment.

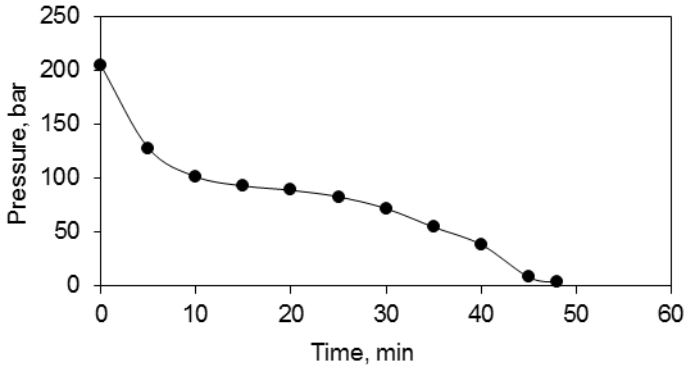

Figure D1 – Pressure change during the depressurization step of the high pressure cell at constant flow rate (0.37 L_{CO2}·min^{-1}).

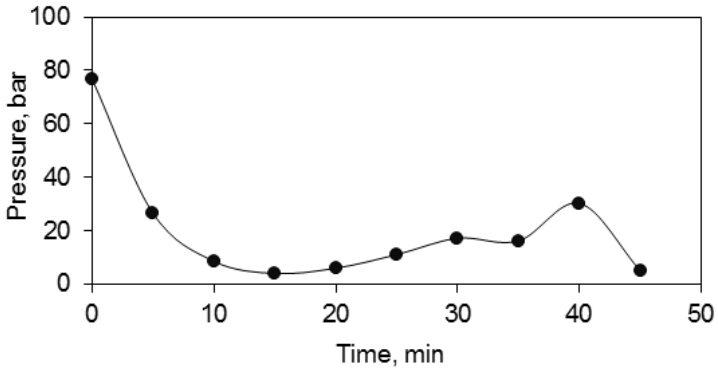

Figure D2 – Pressure drop as a function of time at constant flow rate (0.37 L_{CO2}·min^{-1})